



Netherlands Enterprise Agency

Morphodynamics of Hollandse Kust (zuid) Wind Farm Zone

*>> Sustainable. Agricultural. Innovative.
International.*



HOLLANDSE KUST (ZUID) WIND FARM ZONE

Certification Report Morphodynamics

Netherlands Enterprise Agency

Report No.: CR-SC-DNVGL-SE-0190-02453-2_Morphodynamics

Date: 2016-12-24



Project name: Hollandse Kust (zuid) Wind Farm Zone DNV GL
 Report title: Certification Report Renewables Certification
 Customer: Morphodynamics Tuborg Parkvej 8
 Netherlands Enterprise Agency 2900 Hellerup
 Croeselaan 15 Denmark
 3521 BJ Utrecht The Netherlands
 Contact person: F.C.W. (Frank) van Erp
 Date of issue: 2016-12-24
 Project No.: 10016925
 Report No.: CR-SC-DNVGL-SE-0190-02453-
 2_Morphodynamics

Applicable contract(s) governing the provision of this Report: WOZ1600001

Objective: To confirm that the result of a Morphodynamic study carried out for Hollandse Kust (zuid) Wind Farm Zone (here: Wind Farm Sites (WFS) I, II, III and IV) can be used for design of future offshore wind farms.

Prepared by:	Verified by:	Approved by:
 Asp, Erik 2016.12.25 12:58:29 +01'00'	 Lohmann, Iris Pernille 2017.01.03 10:30:01 +01'00'	 Redanz, Pia 2016.12.24 08:59:14 +01'00'
Erik Asp Principal Specialist	Iris P. Lohmann Senior Engineer	Pia Redanz Head of Section, Loads Copenhagen

Copyright © DNV GL 2014. All rights reserved. This publication or parts thereof may not be copied, reproduced or transmitted in any form, or by any means, whether digitally or otherwise without the prior written consent of DNV GL. DNV GL and the Horizon Graphic are trademarks of DNV GL AS. The content of this publication shall be kept confidential by the customer, unless otherwise agreed in writing. Reference to part of this publication which may lead to misinterpretation is prohibited.

DNV GL Distribution: Keywords:

Unrestricted distribution (internal and external)
 Unrestricted distribution within DNV GL
 Limited distribution within DNV GL after 3 years
 No distribution (confidential)
 Secret

Rev. No.	Date	Reason for Issue	Prepared by	Verified by	Approved by
0	2016-12-16	First issue	Erik Asp	Iris Lohmann	Pia Redanz
1	2016-12-23	Rev 1	Erik Asp	Iris Lohmann	Pia Redanz
2	2016-12-24	Typo corrected	Erik Asp	Iris Lohmann	Pia Redanz



Table of contents

1	EXECUTIVE SUMMARY	1
2	CERTIFICATION SCHEME	1
3	LIST OF REPORTS	1
4	CONDITIONS	1
5	OUTSTANDING ISSUES	1
6	CONCLUSION	1

Appendix A Morphological Investigations

1 EXECUTIVE SUMMARY

The Hollandse Kust (zuid) Wind Farm Zone is located in the Dutch Sector of the North Sea, approximately 22 km from the coastline. As part of the tender preparations, the Netherlands Enterprise Agency (Rijksdienst voor Ondernemend Nederland, RVO) requested a morphology investigation of wind farm sites (WFS) I to IV of the Hollandse Kust (zuid) Wind Farm Zone (WFZ). DNV GL was assigned to validate this Bathymetric study.

2 CERTIFICATION SCHEME

The following codes and standards are applied:

Document No.	Title
DNVGL-SE-0190:2015-12	Project certification of wind power plants

The morphology study will be evaluated based on section 2.3.2 Site Assessment of DNVGL-SE-0190.

3 LIST OF REPORTS

The appendices to this report comprise the detailed DNV GL certification reports which normally include reference standards/documents, list of design documentation as well as summary and conclusion of the DNV GL evaluation.

APPENDIX	Revision	Subject
A	0	Morphological Investigations

4 CONDITIONS

The conditions identified during the technical evaluation are listed in the following. The conditions are assigned to the certification phases in which they need to be considered and evaluated.

The seabed levels within the wind farm area shall be monitored and remedial actions taken before the seabed levels are outside the design upper and lower ranges.

5 OUTSTANDING ISSUES

No outstanding issues have been identified.

6 CONCLUSION

DNV GL find that the morphology study is complete, carried out according to industry best practice, is plausible, and that

- Best Estimate Bathymetry (BEB)
- Lowest Sea Bed Level (LSBL) for the period 2016-2056
- Highest Sea Bed Level (HSBL) for the period 2016-2056

as defined in the documents listed in Appendix A are derived in line with the requirements following section 2.3.2 of the DNVGL-SE-0190 and can be used as basis for determining design seabed levels for Hollandse Kust (zuid) Wind Farm Zone.



APPENDIX A

Morphological Investigations

Evaluation of Morphological Investigations for Hollandse Kust (zuid) Wind Farm Zone

Description of verified component, system or item

Within the wind farm area a morphology study has been performed. The results and the found morphodynamic site conditions are documented by the customer and build the basis for the verification of the current report.

Interface to other systems/components:

Currently, no interfaces to other systems/components are present.

Basis for the evaluation

Applied codes and standards:

Document No.	Revision	Title
DNVGL-ST-0437	November 2016	Loads and site conditions for wind turbines
IEC 61400-3	2009	Wind Turbines – Part 3: Design requirements for offshore wind turbines

Documentation from customer

List of reports:

Ref.	Document No.	Revision	Title
/1/	1230851-000-HY E-0003	Final v2	Morphodynamics of Hollandse Kust (zuid) Wind Farm Zone Prediction of seabed level changes between 2016 and 2051

Evaluation work

Reference /1/ presents the bathymetrical/morphodynamic assessment for the planned Hollandse Kust (zuid) Wind Farm Zone. /1/ contains information regarding:

- Description of morphodynamic features in the wind farm zone
- An analysis of the morphodynamics
- Extrapolation of historical morphodynamic activities for the estimation of future seabed levels

The seabed bedforms at Hollandse Kust (zuid) Wind Farm Zone (HKZ) consist of a combination of Megaripples and Sand Waves.

/1/ concludes that from the geological and geophysical data available non-erodible layers exist, but that they are located too deep to influence migration of the sand waves and the megaripples.

The Megaripples have migration speeds that are so large that many megaripples will pass each Turbine during the lifetime of the wind farms. Therefore, only their dimensions were determined and their representative statistical values were included as an uncertainty band for predicted bed levels.

The Sand waves have been analysed in 3 steps based on the historical and recent seabed bathymetries

- a. Determination of the sand wave migration direction
- b. Determination of the sand wave migration speed
- c. Characterization of the sand wave shape

Future migration

The 2016 HKZ Bathymetry was determined from multibeam survey carried out by Fugro on behalf of RVO: These bathymetrical data together with 2010 survey and other previous surveys were used to determine the seabed dynamics: a) sand wave migration directions, b) sand wave speeds and c) the sand wave characteristics such as wavelength and wave height.

The future bathymetries and corresponding bed level changes have been estimated by artificial shifting of the mobile seabed components of the most recent 2016 bathymetry. In order to account for the variability of the migration speed and migration direction, 9 different combinations of 3 migration directions and 3 migration speeds have been considered. Hereby upper and lower bound future seabed level estimates have been obtained. DNV GL has reviewed this method and has found that the method can be used to determine the long term bathymetrical changes.

In order to account for a) survey, b) megaripples and c) spatial resolution uncertainty, 0.5 m upward and 0.4 m downward bands have been added to the uncertainty. DNV GL has reviewed these uncertainty bands and found them to be on the safe side.

DNV GL has reviewed and agreed on the following main data provided along with /1/:

- Lowest Seabed Level (LSBL) for time spans of 5 year
- Highest Seabed Level (HSBL) for time spans of 5 year
- Best Estimate Bathymetry (BEB) for time spans of 5 year

Conditions to be considered in other certification phases

This section shall list the conditions that need to be addressed in a different certification phase/module. The phase/module should be clearly stated (see also body text above).

The conditions identified during the technical evaluation are listed in the following. The conditions are assigned to the certification phases in which they need to be considered and evaluated.

The seabed levels within the wind farm area shall be monitored and remedial actions taken before the seabed levels are outside the design upper and lower ranges.

Outstanding issues

There are no outstanding issues.

Conclusion

DNV GL find that the morphology study is complete, carried out according to industry best practice, is plausible, and that

- Best Estimate Bathymetry (BEB)
- Lowest Sea Bed Level (LSBL) for the period 2016-2056
- Highest Sea Bed Level (HSBL) for the period 2016-2056



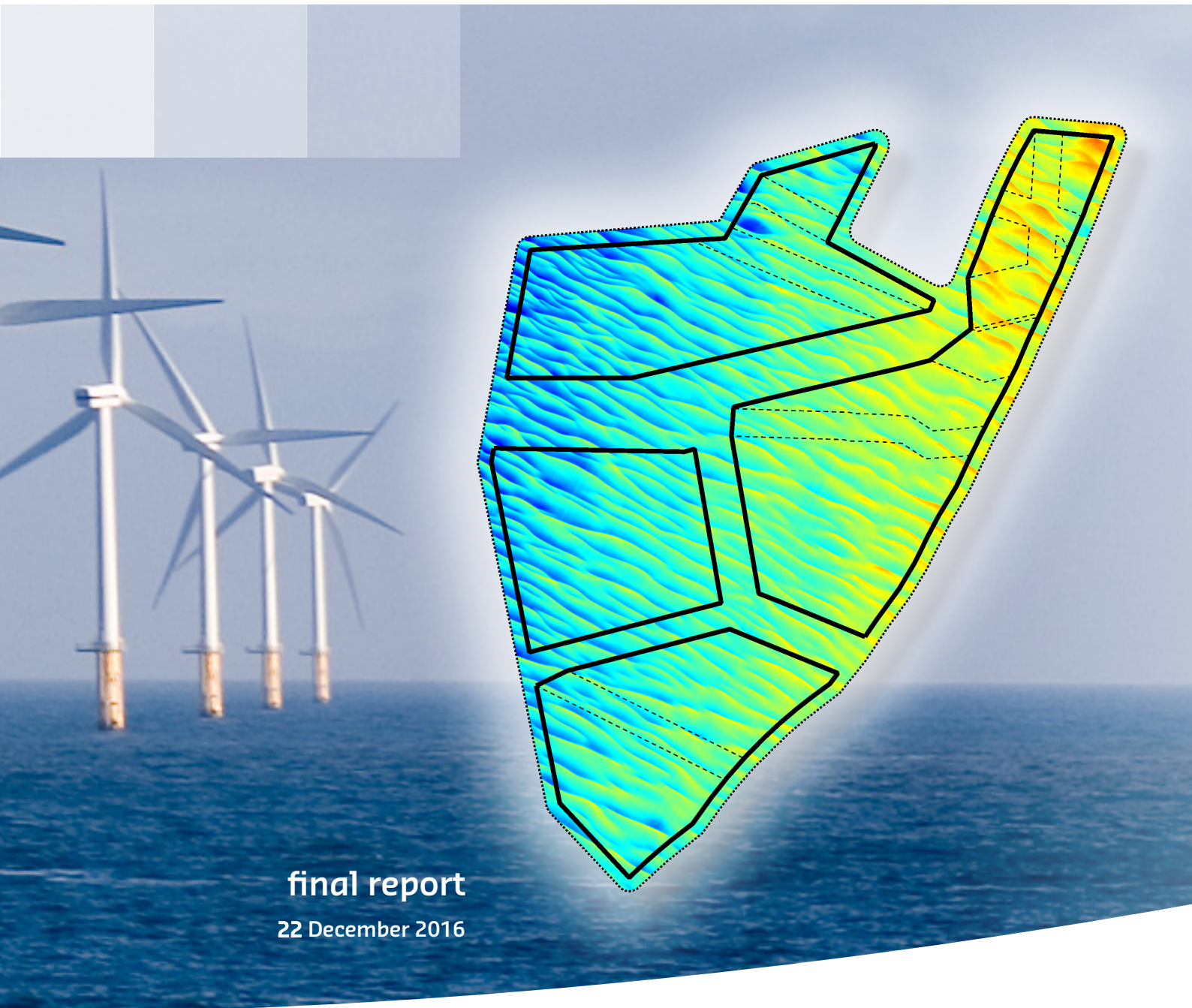
as defined in the documents listed in appendix A are derived in line with the requirements following section 2.3.2 of the DNVGL-SE-0190 and can be used as basis for determining design seabed levels for Hollandse Kust (zuid) Wind Farm Zone.



About DNV GL

Driven by our purpose of safeguarding life, property and the environment, DNV GL enables organizations to advance the safety and sustainability of their business. We provide classification and technical assurance along with software and independent expert advisory services to the maritime, oil and gas, and energy industries. We also provide certification services to customers across a wide range of industries. Operating in more than 100 countries, our 16,000 professionals are dedicated to helping our customers make the world safer, smarter and greener.

Morphodynamics of Hollandse Kust (zuid) Wind Farm Zone



final report

22 December 2016

Morphodynamics of Hollandse Kust (zuid) Wind Farm Zone

Prediction of seabed level changes between 2016 and 2051

Bo Terp Paulsen
Tom Roetert
Tim Raaijmakers
Andrea Forzoni
Roderik Hoekstra
Pim van Steijn

1230851-000

Title

Morphodynamics of Hollandse Kust (zuid) Wind Farm Zone

Client	Project	Reference	Pages
Rijksdienst voor Ondernemend Nederland	1230851-000	1230851-000-HYE-0003	78

Keywords

Seabed morphodynamics, offshore wind, Hollandse Kust (zuid), sand waves, bedform migration

Summary

This report is the result of the morphodynamic analysis of the Hollandse Kust (zuid) Wind Farm Zone (HKZWFZ). The wind farm zone is located off the Dutch coast and is sub-divided into four sites. The morphology in the area is classified as dynamic with significant sand wave migration in the top soil layer. The sand waves are in general oriented perpendicular to the shore and are migrating towards the north-northeast. The underlying bathymetry is considered static at least within the lifetime of the wind farm.

A review of available geological and geophysical data indicate that non-erodible layers exist, but that they are located too deep to influence the sand wave migration. A numerical analysis of the hydrodynamics and sediment transport in the area indicate that the net sediment transport is aligned with the residual tidal flow and towards the north-northeast.

A detailed analysis of the sand wave field is presented for the entire HKZWFZ, as well as for the individual wind farm sites. In total 3904 transects distributed over the wind farm area are analysed. The sand wave migration speeds are determined by a 1D cross-correlation technique and average migration speeds of 0.7 m/year to 3.0 m/year are observed. In general sand waves in the northern part migrate faster than in the southern part and locally migration speeds as high as 5.2 m/year are observed.

A Fourier analysis is applied for determining the spatial characteristics of the sand waves and here wavelengths between 200 and 1000 m and wave heights between 1.1 and 4.0 m are observed. Sand waves are higher and shorter in the western part of the wind farm which is characterised by deeper water depth.

Based on the morphodynamic analysis a best estimate bathymetry (BEB), a lowest seabed level (LSBL) and a highest seabed level (HSBL) are determined. The LSBL and HSBL indicate the lowest and highest seabed levels that are expected during the lifetime of the wind farm (2016-2051). Locally, the maximum seabed lowering that was found for the entire area is -3.6 m and the maximum seabed rising is 7.2 m (the 99% non-exceedance values for lowering and rising are -1.5 m and +4.1 m respectively). Furthermore, the LSBL is compared against both the base of the Holocene formation and identified non-erodible layers. The predicted seabed level changes presented in this study follow from the applied morphological analysis techniques, describing the (uncertainty of the) physics and the natural variability of the analysed morphological system. No additional safety margins for design purposes have been applied.

Copyright © Staat der Nederlanden, 2016. All rights reserved.

The contents of this report were developed by Stichting Deltares, specifically at the request of the Ministry of Economic Affairs. No warranty of any kind, for any particular purpose, is provided or implied with respect to the contents of this report. Use of the information contained in this report is at the sole expense and risk of the person or entity doing so. Deltares disclaims any and all liability for any loss or damage suffered as a result of using the information published in this report.

Title
Morphodynamics of Hollandse Kust (zuid) Wind Farm Zone

Client	Project	Reference	Pages
Rijksdienst voor Ondernemend Nederland	1230851-000	1230851-000-HYE-0003	78

References

Request for Offer, Phase I: *RVO, WOZ1600031, dated 29 July 2016.*

Proposal: *Deltares, 1230851-000-HYE-0001-o-Quotation for Morphodynamical assessment of the Hollandse Kust Zuid Wind Farm Zone, dated 19 August 2016.*

Contract award for Morphological Assessment: *RVO, WOZ1600031, dated 30 August 2016.*

Version	Date	Author	Initials	Review	Initials	Approval	Initials
Draft		Bo Paulsen					
	9 November 2016	Tom Roetert					
Final v1		Tim Raaijmakers		Thaiënne van Dijk			
	13 December 2016	Andrea Forzoni		Dirk Jan Walstra		Klaas Jan Bos	
Final v2		Roderik Hoekstra					
	22 December 2016	Pim van Steijn					

State

final

Contents

Samenvatting (<i>in Dutch</i>)	iii
1 Introduction	1
1.1 Previous studies for the Hollandse Kust (zuid) wind farm zone	2
1.2 Objectives and deliverables	2
1.3 Structure of this report	2
2 Background information	3
2.1 Geodetic parameters	3
2.2 Applied data	3
2.2.1 Seabed surveys	3
2.2.2 Geological data	6
2.3 Generic characterization of morphodynamic seabed features	7
2.3.1 Typical sand wave characteristics	8
2.3.2 Modelling of sand wave processes: growth, decay and migration	8
2.3.3 Variation in sand wave characteristics	10
3 Morphodynamic characterization of the Hollandse Kust (zuid) wind farm zone	13
3.1 Introduction to the area	13
3.2 Description of splitting static and mobile parts of the bathymetries	15
3.3 Large-scale seabed dynamics	17
3.4 Geological and geophysical characterization	19
3.4.1 Methodology and data analysis	19
3.4.2 Quaternary geology	19
3.4.3 Geological units and expected sequence	20
3.4.4 Grain size distribution in uppermost 3 m	23
3.4.5 Summary	27
3.5 Tidal flow and global net-sediment transport	28
3.5.1 Model set-up	28
3.5.2 Model validation	31
3.5.3 Tidal flow and net sediment transport in the wind farm area	32
3.6 Summary of morphodynamics and geology	34
4 Morphodynamic analysis for rhythmic bedforms	35
4.1 Sand wave analysis	35
4.1.1 Sand wave migration direction	35
4.1.2 Sand wave migration speed	38
4.1.3 Sand wave characterization	41
4.1.4 Summary of sand wave analysis	45
4.2 Megaripple analysis	46
4.3 Analysis of storm effects on morphodynamics	50
4.4 Summary	57
5 Prediction of future seabed levels	58
5.1 Sources of uncertainty	58
5.1.1 Survey inaccuracies	59
5.1.2 Megaripples	59

5.1.3	Finite spatial resolution	59
5.1.4	Assumption of shape retaining sand waves	60
5.1.5	Summary of the uncertainty band	60
5.2	Future bathymetries and bed level changes for the period 2016-2051	60
5.3	Best Estimate Bathymetry (BEB)	62
5.4	Lowest SeaBed Level (LSBL)	63
5.5	Highest SeaBed Level (HSBL)	66
5.6	Classification zones for offshore foundations and cables	68
6	Conclusions and considerations	72
6.1	Conclusions	72
6.2	Considerations for cables and foundations in HKZWFZ	73
6.2.1	Cables	73
6.2.2	Foundations	74
6.2.3	Identification of potential risks related to morphodynamic and mobile seabeds	74
	References	76
	Appendices	
A	Description of additional data	A-1

Samenvatting (*in Dutch*)

De Rijksdienst voor Ondernemend Nederland (RVO) heeft Deltares opdracht gegeven om een morfodynamische analyse uit te voeren voor het nieuwe windenergiegebied Hollandse Kust (zuid) (HKZWFZ = Hollandse Kust (zuid) Wind Farm Zone) voor de kust van de provincie Zuid Holland. Het gehele gebied bestaat uit 4 kavels en beslaat een oppervlak van ca. 356 km².

Het doel van de morfodynamische analyse is om de verschillende bodemvormen in kaart te brengen en de mogelijke bodemveranderingen in de periode 2016 – 2051 te kwantificeren, zowel in opwaartse als neerwaartse richting. Met deze resultaten kunnen de windparkontwikkelaars vervolgens de ondersteuningsconstructies en kabeltracés ontwerpen.

De morfologie van HKZWFZ kan worden gekarakteriseerd als dynamisch met significante zandgolf-migratie in de bovenste bodemlaag. De zandgolven staan over het algemeen loodrecht op de kust en migreren in noord-noordoostelijke richting. De onderliggende bathymetrie wordt beschouwd als statisch (tenminste gedurende de levensduur van het windpark).

Een analyse van de beschikbare geologische en geofysische data wijst op de aanwezigheid van een niet-erodeerbare laag, welke echter te diep ligt om de zandgolf-migratie te beïnvloeden. Een numerieke analyse van de hydrodynamica en sediment transport in het gebied geeft aan dat het netto sediment transport in lijn is met de residuele getijdestroming en gericht naar het noord-noordoosten.

Een gedetailleerde analyse van het zandgolfveld is gepresenteerd voor het HKZWFZ, alsmede voor de individuele kavels. In totaal zijn er 3904 transecten verdeeld over het windenergiegebied geanalyseerd. De zandgolf-migratiesnelheden zijn bepaald aan de hand van een 1D kruiscorrelatie techniek en gemiddelde migratiesnelheden van 0.7 tot 3.0 m/jaar zijn geobserveerd. Over het algemeen migreren de zandgolven in het noordelijke gedeelte van HKZWFZ sneller dan in het zuidelijke gedeelte en lokaal zijn migratiesnelheden van 5.2 m/jaar geobserveerd. Vervolgens is een Fourier analyse toegepast om de ruimtelijke karakteristieken van de zandgolven te bepalen. In het HKZWFZ zijn er golflengtes tussen de 200 en 1000 m en golfhoogtes tussen de 1.1 en 4.0 m geobserveerd. Zandgolven zijn hoger en korter in het westelijke gedeelte van het windenergiegebied, dat wordt gekenmerkt door grotere waterdieptes.

Op basis van de morfodynamische analyse zijn een Best Estimate Bathymetry (BEB), een Lowest SeaBed Level (LSBL) en een Highest SeaBed Level (HSBL) bepaald. De LSBL en HSBL duiden de laagste en hoogste bodemniveaus aan welke verwacht worden gedurende de levensduur van het windenergiegebied (2016 – 2051). Lokaal kunnen er veranderingen in het bodemniveau variërend van -3.6 tot 7.2 m optreden (de 99%-overschrijdingswaarden voor bodemdaling en –stijging zijn respectievelijk -1.5 en +4.1 m). Als extra kwaliteitscontrole is het LSBL vergeleken met de basis van de Holocene formatie en de top van de niet-erodeerbare laag. Beide vergelijkingen leerden dat er geen onrealistische waarden voor de bodemdaling zijn voorspeld in deze studie.

De voorspelde veranderingen in de bodemniveaus volgen uit de toegepaste, state-of-the-art analysemethoden en zijn gebaseerd op de beschikbare bodemmetingen. Onzekerheden in de (nauwkeurigheid van de) bodemdata, de fysieke processen verantwoordelijk voor de bodemdynamiek en de natuurlijke variatie zijn zo goed mogelijk meegenomen in de onzekerheidsbanden. Er zijn geen additionele veiligheidsfactoren voor ontwerp-toepassingen op de resultaten toegepast.

1 Introduction

In 2013 more than 40 organisations and the Dutch Government entered into the Energy Agreement for Sustainable Growth (Energieakkoord voor Duurzame Groei). An important part of this agreement includes scaling up of offshore wind power development. The Ministry of Economic Affairs presented a road map outlining how the Government plans to achieve its offshore wind goals in accordance with the timeline agreed upon in the Energy Agreement.

The road map sets out a schedule of tenders offering 700 MW of development each year in the period 2015 – 2019. The Dutch Government has developed a systematic framework under which offshore wind farm zones are designated. Any locations outside these wind farm zones are not eligible to receive a permit. Within the designated wind farm zones the government decides the specific sites where wind farms can be constructed using a so-called Wind Farm Site Decision ('Kavelbesluit'). This contains conditions for building and operating a wind farm on a specific site. The Dutch transmission system operator TenneT will be responsible for grid connection.

Winners of the site development tenders will be granted a permit to build a wind farm according to the Offshore Wind Energy Act (Wet Windenergie op zee), a SDE+ grant and offered a grid connection to the main land. The Ministry provides all relevant site data, which can be used for the preparation of bids for these tenders. This morphodynamic study is part of the site data for Hollandse Kust (zuid) Wind Farm Zone (HKZWFZ).

The wind farm is divided in four wind farm sites (WFS): WFS-I, WFS-II, WFS-III and WFS-IV named anti-clockwise starting from the north-western corner as illustrated in Figure 1.1

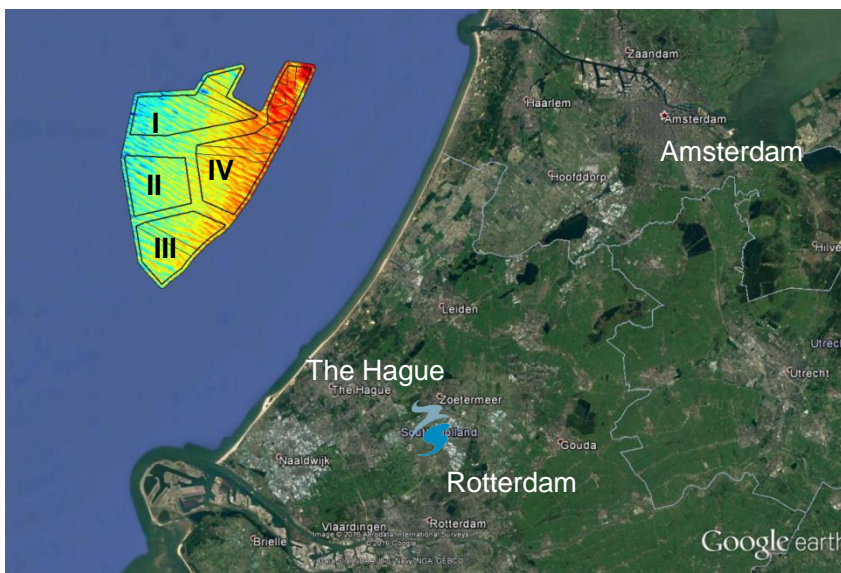


Figure 1.1 Location of the HKZWFZ off the Dutch coast.

1.1 Previous studies for the Hollandse Kust (zuid) wind farm zone

A first quick scan of the HKZWFZ was performed by Deltares (2014b). Herein, a general overview of the area is presented including geology, morphology and hydrodynamics. This study was further extended by Deltares (2015a), where geology and morphology were investigated using data sources that were available at that time. Included in this extended study were also recommendations to RVO for the measuring campaign executed by Fugro (2016).

Based on the measuring campaign by Fugro (2016), this study presents a detailed investigation of the morphodynamics in the HKZWFZ. The analysis is based on both the geological and geophysical investigations by Fugro (2016) as well as historical geophysical information.

Please note that more information about site studies for HKZWFZ is available on:

<http://offshorewind.rvo.nl/studieszh>

1.2 Objectives and deliverables

The objective of this study is to provide RVO and companies tendering for the HKZWFZ with detailed information on the morphodynamics in the wind farm zone. The report contains the following information:

- A detailed description of morphodynamic features in the wind farm zone;
- An analysis of the morphodynamics;
- Extrapolation of historical morphodynamic activities for the estimation of future seabed levels.

To support the morphodynamic analysis, the geological, geophysical and hydrodynamic conditions in the wind farm zone are analysed as part of this report to ensure that all relevant physical processes are taken into account.

The outcomes of this analysis are presented in:

- A concise report presenting the analysis and main results (this document)
- A webinar on 24 January 2017
- A GIS archive with present and predicted future seabed levels.

1.3 Structure of this report

The remainder of this report is organized as follows. First in Chapter 2, background information about this study, applied data sources and seabed morphodynamics in general is given. In Chapter 3, a morphodynamic characterization of the Hollandse Kust (zuid) wind farm zone is presented including a description of the geology in Section 3.4 and the hydrodynamic conditions in Section 3.5.

After the characterisation of the area the morphodynamic analysis is carried out and the results are presented in Chapter 4. The analysis focusses on rhythmic bedforms where sand waves are discussed in Section 4.1, megaripples in Section 4.2 and the influence of a storm event in Section 4.3. Based on the morphodynamic analysis, future seabed levels are predicted for the life time of the wind farm in Chapter 5. Conclusions and considerations are presented in Chapter 6.

2 Background information

In this section background information applied in this study is summarized. First in Section 2.1, the geodetic information is presented. In Section 2.2 the applied seabed surveys (Section 2.2.1) and geological information (Section 2.2.2) is introduced. A general introduction to morphodynamics with a focus on sand wave migration is given in Section 2.3.

2.1 Geodetic parameters

Similar to previous studies by Deltares (2014b, 2015a) and to the survey report by Fugro (2016), all geographical coordinates are based on the ETRS1989 horizontal datum, which is based on the GRS80 ellipsoid, and the UTM-31N projection. Vertical levels are relative to Lowest Astronomical Tide (LAT); see Table 2.1 for the parameters.

Parameter	Value
Horizontal datum	ETRS89 (EUREF89)
Spheroid	GRS 1980
Spatial Reference System Identifier EPSG	4258
Semi-major axis (a)	6378137.00 m
Semi-minor axis (b)	6356752.314 m
Inverse flattening (1/f)	1298.257222101000
Flattening (f)	0.003352810681182
First eccentricity	0.081819191042816
First eccentricity squared (e ²)	0.006694380022901
Second eccentricity (e')	0.082094438151917
Projection	UTM zone 31 North
Latitude of grid origin	0° 00' 00.000"
Longitude of grid origin	3° 00' 00.000"
Grid Easting at grid origin	500000
Grid Northing at grid origin	0.00
Scale factor at longitude of origin	0.9996
Vertical datum	LAT GEONZ97 (Noordzee)

Table 2.1 Geodetic parameters used in this study

2.2 Applied data

2.2.1 Seabed surveys

Existing 'historical' bathymetric data for the project site are available from the Netherlands Hydrographic Office (NLHO), Royal Netherlands Navy. At the HKZWFZ site and its surroundings in total sixteen surveys were conducted between 1984 and 2012. The scientific validation of this survey policy was investigated in (Deltares, 2011). The datasets are summarized in Table 2.2. The 1984-1985 data are digitised fair sheets, with low horizontal precision and low data density, and are therefore not used in the morphodynamic analysis.

None of the surveys summarized in Table 2.2 cover the entire wind farm area, so patched bathymetries were created, see Figure 2.1. Surveys separated by the smallest possible timespan are grouped and, to the extent possible, the entire area is covered.

This process resulted in two bathymetries corresponding to approximately the year 2000 and year 2010. It must be stressed that even though the bathymetries are referred to as “2000” and “2010” the original time stamp, defined as the day halfway through the period in which the specific patch was surveyed, for each patch is retained and applied in the further analysis. Since information cannot be reused each survey is applied only once. That implies that a small area in the south-western corner of the 2010 bathymetry is missing. During the analysis information in this part will be substituted by information from the other bathymetries, so it will not affect the completeness of the study, but the uncertainty may be slightly larger. It is the impression of Deltares that the data used is suitable for the purpose of the study, however data obtained with single beam echo sounders (SBES) may have a larger uncertainty. Finally it should be noted local discontinuities may exist across bathymetry patches, but this has been accounted for in the analysis as described in Chapter 4.

Year	Survey ID NLHO	Survey Method	Data density	Coverage	Used in this study
1984	15534	SBES	Low	Parts of site I and II	No
1984	15514	SBES	Low	Parts of site III & IV	No
1985	15535	SBES	Low	Part of site II	No
1999	4709	SBES	Average	Parts of site I, II, III & IV	Yes
1999	4823	SBES	Average	Part of site II	Yes
2000	4819	SBES	Average	Part of site II	Yes
2001	7305	SBES	Average	Parts of site I & IV	Yes
2007	13789	MBES	High	Parts of site I, II and III	No
2007	13792	MBES	High	Parts of site I & II	No
2009	14508	MBES	High	Part of site III	Yes
2009	15878	MBES	High	Part of site II	Yes
2011	16205	MBES	Excellent	Part of site III	Yes
2011	16206	MBES	Excellent	Sand wave coverage	Yes
2011	16513	MBES	Excellent	Parts of site I, III & IV	Yes
2012	16685	MBES	Excellent	Parts of site I & II	Yes
2012	16687	MBES	Excellent	Parts of site I, II & IV	Yes

Table 2.2 Overview of available surveys from the NLHO. SBES means Single Beam Echo Sounder, MBES means Multi Beam Echo Sounder. Surveys indicated by shaded blue are included in the “2000” bathymetry and surveys indicated by shaded green are included in the “2010” bathymetry.

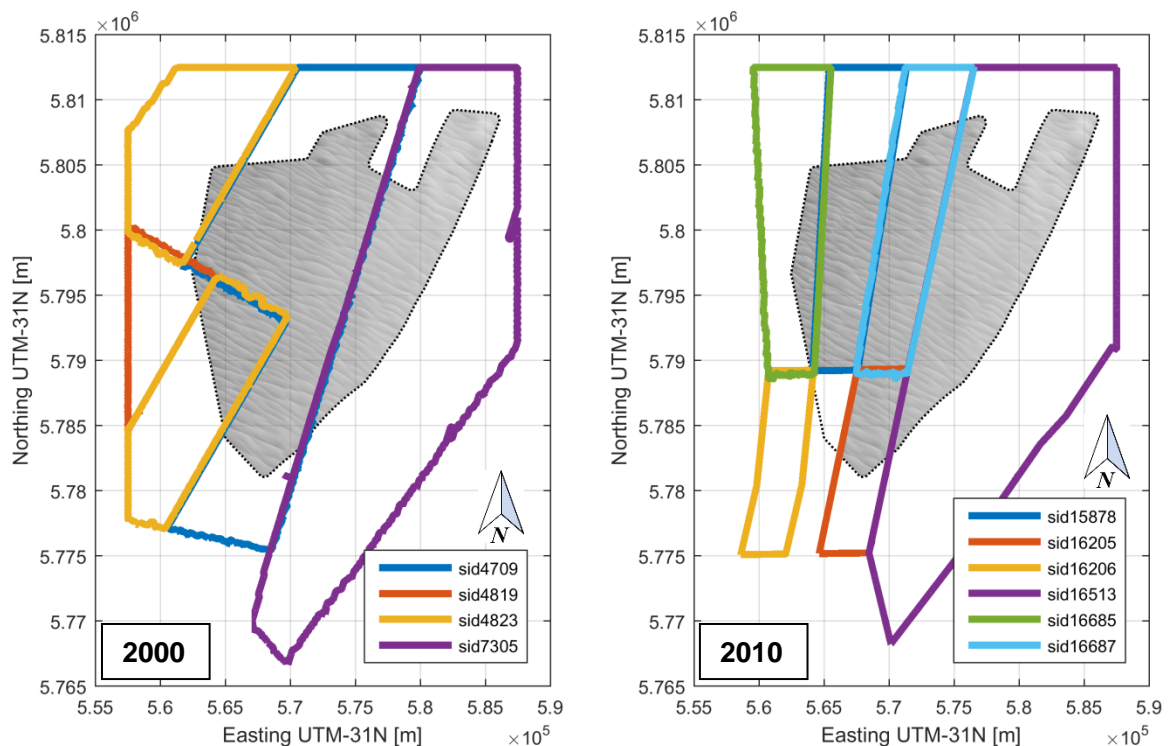


Figure 2.1 Coverage of patches for historical bathymetries. Survey id's (sid) correspond to those shown in Table 2.2.

In addition to the historical data, RVO commissioned Fugro to perform a full bathymetric and geophysical survey of the HKZ wind farm zone. The survey was carried out between 7 March and 18 April 2016 using the survey vessels MV Fugro Pioneer and MV Victor Hensen. The investigation provided bathymetric and shallow seismic data using the following equipment:

1. single- and multibeam survey (SBES/MBES)
2. side scan sonar (SSS)
3. sub-bottom profiler survey (SBP)
4. magnetometer survey (MAG)
5. single- and ultra-high resolution seismic sparker (SCS/UHR)

In this study, the multibeam survey was used to extend the bathymetric time series with an additional high quality dataset in order to compute the expected bed level changes for the period 2016-2051 with greater accuracy. The 2016 bathymetry is plotted in Figure 2.2. The data is available on a 0.5 x 0.5 m grid, but was interpolated to a 5 x 5 m and a 1.0 x 1.0 m grid for the sand wave and megaripple analysis respectively.

Since lithology and compaction of sedimentary layers in the subsurface may affect the erodibility and therefore the rate of seabed morphodynamics, the predicted bed level changes were compared to the sub bottom profile (SBP) data. The predicted bed degradation was compared with the depth contours of the top of a non-erodible layer and the base of the Holocene formations in order to check whether predicted seabed lowering in Section 5.4 would penetrate into the underlying layers. This step was performed to avoid overly conservative results.

Analysing the other Fugro-surveys (e.g. SSS) was not within the scope of this study. This means that, for instance, detected ship wrecks and their influence on local morphodynamics

(e.g. local scour) are not considered in the morphodynamic analysis in this report. Even though not included in this study, it must be stressed the effect of e.g. ship wrecks may significantly change over time and care should be exercised if constructing close to such objects. However, effects will be spatially limited to the vicinity of the structure and normally not more than up to ten times the size of the object.

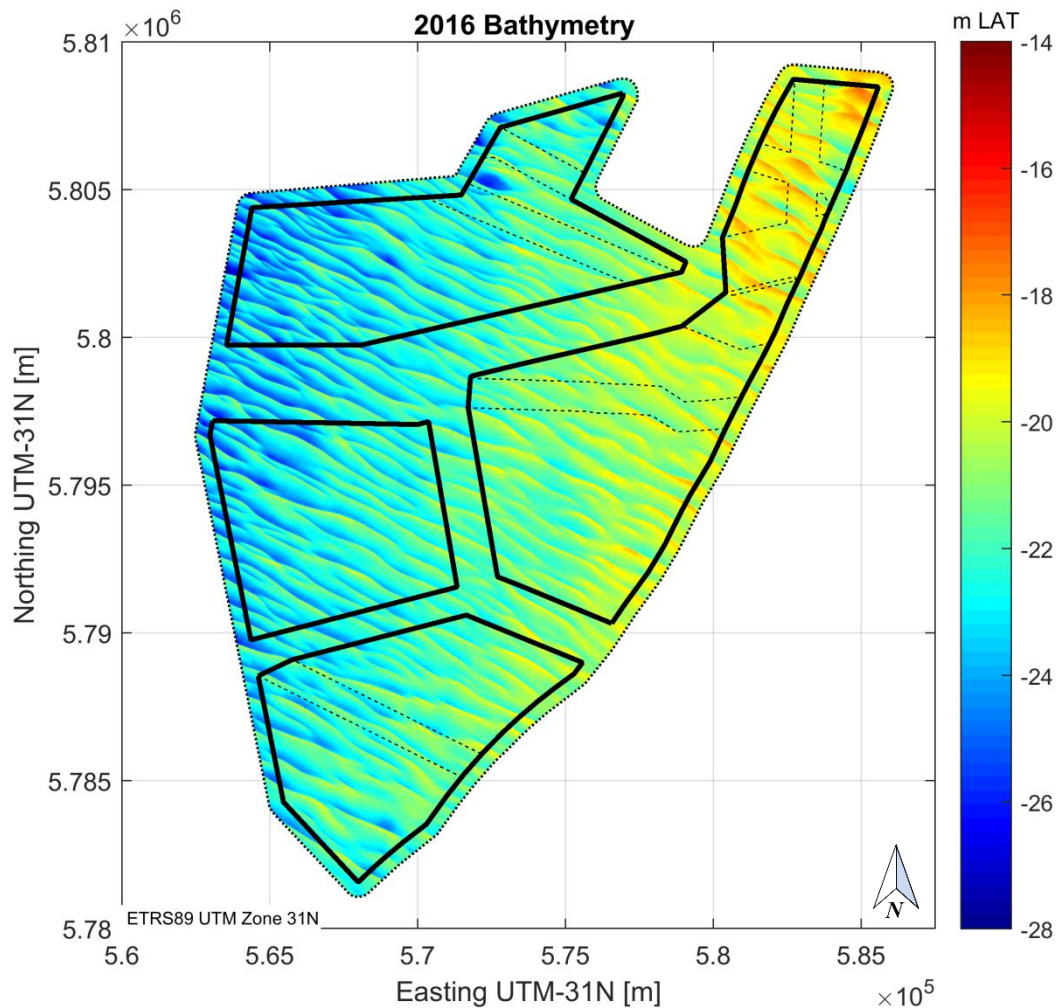


Figure 2.2 Bathymetry of the Hollandse Kust (zuid) wind farm zone: 2016 multibeam data from the geophysical survey by Fugro on behalf of RVO (Fugro, 2016).

2.2.2 Geological data

In order to identify non-erodible layers at the HKZWFZ site, a geological study was performed. Herein, the following data, as provided by Fugro (2016), were used:

- The results from a geotechnical site investigation;
- A geophysical investigation (single- and ultra-high resolution seismic sparker (SCS/UHR));
- A geological model based on both geophysical and geotechnical data.

In addition, 5 boreholes from DINOloket were analysed in order to identify non-erodible layers. DINOloket is the online database of TNO Geological Survey of the Netherlands (www.dinoloket.nl).

The geotechnical investigation included 111 cone penetration tests (CPTs) and 35 geotechnical boreholes. CPT logs provide geotechnical characteristics of the sediments to the penetration depth (e.g. tip resistance and sleeve friction values) allowing for the interpretation of the vertical sediment profile (lithological sequences and associated strata descriptions). The interpreted geological model and associated strata descriptions are based on CPT data using classification methods proposed by Robertson (2009). Geotechnical boreholes provide a detailed description of the lithological and sedimentological characteristics of the subsurface.

The objectives for the geophysical survey, within the context of this report, were to provide a geological interpretation of the subsurface, to produce isopach charts showing the thickness of the main geological formations and to locate any structural complexities or geohazards. The equipment used for the geological investigation consisted of single channel sparker (SCS) and ultra-high resolution multichannel sparker (UHR). The data from this equipment was calibrated on the existing Fugro geotechnical borehole 12-42, located approximately 6 km to the west of the wind farm area.

Based on geophysical and geotechnical data, Fugro built a geological model, described in Fugro (2016), that comprises geological formations and subdivisions in formation members, as interpreted from seismic reflection data, thicknesses of sediment layers, their lateral continuity across the site and the Quaternary lithostratigraphy according to Rijdsdijk et al. (2005).

2.3 Generic characterization of morphodynamic seabed features

Large parts of the sandy seabed of shallow seas, such as the North Sea, are covered with rhythmic bedforms. These features are dynamic and are the result of the complex interaction between hydrodynamics, sediment transport and morphology. Typical parameters of geometry and dynamics that distinguish different types of bedforms (wavelength, wave height and mobility) are presented in Figure 2.3. In the last column, the potential threat to foundations and electricity cables is indicated per bedform.

Ripples are the smallest and fastest migrating seabed features, but because of their limited size they can be disregarded in the analysis. Ripples are, however, relevant for the bed roughness and sediment transport in the area. Megaripples are larger with a height of a few decimetres up to ~1 m. Because of their relatively short wavelength and high migration speed, a turbine foundation will experience many megaripples passing during the lifetime of a wind farm. So, if the sand waves and sand banks would be completely stable (or if sand waves would be non-existent), seabed variations are at least in the order of the height of the megaripples (if present in the area).

Sand waves and sand banks both have dimensions which are significant for foundation design. Where the sand banks often can be considered to be stationary for the lifetime of a wind farm, the sand waves typically migrate fast enough to cause (up to) meters of seabed variation, depending on the location on the sand wave relative to the foundation.

	Wavelength	Wave height	Mobility	Threat to foundations and cables
Ripples	O(0.1) m	O(0.01) m	Mobile and transient	Minimal
Megaripples	O(10) m	O(0.1) m	Mobile and transient	Minimal
Sand waves	O(100) m	O(1) m	Mobile and persistent	Large
Sand banks	O(1000) m	O(10) m	Stationary	Minimal

Figure 2.3 Morphodynamic seabed features in HKZWFZ and some typical characteristics. Capital "O(.)" indicate "In the order of".

2.3.1 Typical sand wave characteristics

As explained in the previous section, sand waves are considered the most threatening seabed feature to offshore structures. Sand waves are normally created due to the tidal flow and may be as large as 25% of the water depth (McCave, 1971), have wavelengths (distance between two successive crests) in the order of hundreds of meters (Ashley, 1990; van Dijk et al., 2005) and may migrate at a speed up to tens of metres per year (van Dijk et al., 2005; Dorst et al., 2009; Van Santen et al., 2011). If sand waves are removed by dredging they may regenerate within a time period of years (Knaapen et al., 2002). In the southern North Sea, sand waves are observed in water depths of 20-40 m, flow velocity amplitudes of around 0.65 m/s and median grain sizes of 0.35 mm (Borsje et al., 2009).

Sand waves may be superimposed by megaripples, which have wavelengths of tens of meters and heights up to 1 m. These megaripples are flow-transverse bed patterns and migrate with a rate of about up to 0.5 m/day (Ashley, 1990).

2.3.2 Modelling of sand wave processes: growth, decay and migration

An early model for offshore sand wave migration was proposed by Deigaard et al. (1986) who presented a calculation model for equilibrium sand waves in an offshore environment. The model was further extended by Staub et al. (1990) to include effects such as non-equilibrium sand waves, generation of ripples and 2D horizontal effects.

Hulscher (1996) showed that sand wave formation can be explained as an inherent instability of the sandy seabed subject to tidal motion. The interaction of the oscillatory tidal current with a bottom perturbation gives rise to a tide-averaged, vertical residual circulation, where net sediment transport is directed from the troughs towards the crests of sand waves (see Figure 2.4). This residual circulation induces a net sediment flux towards the crest of sand waves, which leads to sand wave growth if it overcomes the opposite effect of gravity. The migration of sand waves is caused by an asymmetry in the residual circulation cells, due to tidal asymmetry and residual currents (Németh et al., 2002; Besio et al., 2004).

The model by Hulscher (1996) describes the hydrodynamics by using the three-dimensional shallow water equations. The turbulent stresses are accounted for by combining a constant eddy viscosity with a partial slip condition at the bed and sediment transport is only modelled as bed load transport. Despite the strongly schematized representation of the physical

processes, the occurrence of sand waves in the Southern North Sea was predicted reasonably well (Hulscher et al., 2001). Besio et al. (2006) extended the model proposed by Hulscher (1996) by introducing a depth-dependent eddy viscosity in combination with a no-slip condition at the bed. Moreover, both bed load and suspended load are included in the model, showing an opposite effect on sand wave formation (growth and decay respectively). Comparison of the model outcome with field data showed that the model was able to reproduce the sand wave length at different locations on the Belgium Continental Shelf fairly well (Cherlet et al., 2007).

More recently, successful efforts were undertaken to model even more realistically the physical sand wave processes by applying a numerical shallow water model (Delft3D), in which complex tidal currents, waves, sediment variations (both horizontal and vertical), turbulence and sediment transport (bed load and suspended transport) can be modelled. In Borsje et al. (2013) it was demonstrated that when boundary conditions, grid resolution and boundary conditions are treated carefully and a $k-\epsilon$ -turbulence model was used, even better resemblance of sand waves was achieved compared to the non-linear sand wave stability models; especially sand wave lengths were better reproduced. In Borsje et al. (2014) the same process-based model (Delft3D) was used to demonstrate the influence of suspended sediment transport on the occurrence and (if present) dimensions of sand waves (see next section for more information).

Most of the applications with process-based models are in 2D and for undisturbed seabeds (without the presence of “disturbing” structures, potentially affecting the processes of sand wave growth and migration). One of the first attempts to investigate the effect of a rock berm (e.g. protecting a pipeline or cable) on long-term sand wave stability was performed by Matthieu et al. (2012). It was shown that even relatively small disturbances caused by rock berms can affect the tidally averaged recirculation cells and may modify the sand wave shape locally around the rock berm.

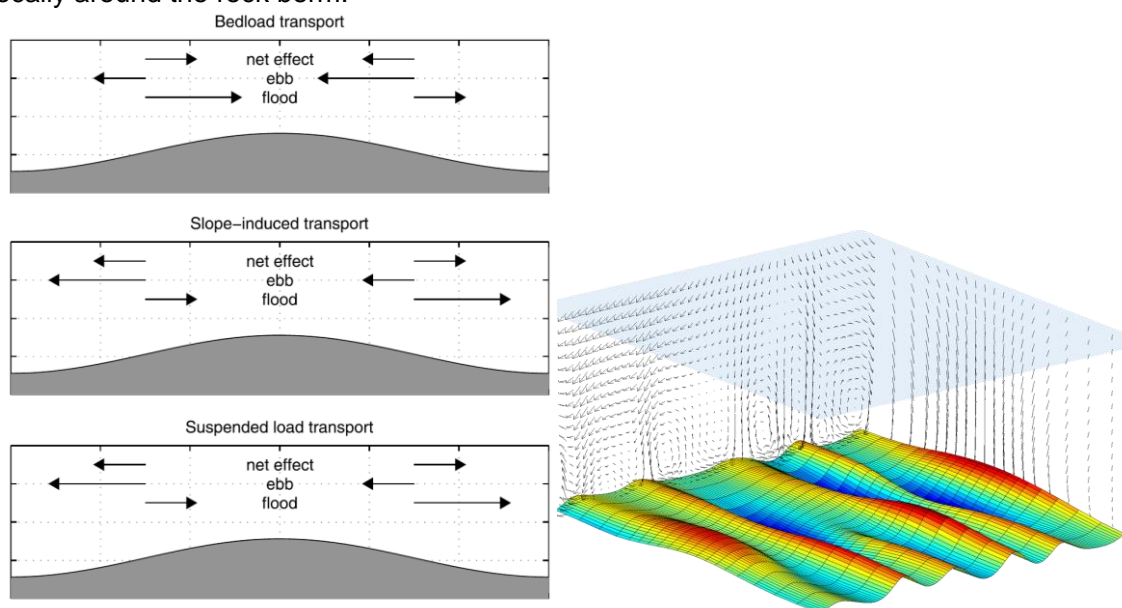


Figure 2.4 Left: Schematic overview of the three dominant processes in sand wave formation: bed load transport (net flux towards the crest: causing sand wave growth), slope-induced transport (causing sand wave decay), and suspended load transport (causing sand wave decay). Distinction is made between the fluxes during the flood and the ebb phase. Fluxes and sand wave dimensions are not to scale (Borsje et al., 2014). Right: 3D impression of tidally-averaged flow pattern around sand wave field (tidal recirculation cells).

Modelling sand waves in a full 3D-model (e.g. right image in Figure 2.4) requires a serious computational effort and is currently not yet feasible for areas as large as HKZWFZ. Also the interaction of structures with 3D sand wave fields is a rather unexplored field of research. Numerical modelling performed in this study therefore focuses on net sediment transport patterns rather than actual sand wave migration (as will be explained in Section 3.5).

2.3.3 Variation in sand wave characteristics

In the Dutch part of the North Sea bathymetric bedforms, such as sand waves, generally remain the same over decades with only limited local changes. Even though, sand wave lengths may change a few to tens of meters between surveys in time. Compared to their wavelengths of hundreds of meters, this change is not influencing the overall pattern. That bed patterns in general remain the same over decades is further discussed in Van Santen et al. (2011). Their Fig. 3.24 displays bathymetric cross sections of offshore sand banks with superimposed sand waves for an area in the southern North Sea. The similarity of patterns for site 3 of the HKZWFZ is shown in Figure 2.5, where the sand wave field from a historical and a recent survey is shown. In the 16 year period between the two surveys the sand waves have migrated in the order of 10 m, but the general sand wave shape is unaltered.

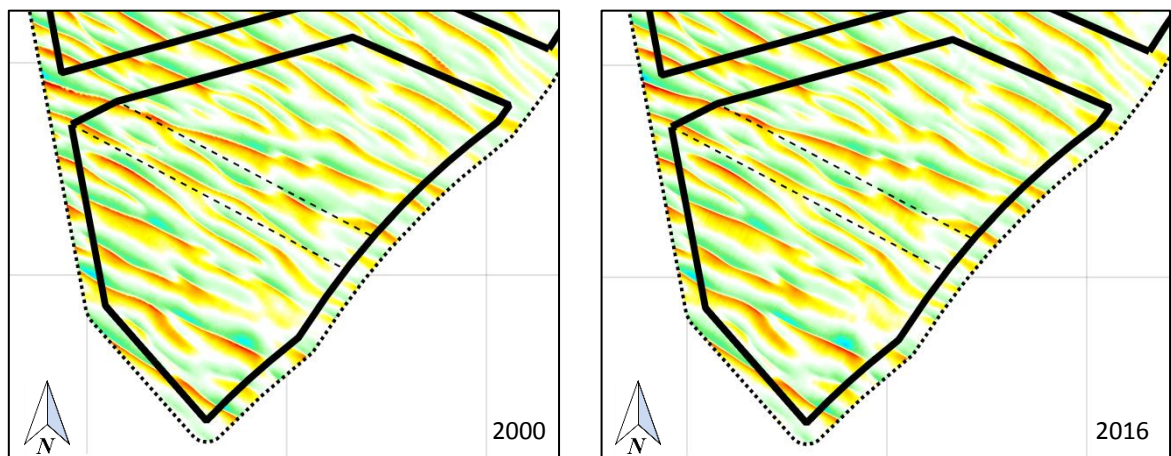


Figure 2.5 Historical and recent sand wave field for site 3 of the Hollandse Kust (zuid) wind farm zone.

Variation of sand wave dimensions

Van Santen et al. (2011) suggested that the spatial variation in sand wave lengths may be related to current velocity, but seems unaffected by water depth and elongation of the tidal ellipse. Borsje et al. (2014) found critical conditions for sand wave formation, which are related to the locally dominant transport mode. As soon as suspended load is the dominant transport mode, sand wave fields are absent. The lower limit of sand wave occurrence is found at a Rouse number of 1.9 (Rouse number is defined as the ratio between sediment settling velocity and shear velocity), which roughly corresponds to a situation in which the grain size is smaller than 0.225 mm and the flow velocity amplitude becomes larger than 0.775 m/s.

Sand wave heights may change following sand wave growth or decay, due to the seasonal variation in environmental parameters (Buijsman et al., 2008a, 2008b) or storms (e.g. Houthuys et al., 1994) and (Sterlini et al., 2009). Differences in height may be short term (yearly or event-related) and long term (decades) and may be in the orders of decimetres to metres.

For sand waves in the tidal inlet Marsdiep (water depths around 24 m below MSL, average wavelength 190 m, average height 3 m), determined from a high temporal resolution time series between 1998 and 2005, Buijsman et al. (2008b) found a seasonal variation in sand wave height, where sand waves were 0.5 m lower in spring compared to autumn.

Variations in growth and decay were also reported at offshore locations, for example offshore Rotterdam at a water depth of 30 m below LAT, some sand waves decreased in height in the period 1999-2002 and then increased in height in the period 2002 – 2007 (e.g. site 1 in Van Santen et al. (2011)). Farther offshore, at the North Hinder Traffic Separation Scheme and at water depths of approximately 33 m below LAT, sand waves with an average wavelength of 270 m and average wave height of 4.8 m were found to grow steadily in height (Van Santen et al., 2011). Here, the crest heights of sand waves increased with roughly 2 m in the period between the early 1990s and 2006.

Variation in sand wave migration

Apart from the spatial variation in dynamic behaviour of sand waves (e.g. van Dijk et al., 2005; Van Dijk et al., 2008) and (Dorst et al., 2011), the migration direction and migration rates of sand waves may vary in time at one location (e.g. Van Santen et al., 2011). The migration direction of sand waves is generally in the direction of the residual current, but may reverse due to higher tidal constituents (Besio et al., 2004) or – in coastal settings – due to advection of sediment and estuarine circulation (Buijsman et al., 2008b).

Migration rates depend on the residual current velocity, but may also be controlled by wave action, both by the stirring of sediment and thereby adding to the sediment transport, increasing migration rates (van Dijk et al., 2005), and by the directions of the waves with respect to the residual tidal current, thereby decreasing migration rates when wave and current directions are opposed (Sterlini et al., 2012).

Sand wave variation due to storms

In general, the morphology of sand waves (lengths, heights, steepness and asymmetry), as well as changes in dynamics (growth, migration) can change in time, e.g. due to seasonal influences and occurrence of storm events (Deltares, unpublished data). The measured bathymetry may therefore depend on when surveys were carried out.

The effect of storms on sand wave characteristics is in general not well established. Few studies report that storms will lower the sand wave heights due to the action of surface waves. Observations before and after a storm were carried out at the Middelkerke Bank on the Belgian Continental Shelf. The area has a water depth of 10 m to 15 m and sand waves with heights of 1 m to 3 m. Houthuys et al. (1994) found that the crests of the sand waves on the top of the bank decreased in height by 0.3 - 1.2 m as an effect of storms with deposition in the adjacent troughs. This indicates that storms may smooth the morphological profile and cause sand wave migration towards the top of the bank. Also, megaripples with heights of 0.2-0.5 m on the north-west flank of the bank disappeared after the storm. However, in some parts, both deep and shallow, the smoothing was not significant. On the other hand, storms may also create bedforms, such as hummocks, which are 3-dimensional bedforms with wavelengths in the order of meters (Passchier et al., 2005; Peters et al., 2012).

Under high surface waves, sediment is stirred up and is transported by the tidal current. van Dijk et al. (2005) show in sensitivity plots that the orbital motion at the bed below surface waves of $H_s=3$ m is sufficient to cause sediment transport at the bed at 25 m water depth for sediment grain sizes of up to 300 μm . Records of significant wave height in the shallow

Southern Bight of the North Sea reveal that surface waves of 3 m occur several times per year, mostly during the winter season. During periods of fair-weather conditions, the height of sand waves may then again increase (Terwindt, 1971; Buijsman et al., 2008a). Therefore, both the magnitude and frequency of storms play a role in the reduction of sand wave heights.

The increased sediment transport due to high surface waves also influences the migration rate of sand waves (van Dijk et al., 2005; Sterlini et al., 2012). Opposing directions of wave propagation and tidal currents may decrease the migration rate. An additional factor affecting the migration rate of sand waves is the wind- and surge-driven current, which increases the sediment transport during storms and causes sedimentation in the waning stage of the storm (Papili et al., 2014).

Current research projects specifically investigate the impact of storms on sand wave geometry and dynamics, both in empirical and modelling approaches (e.g. NWO research project SMARTSEA and SANDBOX). Further it may be noted that as part of the measuring campaign by Fugro (2016) of the HKZWFZ, a transect across the sand wave field was measured before and after a significant storm (see Section 4.3).

In summary, the large-scaled bathymetric patterns remain more or less similar over decades, but (temporary) changes may occur. The changes in length, height, steepness and asymmetry of individual sand waves are variable in both space and time, and may be opposite in subsequent periods between surveys. Net changes of a period of decades may therefore be more steady, because the short-term variations are averaged out. As seasonal changes may occur (mainly related to occurrence of severe storms), they should be sufficiently covered in this study in the adopted methodology and uncertainty ranges.

3 Morphodynamic characterization of the Hollandse Kust (zuid) wind farm zone

The objective of this chapter is to give a general characterization of the morphodynamics of the HKZWFZ which forms the basis of the analysis in Chapter 4. First in Section 3.1, a general introduction to the area is given. In Section 3.2, filtered bathymetries necessary for the further analysis are introduced. In Section 3.3 large-scale seabed variations in the HKZWFZ are presented. Geological and geophysical features in the wind farm zone are presented in Section 3.4, including a map of non-erodible layers in the subsurface and the spatial distribution of grain sizes in the top sediment layers. Tidal flow patterns and net-sediment transport directions are presented in Section 3.5. Observations for the HKZWFZ are summarized in Section 3.6.

3.1 Introduction to the area

The Hollandse Kust (zuid) wind farm zone (HKZWFZ) is located 12 nautical miles (nm) off the coast of the Dutch province Zuid-Holland (South-Holland). However, it is the intention of the government to expand the HKZWFZ two nautical miles on the east side, see Figure 3.1 and Figure 3.2. Bed levels in the area vary from -15.8 to -27.9 m relative to Lowest Astronomical Tide (LAT). The area is divided into 4 main wind farm development sites (WFS): WFS-I, WFS-II, WFS-III and WFS-IV named anti-clockwise starting from the north-western corner (Figure 3.1). The wind farm zone is further divided due to the presence of several operational and abandoned telecom cables and a pipeline.

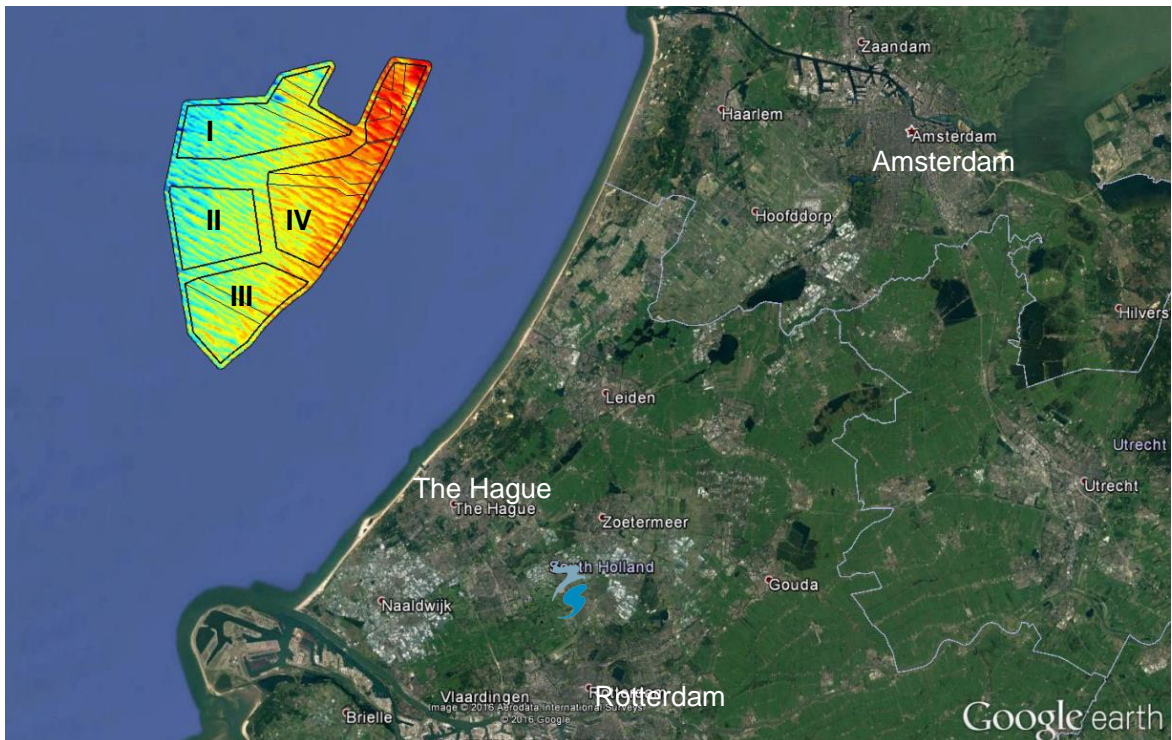


Figure 3.1 Location of the HKZWFZ off the Dutch coast.

The HKZWFZ has a relatively uniform morphology without prominent sand banks (Section 3.3). The area is covered with sand waves migrating towards the north-northeast (Section 4.1). The sand waves are larger towards the west and north and are somewhat smaller towards the east close to the 10 nm boundary.

It may be noted that the wind farm zone is surrounded by the following infrastructure:

- A sand extraction area (north-east side)
- Anchoring area (north)
- Shipping lanes (west)
- Gas exploration (west)
- Gas pipe line (south)

A visual impression of the wind farm zone and its surroundings is presented in Figure 3.2.

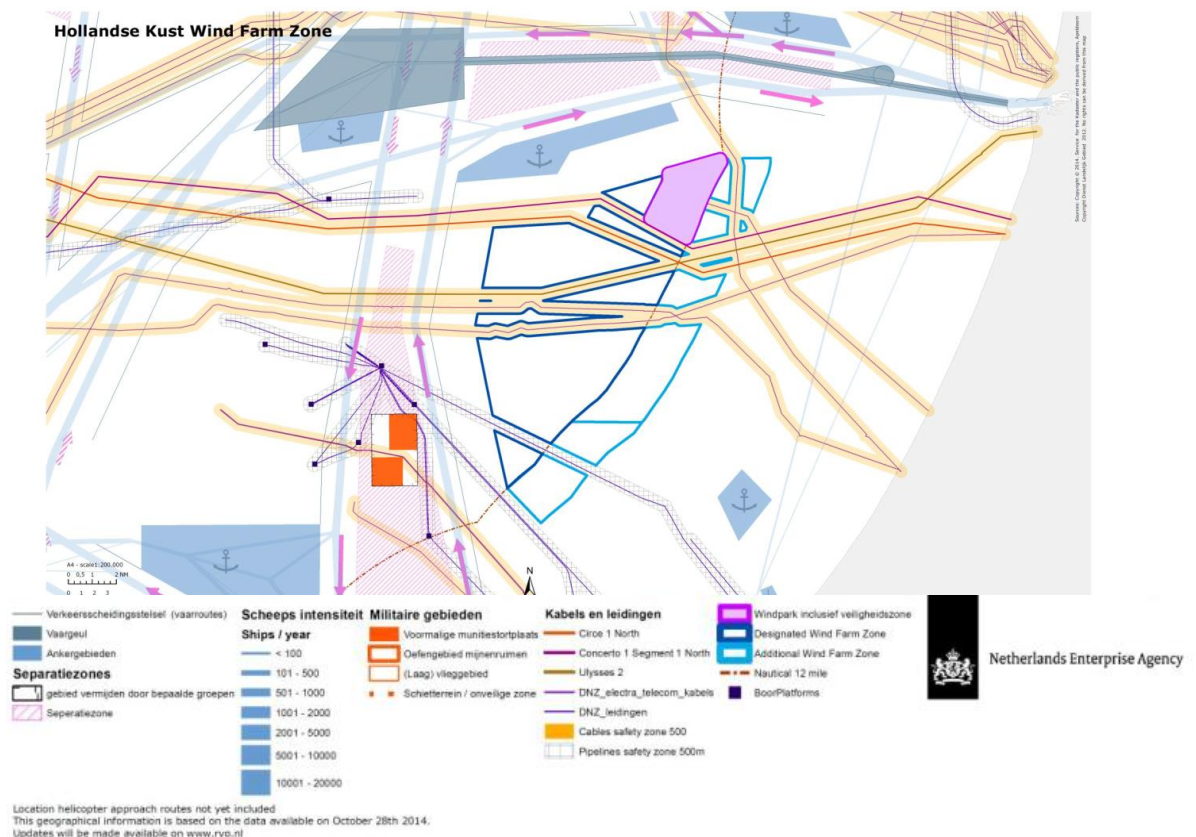


Figure 3.2 Overview of (sub-)site division in the HKZWFZ (blue lines), its intended additional zone (light blue lines) and safety zones related to telecommunication and electricity cables (crossing the area from west to east).

For this study the sand extraction areas (in the north-eastern part of HKZWFZ) are of particular importance, since the dredging activities may influence the seabed morphodynamics in this extraction area. The names of the sand extraction areas are specified in the GIS files supplied by RVO. Figure 3.3 presents the relevant extraction areas in the north-eastern part of HKZWFZ. Based on information by RVO licenses Q10F and Q10R, which allow to dredge up to a maximum depth of 2 m until 31 December 2018 (source: Rijkswaterstaat), are still active and therefore most relevant.

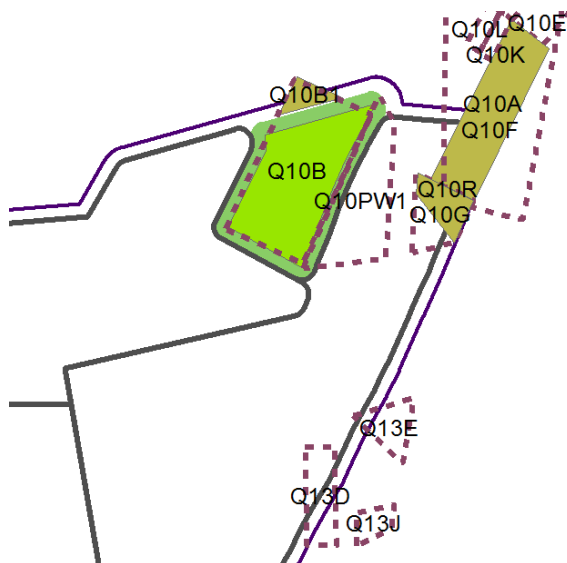


Figure 3.3 Sand extraction zones in the north-eastern part of HKZWFZ; areas “Q10F” and “Q10R” will be operational until December 2018.

In figures presented later in this report the sand mining area is indicated by shaded grey (e.g. Figure 3.5) to indicate that caution should be taken when interpreting the results in this area. In digital deliverables (GIS and xyz data) this area is removed to ensure that data are not wrongly interpreted. It may be noted that the net-sediment transport direction is out of the area towards the northeast (see Section 3.5) and hence the sand mining area is located “downstream” of most of HKZWFZ. That implies that there is limited effect inside the wind farm zone. In any future assessment of the morphology of HKZWFZ it is recommended to start with a new seabed survey after the expiry date of the dredging license and then to proceed with the morphodynamic analysis.

3.2 Description of splitting static and mobile parts of the bathymetries

For the further analysis the migrating part of the bathymetry has to be separated from the underlying, large-scale, static bathymetry. For this purpose a coarse spatial filtering of the bathymetry was applied on the three available surveys. The filter size was chosen such that the mobile bedforms (i.e. sand waves and megaripples) could be removed, while the underlying bathymetry remains unaltered in shape and is not noticeably smoothed by the filtering process. The filtering was carried out with a mean filter with a compact base of 1400 m.

The results for the most recent 2016 bathymetry are presented in Figure 3.4. The top left figure (a) depicts the original unfiltered bathymetry, whereas the filtered “static” bathymetry is shown in the top right corner (b). This bathymetry can be considered a long-term mean bathymetry around which the sand wave elevations fluctuate (analogous to a mean sea level around which the tidal motion and sea waves fluctuate). Throughout this report these bathymetries are referred to as “static”, because this long-term mean bathymetry is considered to remain constant throughout the considered period; see Section 3.3. Please be aware that the term “static” does not mean that the seabed sediment will not become mobile below this level and it is hence *not* a lowest possible seabed level.

Finally, an estimate of the mobile part of the seabed is obtained by subtracting the filtered static bathymetry from the original unfiltered bathymetry. Therewith, the remaining field, i.e. bed levels due to sand waves and megaripples, is expressed around a zero mean. Since the megaripples are much smaller than the sand waves they are not clearly visible in Figure 3.4 (c). This mobile bathymetry is used for the seabed predictions presented in Chapter 5.

To prevent noise in the sand wave analysis, an additional filtering has been carried out to remove the megaripples. Again, a mean filter was used, but with a much smaller base of 15 m, which is sufficient to remove the megaripples, but does not significantly influence the sand waves, which are characterized by much larger length scales.

Similar filtered bathymetries are computed for the two historical bathymetries denoted “2000” and “2010” (see Section 2.2.1), but these are not presented here.

In the remainder of this document we will use the definitions of the various spatial bathymetrical data fields as explained in Table 3.1.

Short name	Description	Long-term mean seabed	Sand waves	Mega-ripples
2016 Bathymetry	Full measured bathymetry by Fugro	√	√	√
Static Bathymetry	Long-term mean bathymetry (for the considered period / lifetime of HKZWFZ)	√	X	X
Mobile Bathymetry	Filtered bathymetry with sand waves and megaripples only	X	√	√
Sand Wave Field	Filtered bathymetry with sand waves only	X	√	X
Megaripple Field	Filtered bathymetry with megaripples only	X	X	√

Table 3.1 Definitions of various bathymetrical data fields used in this study.

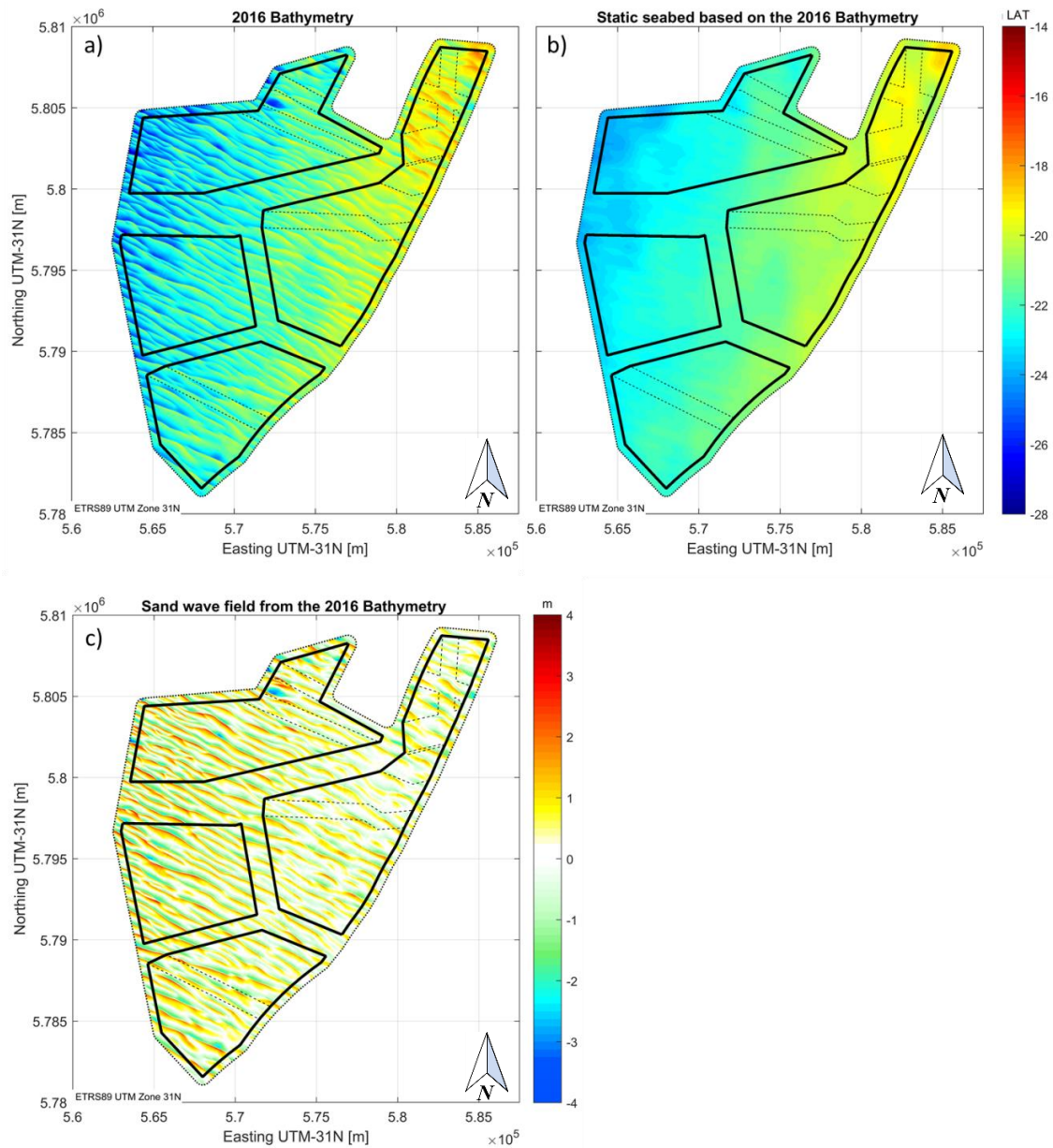


Figure 3.4 Example of bathymetry filtering: a) Original unfiltered bathymetry, b) Filtered Static Bathymetry and c) Mobile Bathymetry obtained by subtracting the Static Bathymetry from the unfiltered bathymetry.

3.3 Large-scale seabed dynamics

In this section the large-scale seabed dynamics of the area are analysed. The analysis is based on temporal difference plots between the different surveys. Large-scale seabed changes associated with overall lowering or rising of (larger parts of) the seabed, can be quantified by computing differences between surveys. Here bathymetrical surveys are interpolated to a common grid and the vertical seabed changes (Δz) are computed per grid point and divided by the time difference between the two surveys (Δt). To ensure that the analysis is not influenced by the dynamic rhythmic bedforms, such as sand waves and megaripples, the spatially filtered Static Bathymetry is applied in the analysis (Section 3.2).

The results are shown in Figure 3.5, where it may be noted that for the patched bathymetries the original time stamp is used for computing the yearly variation. In the figures limited

variations (in the order of cm's per year) can be observed. The limits of the colour bar, ± 0.1 m/year, are chosen to resemble realistic natural variations and not the span of the data. This choice clearly illustrates that vertical seabed variations are limited. The slightly reddish area, indicating a seabed rise in Figure 3.5-a and c, is only observed for the 2000 Bathymetry and seems to be related to the 2001-survey (id 7305, see Table 2.2), adjacent to the 1999-survey (id 4709). It is possible that the observed change is amplified by the two-year difference between the surveys rather than a contrast in seabed change. Another source of uncertainty is the comparison of SBES (2000 Bathymetry) and MBES data (2016 Bathymetry), which may cause an overestimation of the bed level differences. Seabed lowering (bluish) of a few centimetres per year is computed for the central and north-western areas, which is considered to be caused by the survey method instead of a natural process.

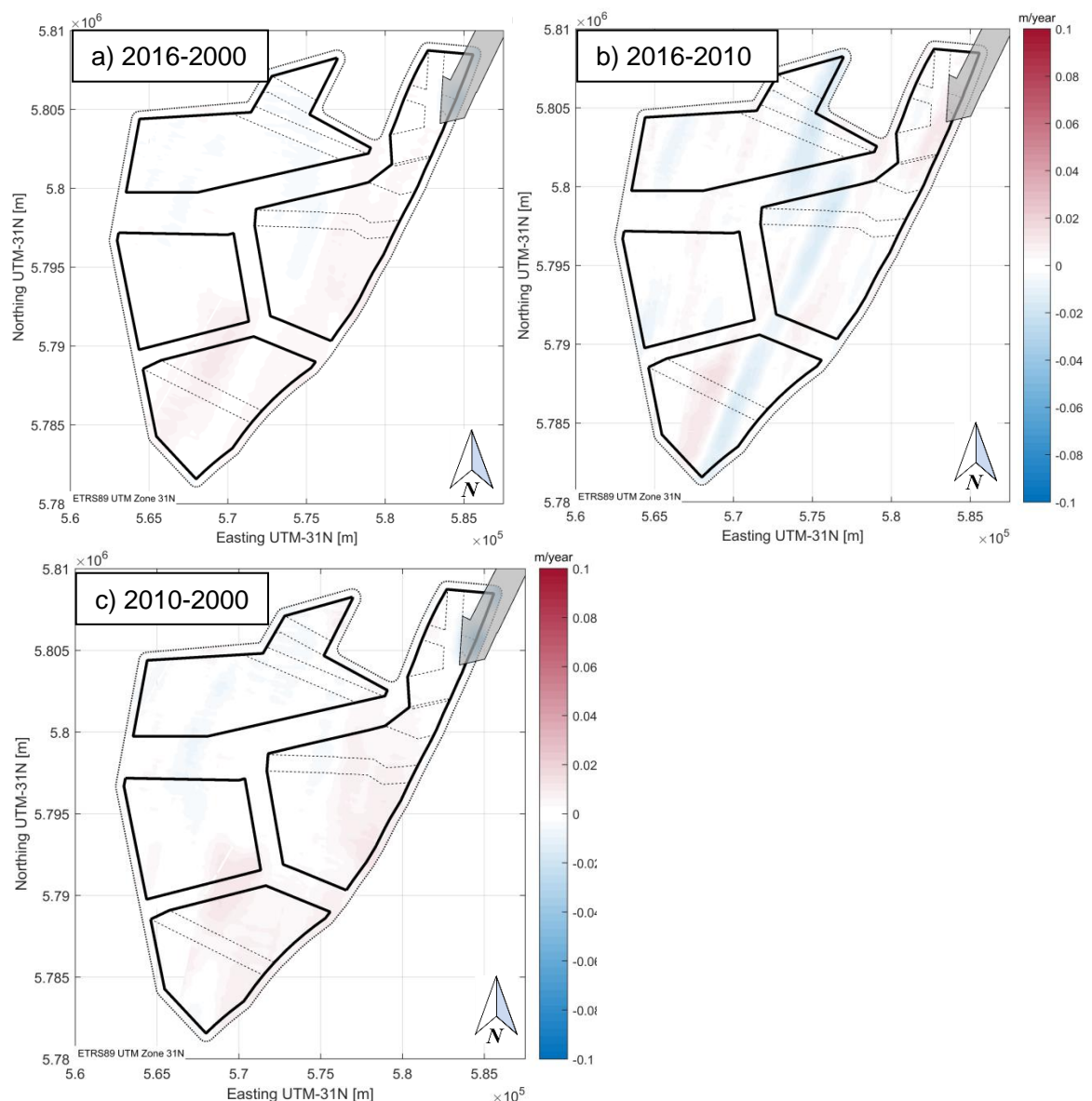


Figure 3.5 Average annual seabed variation observed between available surveys. The greyed out area in the top right corner indicates the sand mining pit. Colours are variations in m/year.

In Figure 3.5-c a seabed lowering is observed in the sand mining area indicated by a grey patch in the top right corner. The lowering is significant, but caused by (almost instantaneous) man-made activities and the computation of yearly average seabed changes is meaningless. For the remaining part of the wind farm zone the changes (white) are insignificant.

The vertical bed level differences of maximum ± 2 cm/year are observed over the considered 16 years period which implies that the large-scale seabed lowering or rising is insignificant and hence the morphodynamic analysis of Chapter 4 will focus on the migrating rhythmic bed-forms, such as sand waves. The earlier assumption (Section 3.2) that the Static Bathymetry, obtained after filtering out the rhythmic bedforms, can indeed be considered static is thus confirmed.

3.4 Geological and geophysical characterization

In this section the geological characteristics of the HKZWFZ are analysed. The goal of the analysis is to establish how the composition of the substrate in the area may affect future seabed level variations. Specifically, the analysis focused on the presence of non-erodible layers within the upper 20 m of the substrate. Non-erodible layers are clay, silt, or peat layers characterized by high stiffness and resistance to erosion.

The analysis is based on data from the recent measurement campaign by Fugro (2016) and sedimentological measurements from DINOloket, see Section 2.2.2. The analysis is limited to parameters relevant for the morphodynamics. This section is organized as follows. First in Section 3.4.1 the methodology and the applied data are summarized. In Section 3.4.2 a general overview of the geomorphological evolution of the area during the Quaternary is given. The geological units are described in Section 3.4.3 including a description of non-erodible layers. In Section 3.4.4 the grain size of the top soil layers is presented, and finally in Section 3.4.5 conclusions and observations are summarized.

3.4.1 Methodology and data analysis

The analysis is based on relevant literature describing the Quaternary geology of the area together with recent grain size analyses from four locations, extracted from DINOloket, that were also included in the analysis. The geological grids were used to calculate the thickness of the different formations and to determine in which formation non-erodible layers occur (see Figure 3.7 and Table 3.2). Non-erodible layers were identified from boreholes (sediment cores) and CPT's. The information on non-erodible layers (depth, thickness) was digitized, visualized and interpolated in ArcGis. Finally, the grain size data from boreholes was used to create sediment size distribution maps of the upper 3 m of the sedimentary package.

Note that a compact natural neighbour data interpolation was used to create surfaces. This allows a clearer visualization of trends and the extrapolation of data to areas without measurements. However, this statistical method is not based on geology. Therefore, the interpolated surface should be interpreted only as an indication of whether a non-erodible layer is present and about its possible depth.

3.4.2 Quaternary geology

Since 1 million years ago, glaciations have altered the landscape of the North Sea. The ice masses shifting on land and sea led to river diversion and sediment rerouting. The changes in ice volume during glacial-interglacial phases led to global changes in sea level, which affected coastline configuration, as well as the location and the type of sediments accumulated.

In the study area, deltaic and fluvial deposits were accumulated during the Lower to Middle Pleistocene (Yarmouth Roads Formation). After the Saalian ice age, a shallow sea covered the area leading to the deposition of marine sands and clays in a shoreface, lagoonal or estuarine environment (Eem Formation). As sea level fell at the onset of the last ice age (Weichselian), brackish marine clays and lagoonal or lacustrine laminated clays were deposited, identified as the Brown Bank Member. During the youngest glacial period, the Weichselian, the Rhine-Maas fluvial system developed throughout the North Sea south of the ice sheet (Busschers et al., 2007). The deposits of this period are wind-blown sands and fluvial channel-fills. These deposits are overlain by shallow marine sand, possibly deposited during the transgression at the end of the Weichselian. Both the lower fluvial and the upper marine deposits are identified as the Kreftenheye Formation.

Since the last glacial maximum, sea level rise induced transgression and led to flooding of the former fluvial systems in the North Sea. The Rhine and Meuse rivers shifted from braiding to meandering systems and their mouth developed to tidal deltas (van Heteren et al., 2008). Most of these deposits were subsequently eroded by waves (Hijma et al., 2009; Hijma et al., 2010). They are preserved as scattered, thin, muddy, lagoonal and tidal flat deposits overlain in most places by sand sheets. In the area of study the surficial sediments consist of shelly, well-sorted marine sands associated with sand waves. These are ascribed to the Southern Bight Formation.

3.4.3 Geological units and expected sequence

Four main lithostratigraphic units are present in the study area: the Southern Bight Formation, the Kreftenheye Formation, the Brownbank Member of the Eem Formation and the Eem Formation. A general description of the geological units and an overview of the typical geological sequence are given in Table 3.2. This description is based on the quick scan report (Deltares, 2015a), on Fugro geotechnical and geophysical data (Fugro, 2016) and on the TNO descriptions in the DINO-database.

The Southern Bight Formation (Bligh Bank Member) represents the surficial sand layers in the entire study area. The unit is generally 4 m thick with a slight increase due to crests of the sand waves (Figure 3.6). The Kreftenheye Formation is characterized by sandy and clayey fluvial deposits. The lowest part of the formation is characterized by channelized deposits formed by fluvial channels which incised into the underlying Brown Bank Member of the Eem Formation and consequently filled in with sand. The Eem Formation is characterized by shallow marine and estuarine deposits. The upper part of the formation is formed by clayey deposits (Brown Bank Member), whereas the lower part is formed by sandy deposits. The Brown Bank Member thickness varies considerably and underlies only parts of the area of study.

Unit	Thickness	Lithology
Southern Bight Formation	3-6 m typically 4 m	Brown-yellow, dense, fine to coarse SAND, with CaCO ₃ , shells and shell fragments (0-20%), sparse clay and silt laminae, locally with gravel.
Kreftenheye Formation	5-25 m typically 10 m	Grey, fine to medium, dense SAND, with gravel (up to 10%), shell fragments, wood fragments, and clay pebbles.
Brown Bank Member	0-13 m	Interbedded firm CLAY, PEAT, SILT and dense SAND.
Eem Formation	8-32 m	Medium dense, fine to coarse SAND with shells, interbedded clay and locally gravel.

Table 3.2 Geological units, thickness and lithological characteristics in the HKZWFZ.

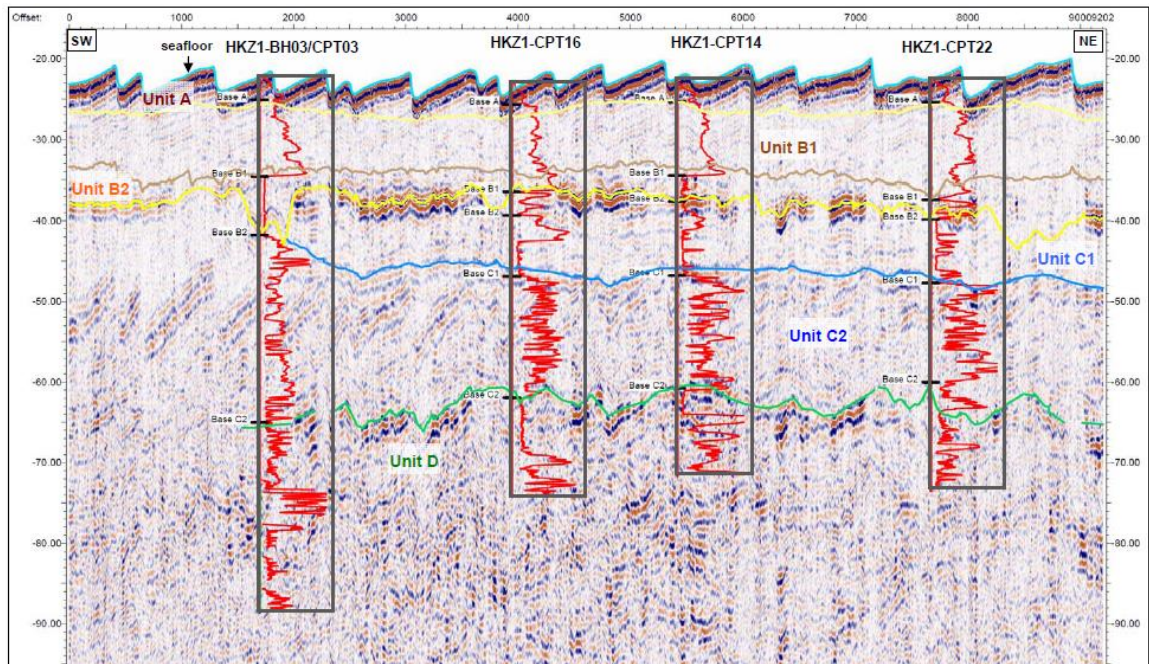


Figure 3.5. Example of interpreted seismic line across the HKZWFZ, taken from Fugro (2016). Vertical scale is depth in metres below LAT. Horizontal scale is distance in metres. CPT cone resistance data (red line) for the geotechnical locations (distance less than 300 m) are projected on the cross section. Unit A = Southern Bight Formation; Unit B1 and B2 = Kreftenheye Formation; Unit C1 = Brownbank Member of the Eem Formation; Unit C2 = Eem Formation.

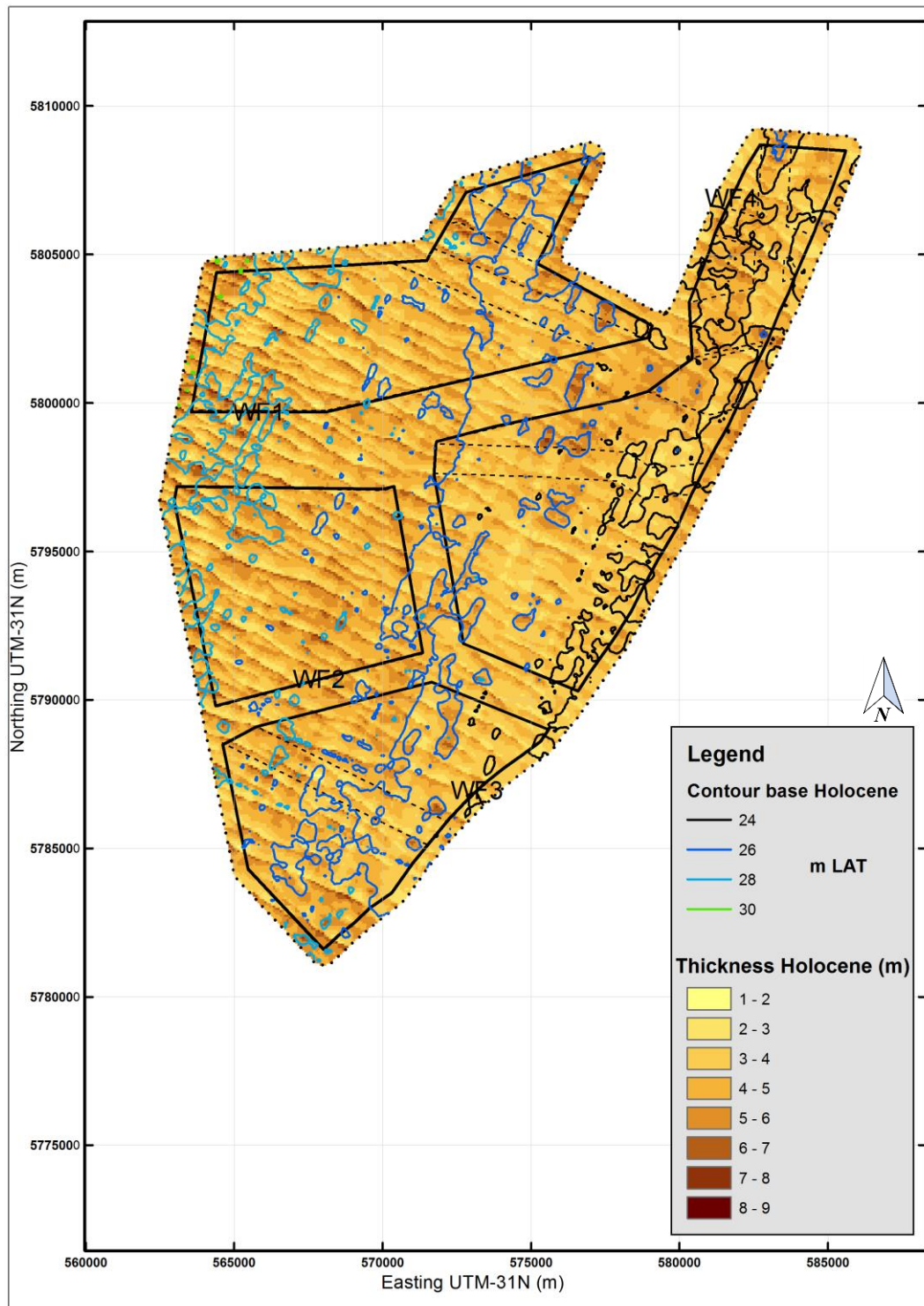


Figure 3.6. Thickness of the Holocene sediments and superimposed contour map of the base of the Holocene. The Holocene deposits are thicker towards the northwest. Maximum values are reached on the crests of sand waves. The base of the Holocene deepens towards the northwest.

3.4.3.1 Occurrence of non-erodible layers

The Southern Bight Formation is presently the uppermost geological layer of the seafloor. It is essentially formed by tide- and wave-induced reworking of fluvial sediments of the Kreftenheye Formation. An exposure of the Kreftenheye Formation at the seafloor is not expected to affect the seafloor morphodynamics. Still, the occurrence of clay, particularly in the lower part of the Formation, gravel layers, sharp changes in sand grain size, and the alternation of sand and clay may alter the seafloor dynamics. The most extensive non-erodible unit is the Brown Bank Member of Late-Pleistocene age. The exposure of this unit at the seafloor would likely result in absence of sand waves. In addition, it could lead to the formation of scour holes when parts of this unit would be eroded, as observed onshore in rivers. Other non-erodible layers also occur in the Eem Formation, even though less extensive and thick.

Non-erodible layers are absent within the uppermost 5 m with the exception of one locality in WFS-IV, where a 1.8 m thick layer of silt is present, see Figure 3.7. Between 5-10 m depth below the seafloor more non-erodible layers (clay and silt) occur within the Kreftenheye formation in the areas WFS-II, WFS-III, and WFS-IV (Table 3.3). These layers have variable thicknesses (from decimetres to meters). Below 10 m depth, non-erodible layers occur within the Kreftenheye Formation, the Brown Bank Member and the Eem Formation.

	upper 5 m	upper 10 m	Formation containing non-erodible layers
WFS-I			Kreftenheye Formation, Brown Bank Member
WFS-II		x	Eem Formation, Kreftenheye Formation
WFS-III		x	Kreftenheye Formation, Eem Formation
WFS-IV	x	x	Kreftenheye Formation, Brown Bank Member

Table 3.3 Details of occurrence of non-erodible layers for the four wind farm sites (WFS)

3.4.4 Grain size distribution in uppermost 3 m

The borehole data from Fugro (sediment cores) indicate an important lateral variability of sediment grain sizes in the area within the first few meters below the seafloor. To illustrate this the grain size distribution is presented for the first three meters below seabed level in intervals of 1 m. The classification of sediment grain size classes adopted in this report is presented in Table 3.4. Based on the sparse borehole data, it is not possible to quantify how much of this variability is caused by seafloor morphology, namely coarser sand in the sand wave's crests and finer sand in the troughs. In the first meter below the seafloor (Figure 3.8) sediment grain size varies from fine to coarse sand. The coarsest sediments (medium to coarse sand) are found in the south (WFS-III) and in two small areas in WFS-II and WFS-IV.

Next, the sediment grain size is described at a specific depth, i.e. at iso-surfaces defined with respect to the average Static Bathymetry, defined in Section 3.2.

At 0-1 m depth sediment size tends to increase southwards (Figure 3.9). In the north the sediment is characterized as fine to medium sand, whereas in the south it is medium to coarse sand, with three maxima in WFS-III, WFS-IV and WFS-I (see Figure 3.9). Between 1 and 3 m depth (Figure 3.10) the sediment grain sizes increase laterally from the northeast towards the southwest. The finest sediments (silts and fine sands) are located in the centre of the wind farm zone in sites WFS-II and WFS-IV, and increase with depth.

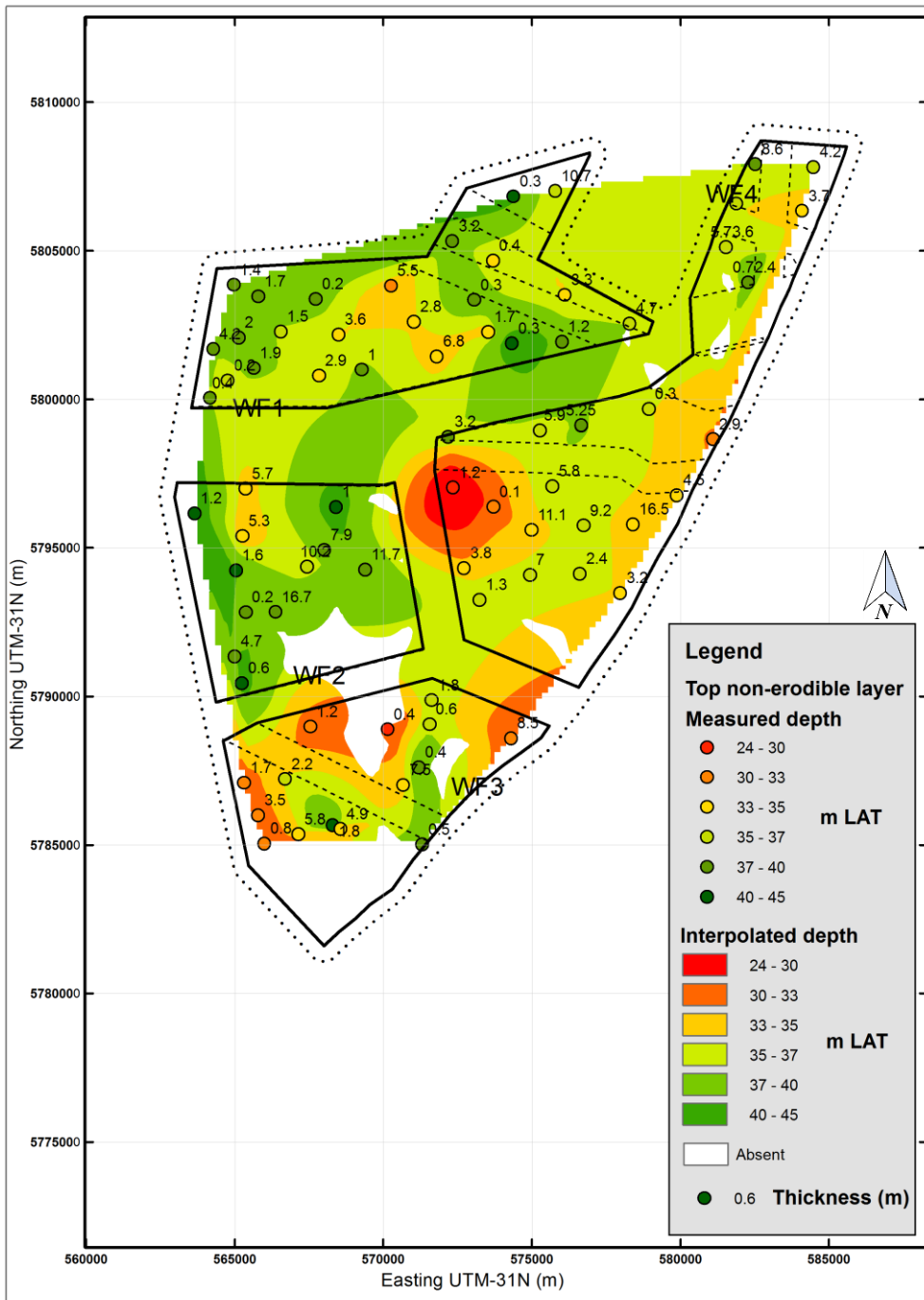


Figure 3.7 Depth of the uppermost non-erodible layer (clay/silt) within the uppermost 20 m of the sedimentary package. The depth of the non-erodible layer is expressed in colours in all observation points (CPTs) and as an interpolated surface (meters depth with respect to LAT). These values represent the non-erodible layer depth in meters, measured from the seabed until the non-erodible layer. The numerical values indicate the thickness of the non-erodible layer.

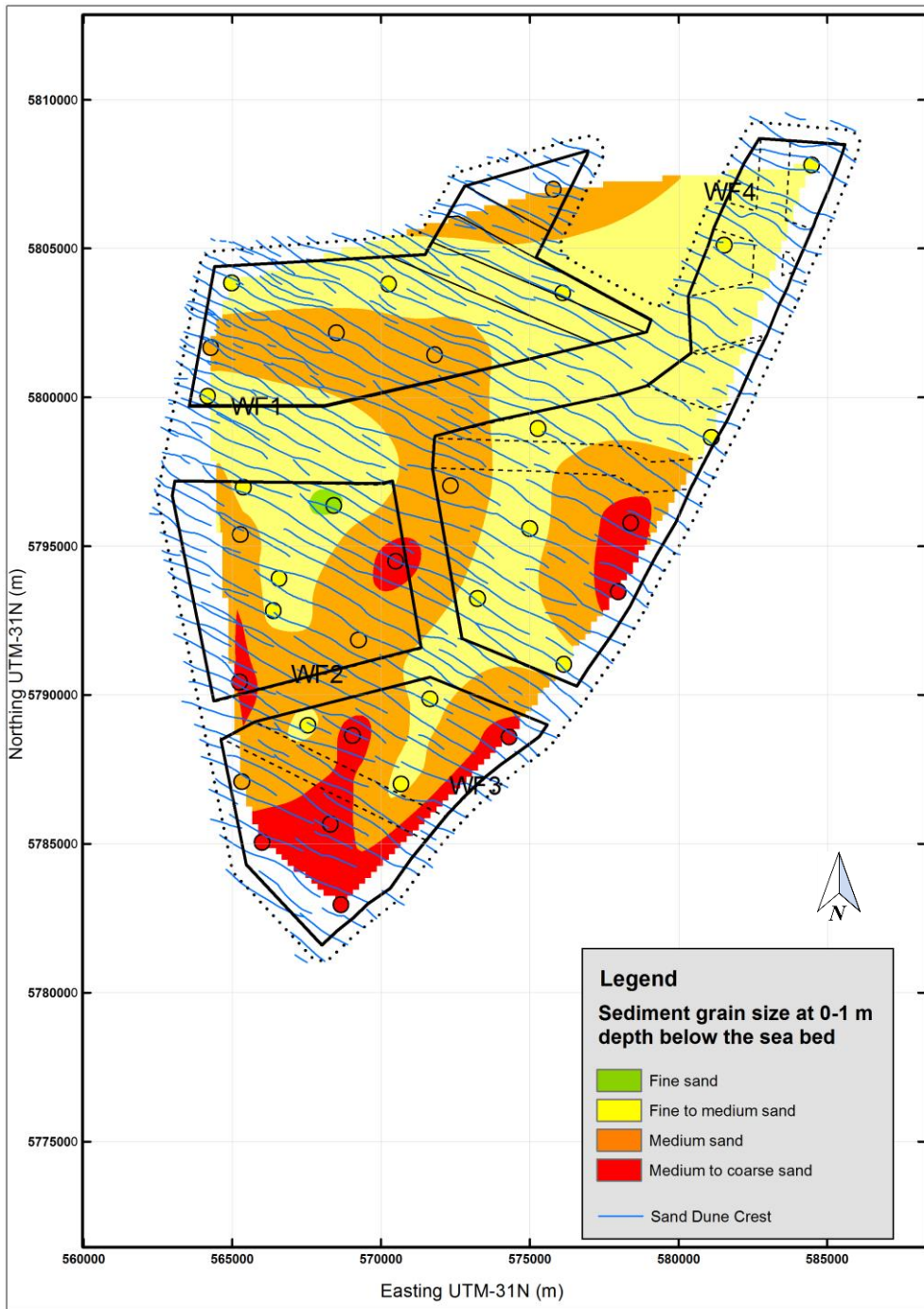


Figure 3.8 Sediment size at 0-1 m depth below the seabed. Note that a compact natural neighbour data interpolation was used to create the interpolated surface. Due to the sparse borehole data and to the morphology of the seabed (crest and troughs), the interpolated surface should be interpreted only as an indication of the sediment grain size.

Sediment grain size class	Sediment particle size (μm)
Silt	4-63
Very fine sand	63-125
Fine sand	125-250
Medium sand	250-500
Coarse sand	500-1000

Table 3.4 Sediment grain size classes and corresponding sediment particle size range

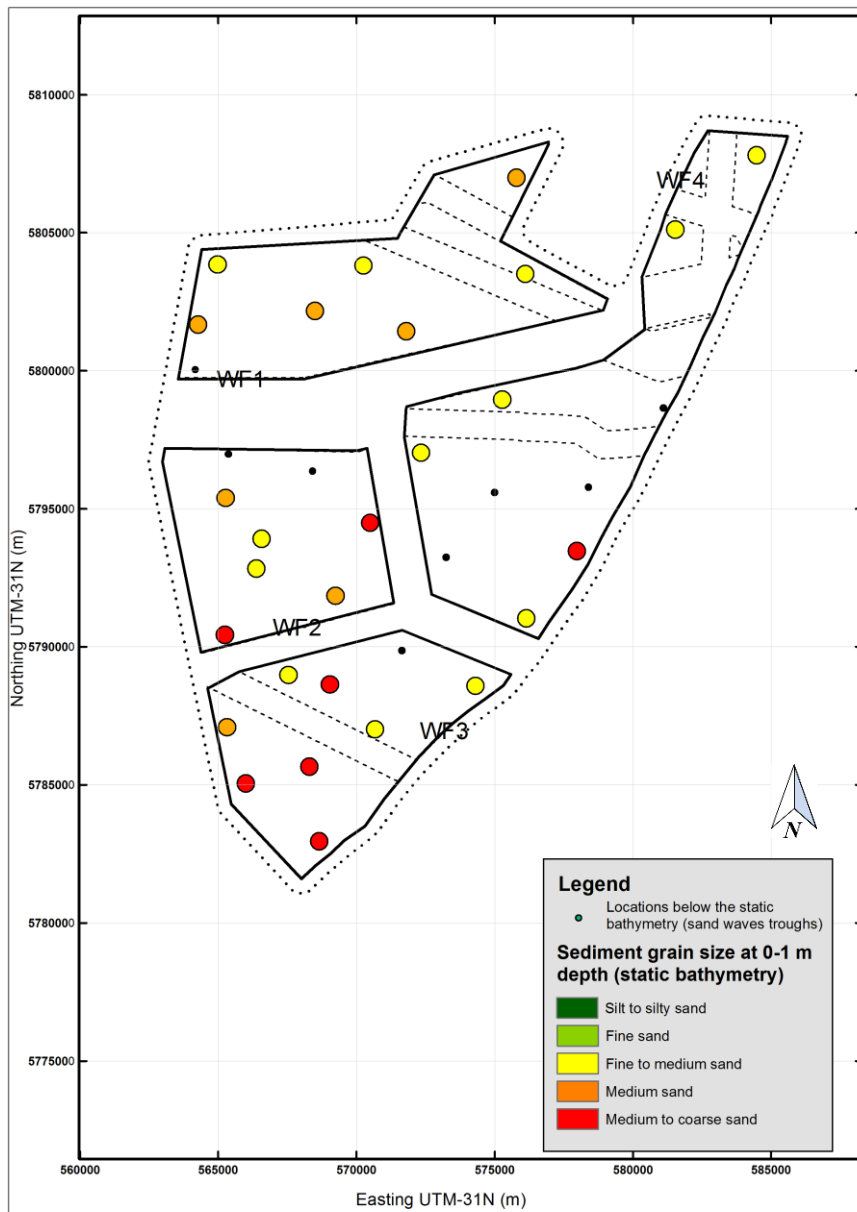


Figure 3.9 Sediment size at 0-1 m depth with respect to the spatially averaged (static) bathymetry. In order to account for seafloor morphology we did the following: where borehole tops were above the Static Bathymetry, we used the value of grain size at the depth corresponding to the Static Bathymetry, ranging from 0 to 1.5 m below the top of the borehole (seafloor). Where borehole tops were more than 0.5 m below the Static Bathymetry, we did not consider these locations.

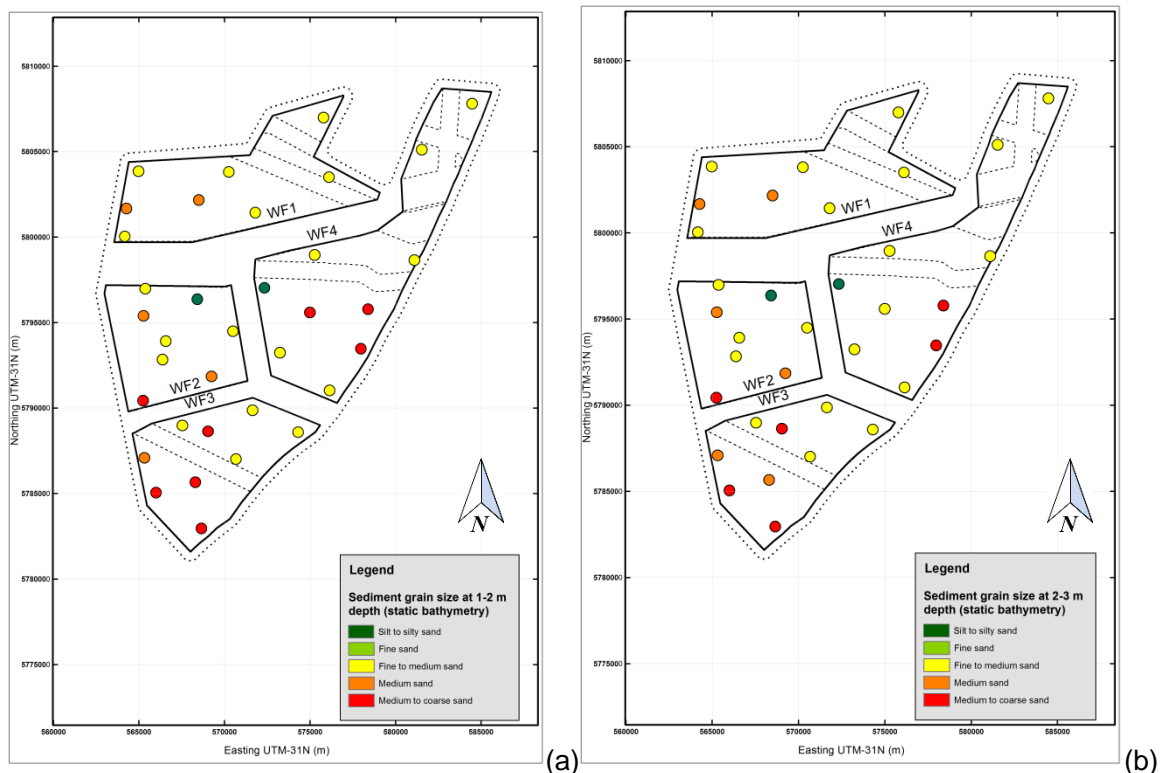


Figure 3.10 Sediment grain size at (a) 1-2 m and (b) 2-3 m depth with respect to the spatially averaged (static) bathymetry surface.

3.4.5 Summary

The subsurface of the HKZWfZ-area is characterized by marine (Holocene Southern Bight Formation) and fluvial-estuarine deposits (Pleistocene formations). Within the upper 20 m of the sedimentary package non-erodible clay and silt layers occur in the Pleistocene formations, typically at depths between 35 and 40 m (LAT). Only in WFS-IV a non-erodible silt layer is present within the upper 5 m below the surface, at 25 m depth (LAT), 1.5 m below the spatially averaged (static) bathymetry .

The sediment grain size varies from fine-medium to medium-coarse sand at the seafloor and within the upper meter below the seafloor. The coarsest sediments (medium to coarse sand) are present in the south (WFS-III) and in two small areas in WFS-II and WFS-IV.

With the Static Bathymetry as a reference, sediment grain size tends to increase laterally from the north towards the south. The finest sediments, below 1 m depth with respect to the Static Bathymetry, are located in the centre of the wind farm zone within WFS-II and WFS-IV.

With the sand wave base at 1 m below the Static Bathymetry these observations imply that:

- 1) Non-erodible layers present in the subsurface are not likely to affect the seafloor morphodynamics because they are too deep to be exposed due to morphodynamic activity including sand wave migration.
- 2) The heterogeneity in sediment grain size at and under the seafloor, however, may affect the geometry (length and height) of the sand waves and the morphodynamic development of the seafloor.

3.5 Tidal flow and global net-sediment transport

Numerical modelling of tidal flow and net-sediment transport was performed to obtain an estimate of the spatial variation of sand wave dimensions and their directions and migration rates over HKZWFZ. These values will be compared to the values determined by the data-driven methods discussed in Chapter 4 to increase the reliability of the results.

It is well established that the net-sediment transport and the tidal flow are good indicators for the morphodynamic activity in the top sediment layer including sand wave migration (Besio et al., 2004). For an offshore area like the HKZWFZ, without significant river outflow or other sources of sediment, the main driver for the net sediment transport is an asymmetry in the oscillating (tidal) flow and related sediment transport (see Section 2.3.2).

To get further insight into the area and the physical processes influencing the morphodynamic activity, numerical computations with combined tidal flow and sediment transport have been carried out. A detailed 2D-horizontal model with accurate bathymetry and high spatial resolution was established to estimate the averaged flow and sediment transport patterns in the area. It may be noted that, even though the computations are carried out on a stationary bathymetry, the sediment transport is explicitly included in the computations to account for the non-linear fluid-sediment interaction.

The section starts with a concise description of the model set-up. Subsequently the computed flow velocities and net sediment transports in the HKZWFZ are presented. The model is carefully validated against recent hydrodynamic measurements from a metocean buoy in the HKZWFZ area. These measurements were carried out by Fugro and presented in a validation report by Deltares (2016a).

3.5.1 Model set-up

The model was set-up in a train of three different model domains, presented in Figure 3.11. The large-scale Dutch Continental Shelf Model (DCSMv6, in blue) was used to derive boundary conditions for two smaller-scale domains Holland Coast model (red) and HKZ model (black) respectively. The three models are working to the required level of detail to model the hydro- and sediment dynamics in the HKZWFZ. It may be noted that due to the very high spatial resolution of the model the computational grid is not visible in the figure. The DCSM model is property of Rijkswaterstaat and runs in operational mode to provide boundary conditions for detailed model applications in the North Sea area and around the Great Britain island. It is extensively calibrated, mainly against water levels measurements carried out in the North Sea. More information on the set-up and calibration of the DCSM model can be found in Zijl et al. (2013).

The DCSM model provides boundary conditions in the form of water levels and flow velocities for the Holland Coast model domain presented in red in the right panel of Figure 3.11. These boundaries are generated by a hindcast simulation of three months (June till August 2016) using astronomic boundary conditions in combination with meteorological data. The Holland Coast model is connected to the shore and runs from Den Helder (in the north) to Hoek van Holland (in the south). The resolution is a factor 5 higher relative to the DCSM model; see Table 3.5. On the northern and southern boundaries, the Holland Coast model is forced with velocities from the DCSM model. The western offshore boundary is forced with water levels.

The most detailed HKZ model domain is coupled to the Holland Coast model and has a factor 5 higher resolution resulting in a resolution of ~50 m, which allows for a fair representation of the shape of the sand waves in the area.

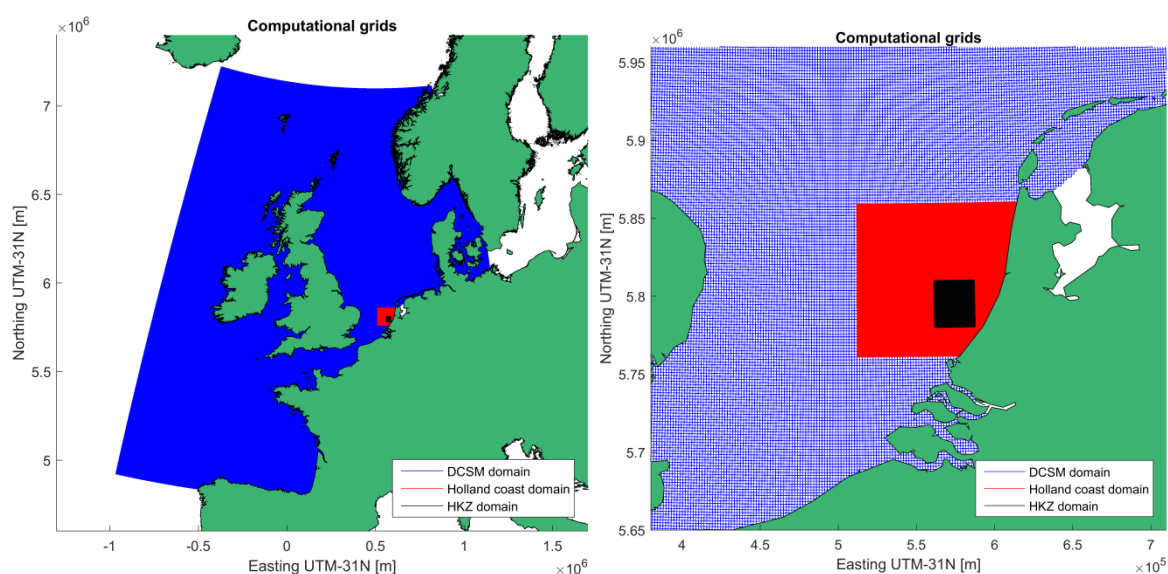


Figure 3.11 Map view of the three model domains: Dutch Continental Shelf Model (DCSMv6, in blue), Holland Coast model (in red), HKZWFZ model (in black).

Figure 3.12 presents the bathymetry schematization of the HKZ model, using the 2016 Bathymetry data collected by Fugro (2016), interpolated to a 5 by 5 m grid, and outside the wind farm area supplemented with historical survey data collected by NLHO according to hydrographic standards (IHO, 1988). The bathymetry data was available on a 5 by 5 m grid resolution, but has been down-sampled to facilitate the interpolation process on the computational grid. The depth in the HKZ area (marked by the outer black polyline) ranges from approximately -15.8 m below LAT in the northeast corner to -27.9 m below LAT in the most westerly part. The sand waves in the HKZ area are clearly reflected in the model bathymetry, with a typical wavelength of several hundreds of meters and having average crest orientations from west-northwest to east-southeast. The green pits to the east of the HKZWFZ, are designated sand mining pits which have been excavated in the past. In Figure 3.12 one of these areas is indicated with a blue arrow.

Table 3.5 summarizes the most relevant characteristics of the three model domains introduced in this section.

	DCSM (in blue)	Holland Coast model (in red)	HKZWFZ model (in black)
Model type	Curvilinear equidistant	Curvilinear equidistant	Curvilinear equidistant
Spatial coverage	2300 by 1700 km	100 by 100 km	26 by 30 km
Resolution	1.8 to 1.8 km	0.27 by 0.27 km	53 by 53 m
Source of bathymetry	NOOS & ETOPO2	DSCM depth file and survey data NLHO	Fugro data and survey data NLHO
Forcing boundary conditions	Astronomic boundary conditions with 38 tidal constituents	Boundary conditions derived from DCSM model	Online coupled to Holland Coast model
Calibration/verification	Calibrated mainly on water levels	Water levels and currents validated against Fugro measurements	Water levels and currents validated against Fugro measurements

Table 3.5 Model domain properties including approximate values for the spatial coverage and grid resolution.

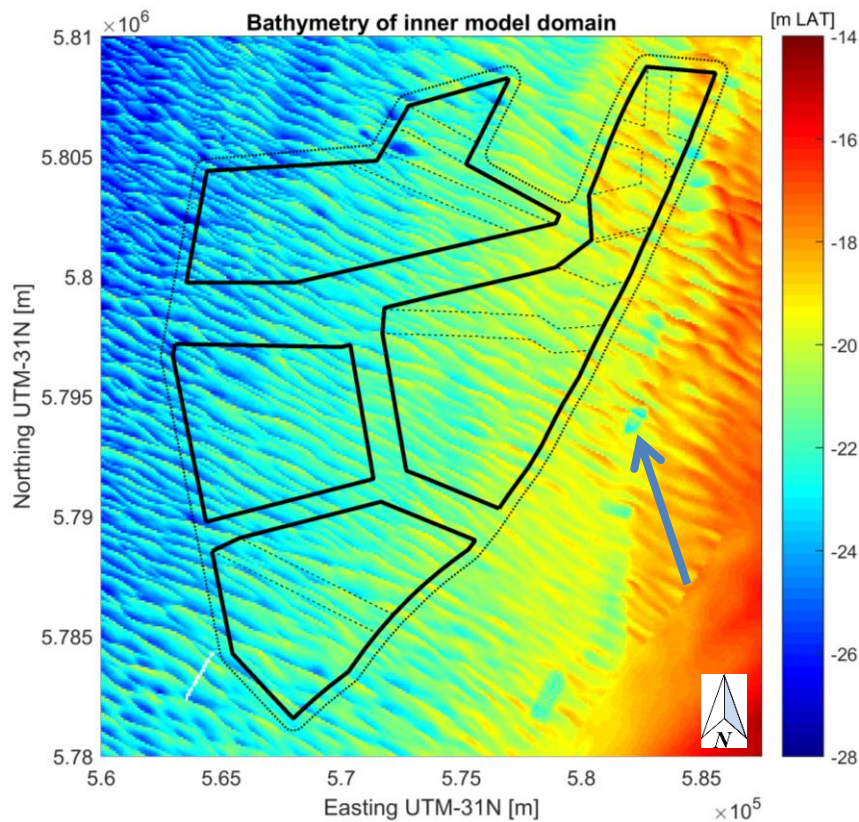


Figure 3.12 Bathymetry used for the HKZ model domain (black outline in Figure 3.11)

The model is set up in depth-averaged (2D-horizontal) mode, which means that the computational grid is not discretised in the vertical. The aim of this study is to get further insight into the net sediment transport (the sum of suspended load and bed load) which is correlated to morphodynamic activity including sand wave migration. Since the sand wave migration in the offshore of the North Sea is mainly driven by the tide, a 2D approach is justified. The net sediment transport rate is derived by time averaging the sediment transport over several spring-neap tidal cycles, since the spring-neap cycle is the most dominant feature in the variation of the hydrodynamics relevant for sand wave migration.

The sediment transport module of Delft3D (Delft3D - SED) has been applied to compute to sediment transport. This module has an online coupling to the Delft3D – FLOW module which means that sediment transport is computed for every computational timestep of the simulation. The default settings have been applied in the sediment transport computation, which can be found in the Delft3D - FLOW manual Deltares (2014a). The adopted sediment diameter (D_{50}) is defined at 250 μm and has been derived from the data presented in Section 3.4. Sensitivity runs have been performed to verify the influence of different sediment diameter settings on the final results. Varying the sediment diameter turned out not to have a significant influence on the relative spatial sediment transport patterns and are therefore not further discussed.

3.5.2 Model validation

In this section the numerical model is validated against recent hydrodynamic measurements Deltares (2016a). Currently data is available for the months June and July 2016. The model was run in hind-cast mode for the same period to be able to validate the modelled flow velocities against the measurements.

Figure 3.13 presents the validation of modelled water levels (top panel), depth-averaged flow velocities (middle panel) and flow direction (bottom panel) against the hydrodynamic measurements, for half a spring-neap cycle. As seen in the figure the tidal water levels and flow is fairly well represented by the DCSM model (in blue) and the HKZ model (in red). Although the peak velocities are not consistently matched, the tidal asymmetry is well reflected.

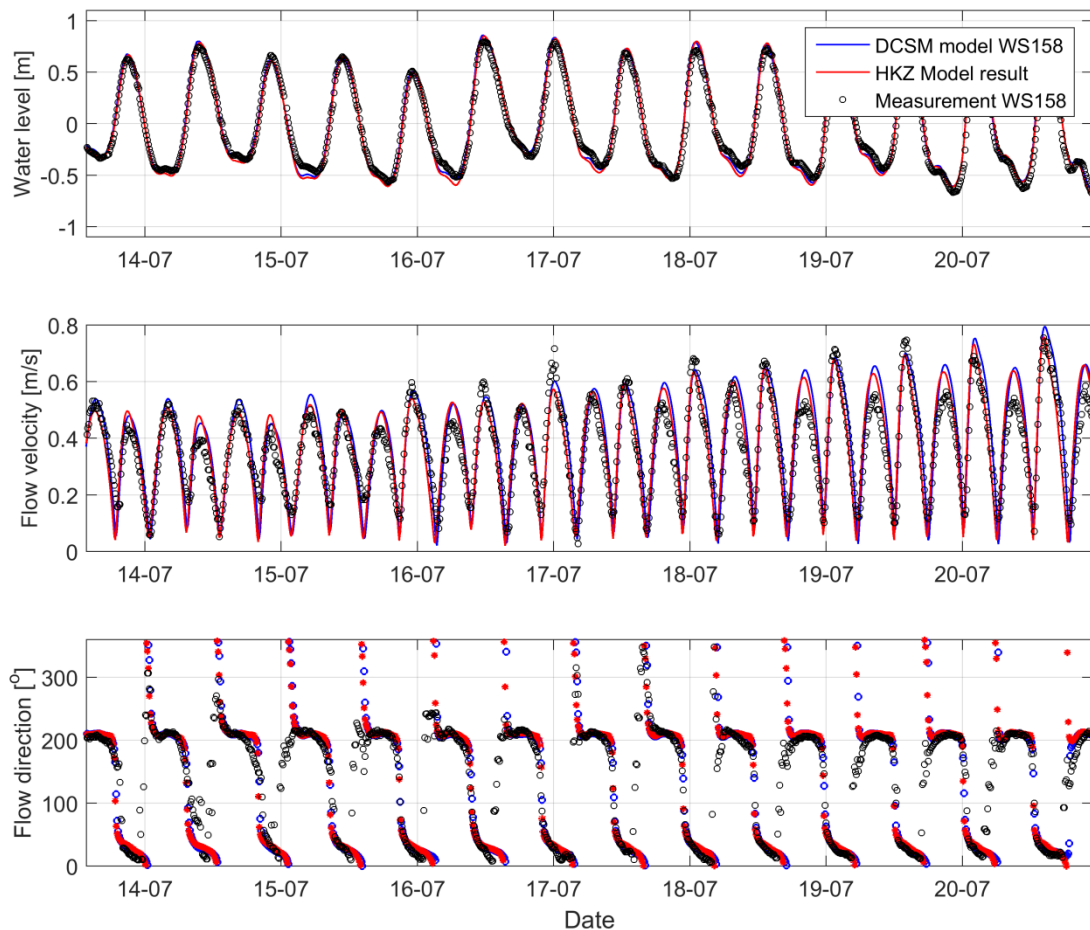


Figure 3.13 Time series plots of measured and modelled water levels (top panel), depth-averaged flow velocity (middle panel) and flow direction (bottom panel).

Figure 3.14 presents scatter plots, reflecting the correlation of modelled and measured water levels (left panel) and the correlation of modelled and measured flow velocities (right panel). The linear correlation coefficient is $r=0.98$ and $r=0.92$ for water levels and flow velocities respectively. In both cases the correlation coefficient is considered high.

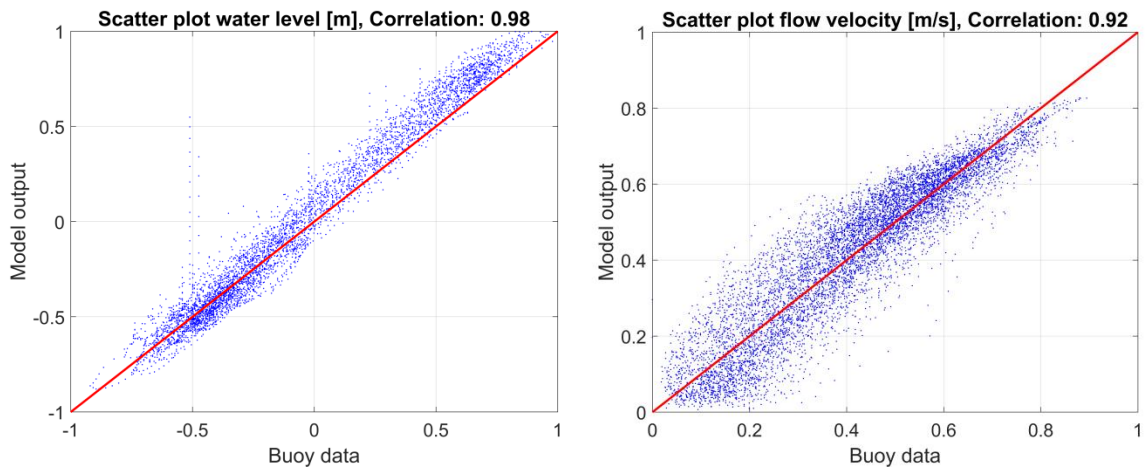


Figure 3.14 Scatter plots presenting the correlation of modelled and measured water levels (left) and flow velocity (right). The red line represents perfect linear correlation $r=1.0$.

3.5.3 Tidal flow and net sediment transport in the wind farm area

Figure 3.15 presents tidal ellipses at several locations in the HKZ domain. These tidal ellipses reflect the modelled tidal current velocities and direction for one tidal cycle on an arbitrary day (23 July 2016). This figure clearly shows a consistent asymmetry in the flow velocities, with higher peak velocities in flood direction (north-northeast) than in the ebb direction (south-southwest).

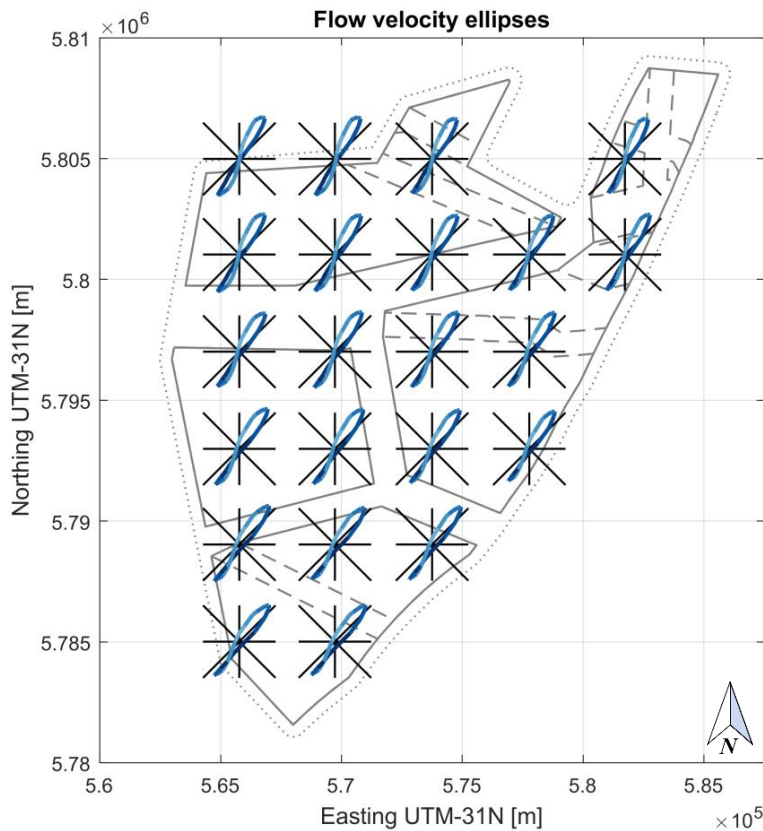


Figure 3.15 Flow velocity magnitude and direction represented in tidal ellipses for one tidal cycle in the simulation period (23 July 2016).

The tide-driven sediment transport is presented in Figure 3.16, in a similar manner as the flow velocities in Figure 3.15. The same asymmetry can be seen, however, it is amplified due to the non-linear relation between flow velocity and sediment transport.

The magnitude of the normalised and filtered net sediment transport in the HKZWFZ is presented in Figure 3.17, for the period 14 June – 26 August 2016. The values in this figure are normalised by dividing all transport values by the maximum net sediment transport. The adopted model approach does not allow for a detailed interpretation of net sediment transport gradients on the sand wave scale. Therefore an averaging filter has been applied to present the results averaged over sand waves. In the figure the arrows indicate the time- and space-averaged direction of the net sediment transport. The relative differences within the area are of particular interest and give insight into the relative rate of sand wave migration. The absolute transport rates have been normalised since the modelled absolute magnitudes cannot be relied upon without a careful validation / calibration, which is beyond the scope of this report. Besides, the absolute values do not have a direct and easy relation with migration rates of sand waves. The absolute value is also of secondary use since the migration speeds are accurately determined using the cross-correlation technique described in Section 4.1.2. It can be observed that the net sediment transport direction is coherent and mainly in north-northeast direction. This trend confirms the results presented earlier in this section for the tidal flow asymmetry. The net transport direction changes over the area from $\sim 43^\circ\text{N}$ in the south to $\sim 20^\circ\text{N}$ in the north. It can also be observed that the net sediment transport magnitude within the HKZWFZ shows a spatial variation, being strongest in the northern part. It should be noted that the areas with the highest net sediment transport seen in the northern part of the wind farm area are correlated with gradients in the underlying bathymetry.

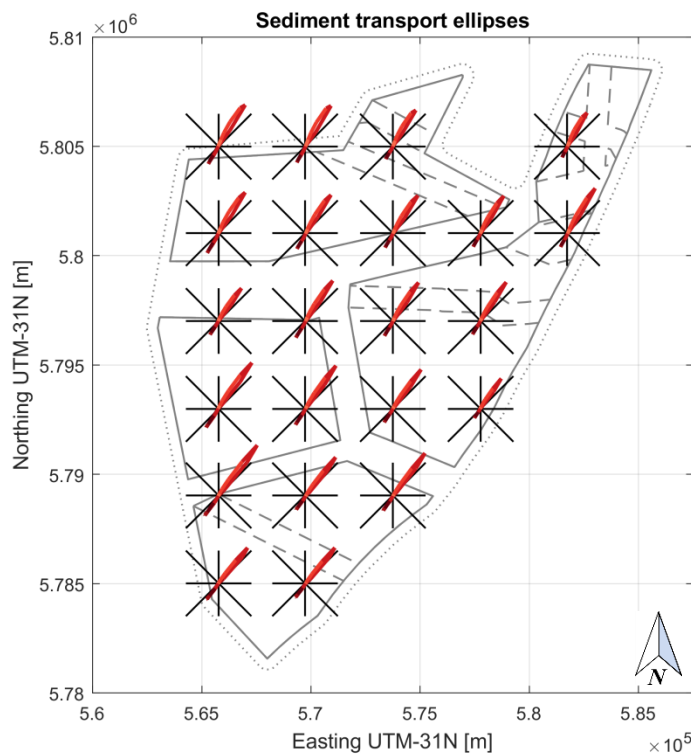


Figure 3.16 Tide-driven sediment transport, represented by tidal ellipses for one tidal cycle in the simulation period (23 July 2016).

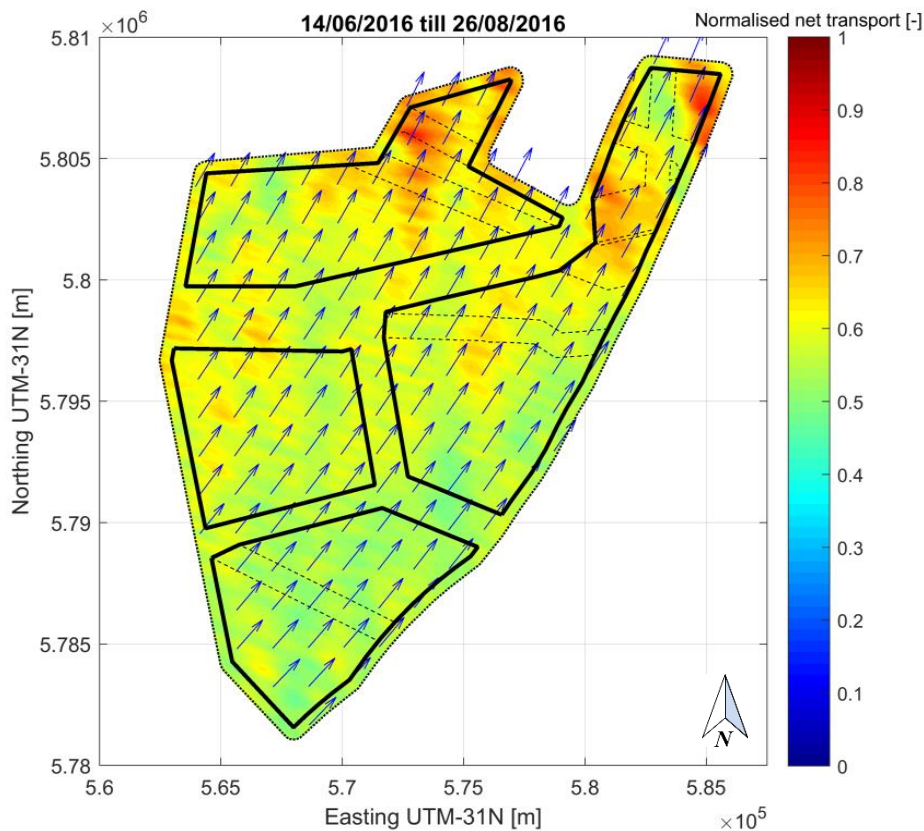


Figure 3.17 Normalised and filtered modelled net sediment transport magnitudes (colour coded) and direction (vectors), derived by averaging the directions and transport rates over 5 spring-neap cycles.

3.6 Summary of morphodynamics and geology

The subsurface of the HKZWFZ-area is characterized by marine (Holocene Southern Bight Formation) and fluvial-estuarine deposits (Pleistocene formations). Within the upper 20 m of the sedimentary package non-erodible clay and silt layers occur in the Pleistocene formations, typically between 35 and 40 m depth (LAT). This is in general well below seabed level and only in WFS-IV a non-erodible silt layer is present approximately 1.5 m below the spatially averaged (static) seafloor. However, this is not expected to influence the sand wave migration.

The sediment grain size varies from fine-medium to medium-coarse sand at the seafloor and within the upper meter below the seafloor. The coarsest sediments (medium to coarse sand) are present in the south (WFS-III) and in two small areas in WFS-II and WFS-IV.

With the sand wave base at 1 m below the Static Bathymetry these observations imply that non-erodible layers present in the subsurface are not likely to affect the seafloor morphodynamics because they are too deep to be exposed due to morphodynamic activity including sand wave migration.

It is concluded that the hydrodynamic model represents the overall flow velocities in the HKZ wind farm area reasonably well, as demonstrated with the validation against recent measurements (Fugro, 2016). A net sediment transport direction towards the north-northeast is observed with a range from 20°N to 43°N and with slightly higher net sediment transport rates towards the northern part of the wind farm zone (about a factor 2 higher).

4 Morphodynamic analysis for rhythmic bedforms

Sand waves are the most dominant seabed feature in the HKZWFZ (Section 3.3) and pose the largest threat (Section 2.3) to offshore foundations and cables if not adequately accounted for in the design. In this chapter a morphodynamic analysis of the rhythmic bedforms in the HKZWFZ is presented. The objective of this chapter is to identify migration speeds and directions which form the basis for the predictions of future seabed levels presented in Chapter 5.

In Section 4.1 a sand wave analysis is performed including a determination of sand wave migration directions, speeds and characteristics such as wavelength and wave height. Statistics about the megaripples are presented in Section 4.2. Furthermore, in Section 4.3 the influence of storms on the Sand Wave Field is analysed. Finally, observations are summarized in Section 4.4.

4.1 Sand wave analysis

The sand wave analysis is based on the historical and recent seabed bathymetries introduced in Section 2.2.1), from which the Mobile Bathymetries were derived (Section 3.2) and consists of the following three steps a) determination of the sand wave migration direction, b) determination of the sand wave migration speed and c) characterization of the sand wave shape.

4.1.1 Sand wave migration direction

Sand waves are in general characterized by a mild sloping stoss side and a steeper lee side oriented in the direction of propagation. Furthermore, sand waves tend to migrate in a direction roughly perpendicular to the crest with a constant form in the direction of the steepest gradient or in the direction of the residual current. In Section 3.5, hydrodynamic computations are presented showing that the net sediment transport direction is in the range from 20°N to 43°N. To further investigate the migration directions a data-driven approach based on the most recent survey is applied in this section.

By differentiating the filtered bathymetry, the direction of the sand wave crest can be estimated. This is illustrated in Figure 4.1, where the direction of the gradient field is shown in the left figure, whereas the magnitude of the gradient along a transect is shown to the right. As seen from the figure, the sand wave crests have significantly larger gradients than the surrounding bathymetry with the direction orientated perpendicular to the crest. The migration direction can hence be estimated by the direction of the steepest gradient. For illustration purpose the number of arrows in Figure 4.1 is down-sampled and hence do not represent the true grid resolution, which also gives a visual effect of diagonal lines. Since the computation of the gradient is sensitive to errors in the bathymetry an additional averaging is carried out along the crest to remove outliers.

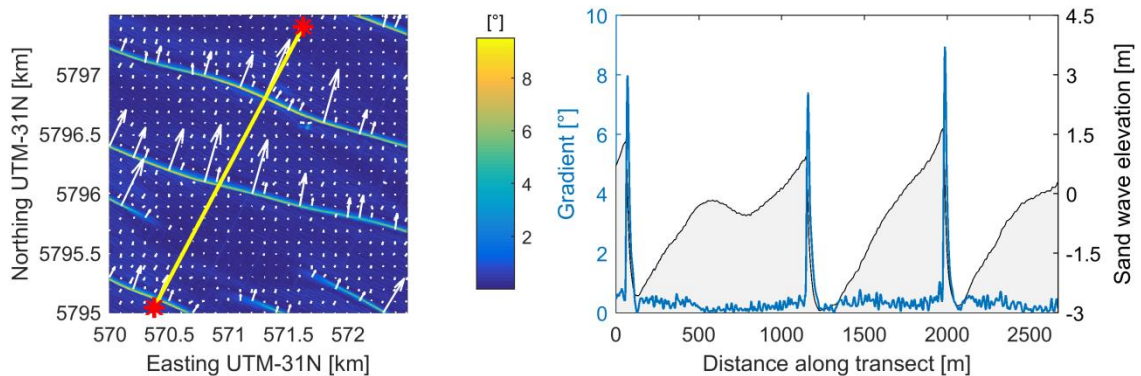


Figure 4.1 Left: Gradient of the Sand Wave Field. Colours and arrows indicate the direction of the point wise gradient. Please note that the number of arrows is down sampled for illustration purposes. Right: The spatial gradient in degrees along the transect indicated in the figure to the left.

Based on the gradient method the sand wave migration direction was estimated for the entire wind farm zone. In Figure 4.2 a map view of the spatially averaged sand wave migration directions is shown. The directions in degrees are relative to the north and defined as “going towards”. A migration direction of $45^{\circ}N$ would thus mean that the sand waves mainly migrate towards the north-east. As seen from the figure, the sand waves are generally propagating towards the north-northeast with a slightly more eastwards direction in the western part of the wind farm zone (WFS-III and WFS-IV).

A statistical representation of the estimated directions is shown in Figure 4.3. In the figure the numbers of observations are shown per degree and an upper and lower bound, defined as two standard deviations ($\pm 2\sigma$), are indicated as well. As seen in the figure, the mean and most frequent observed direction is $28^{\circ}N$ and the two standard deviations correspond to $17^{\circ}N$ and $39^{\circ}N$ respectively. A similar analysis was carried out for the two historical bathymetries presented in Section 2.2.1, and here similar directions were observed.

The directions estimated by the gradient method are well aligned with the net-sediment transport computations presented in Section 3.5. It should be noted that the smoothness of the numerical computations are due to spatial and temporal averaging associated with the computations and the post-processing, which is naturally not observed in directions estimated from the measured bathymetry. In the model computations a slight shift in direction is observed going from the south to the north, which is not observed in Figure 4.2. For prediction of future seabed levels this slight additional shift, observed in the flow modelling, will be included in order to ensure that all possible directions are included in the estimate. Therefore, the upper limit is increased to $43^{\circ}N$. The directions, which will be applied in the estimation of future seabed levels in Chapter 5, are summarized in Table 4.1.

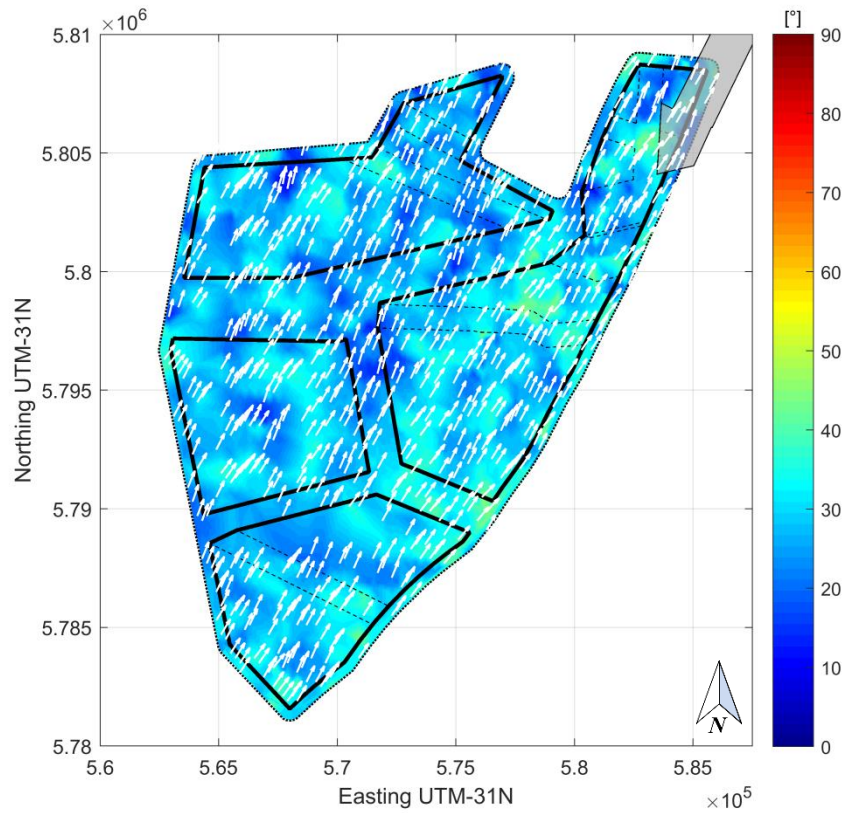


Figure 4.2 Map view of the estimated sand wave migration directions (towards which the sand waves are migrating; degrees north).

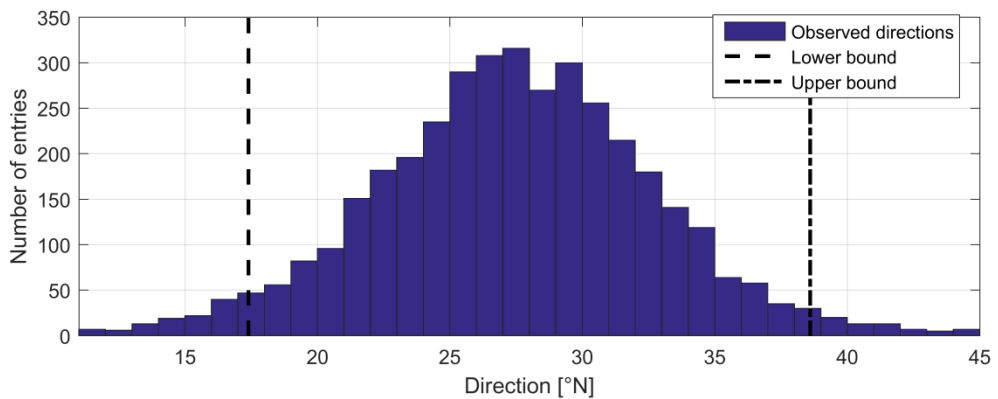


Figure 4.3 Histogram of sand wave orientations estimated by the data-driven gradient method with upper and lower bounds indicated by dashed lines.

Smallest angle of migration	Most likely angle of migration	Largest angle of migration
17°N	28°N	43°N

Table 4.1 Selected smallest, largest and most likely angle of sand wave migration applied in further analysis.

4.1.2 Sand wave migration speed

Once the sand wave migration directions have been estimated by the combination of the gradient method and the sediment transport computations, transects in the directions of propagation can be defined.

For this analysis an optimized cross correlation technique has been established, which allows for automated analysis of several thousand transects covering the entire area as shown in Figure 4.4. The historical bathymetries consist of several survey patches and to ensure consistency across the data sets, transects crossing survey patches (see Figure 2.1) were removed. As seen from Figure 4.4, the chosen transects still provide a significant coverage of the HKZWFZ area. In the white areas information will be obtained by interpolation, but due to the high data density no significant decrease in quality is expected.

The transects have a length of 2000 m, which corresponds to 2 to 5 sand wave lengths. For each transect, information is extracted from the filtered sand wave fields of two independent bathymetries and the spatial offset is computed using a 1D cross-correlation. The cross-correlation determines the migration distance which will give the minimized error between the two bathymetrical transects as illustrated in Figure 4.5. The advantage of the cross-correlation technique is that information from all data points are included in the analysis, which makes the results robust and less sensitive to bathymetry errors often seen in older or low resolution surveys. For each transects the sand waves were identified by a zero-crossing analysis and the cross-correlation was computed for all sand waves individually. In total 3904 transects were analysed and hence more than 10 000 sand wave crossings were used in the estimate of the migration speed.

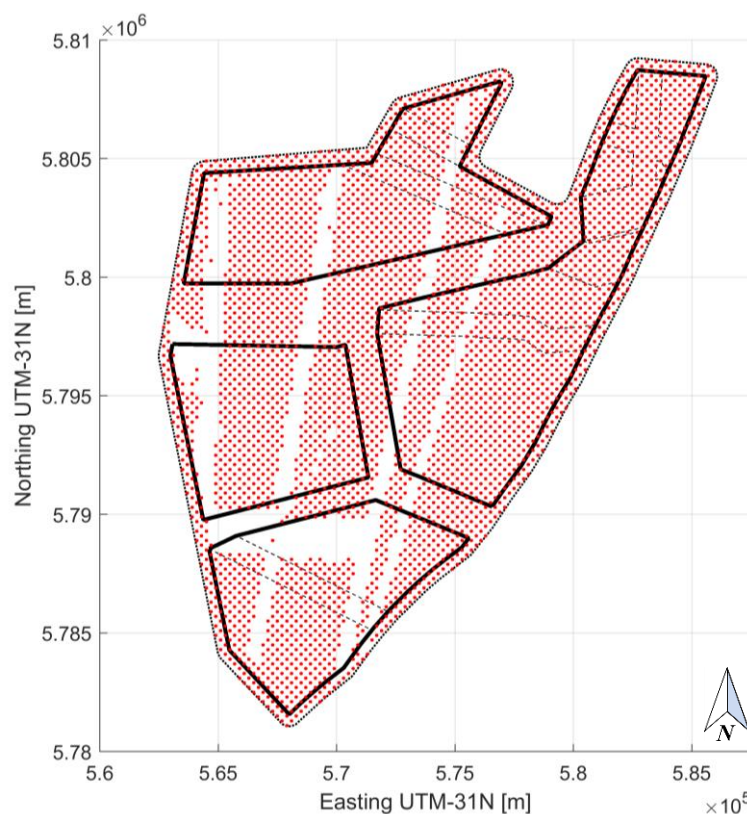


Figure 4.4 Map view of the HKZWFZ, with the centre of all analysed transects indicated by red dots. Total number of transects: 3904.

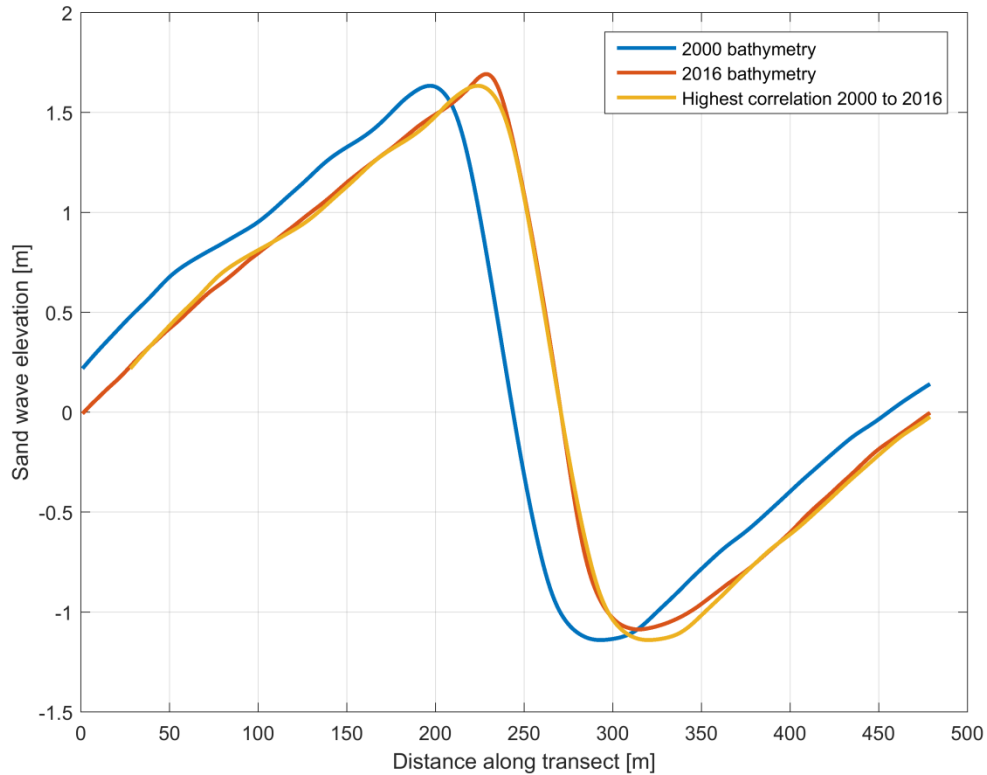


Figure 4.5 Example of cross correlation analysis as carried out for all transects.

Migration speeds have been determined, using the cross-correlation technique, for the three directions identified in Section 4.1.1 and summarized in Table 4.1. In Figure 4.6 the estimated migration speeds are shown for transects with a $28^{\circ}N$ direction, which corresponds to the most frequently observed migration direction (best estimate). As seen from the figure, the sand waves are typically moving with 1.0 to 1.5 m/year in WFS-II, WFS-III and the southern part of WFS-IV. In the central and northern parts of the wind farm zone the sand waves are moving slightly faster, ranging from 2.0 – 3.5 m/year. This is consistent with the hydrodynamic computations presented in Section 3.5 where the net-sediment transport is found to be largest in the northern part of the wind farm area. It may be noted that locally, in the northern part, migration speeds as high as 5.2 m/year are observed.

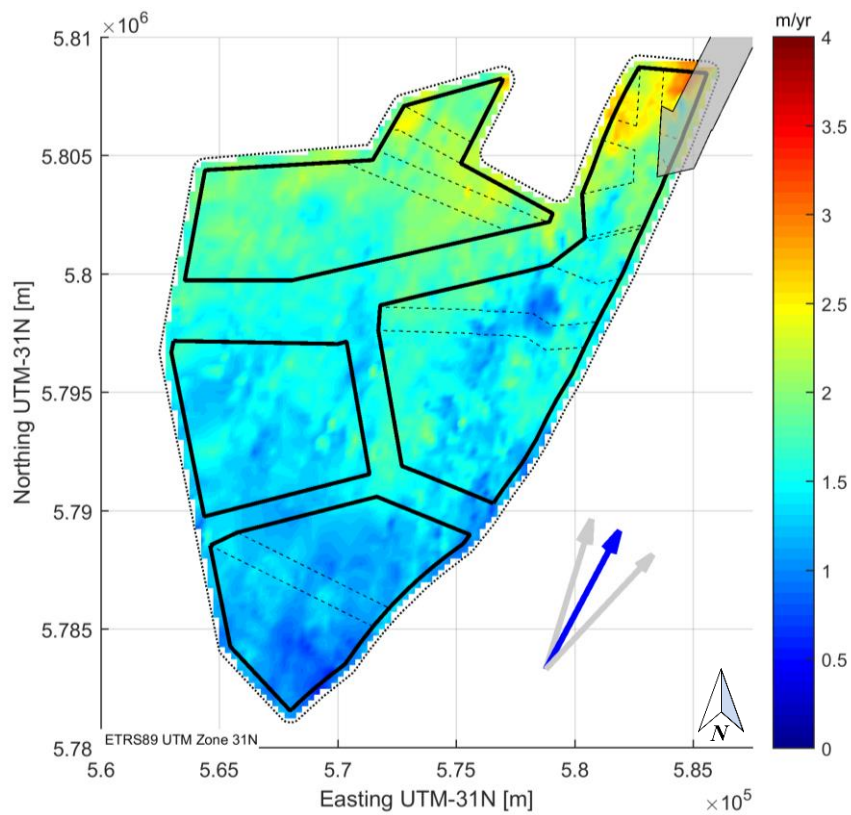


Figure 4.6 Map view of the estimated sand wave migration speed (period 2000 – 2016), based on transects located in a 28°N direction, which corresponds to the most frequently observed migration direction.

In Figure 4.7 non-exceedance plots of the sand wave migration speeds are shown for WFS-I. In the figure, migration speeds for the three directions identified in Section 4.1.1 (17°N, 28°N and 43°N) are shown. Based on the non-exceedance plots, (10%, 50% and 90%) are identified per migration direction as summarized in Table 4.2. As seen from the table typical migration speeds in the wind farm zone are in the range of 0.7 m/year to 3.0 m/year being global 10% and 90% non-exceedance values respectively.

Wind farm site	Migration speed (17°N)	Migration speed (28°N)	Migration speed (43°N)
	10% / 50% / 90% [m/yr]	10% / 50% / 90% [m/yr]	10% / 50% / 90% [m/yr]
I	1.5 / 2.0 / 2.5	1.5 / 2.0 / 2.5	1.5 / 2.1 / 2.7
II	1.2 / 1.5 / 2.0	1.2 / 1.5 / 2.0	1.2 / 1.5 / 2.1
III	0.8 / 1.2 / 1.7	0.8 / 1.2 / 1.6	0.7 / 1.2 / 1.9
IV	0.9 / 1.7 / 2.6	0.9 / 1.5 / 2.6	0.9 / 1.7 / 3.0
All sites	1.1 / 1.7 / 2.5	1.1 / 1.7 / 2.3	1.0 / 1.7 / 2.6

Table 4.2 Sand wave migration speeds estimated per wind farm site and per migration direction.

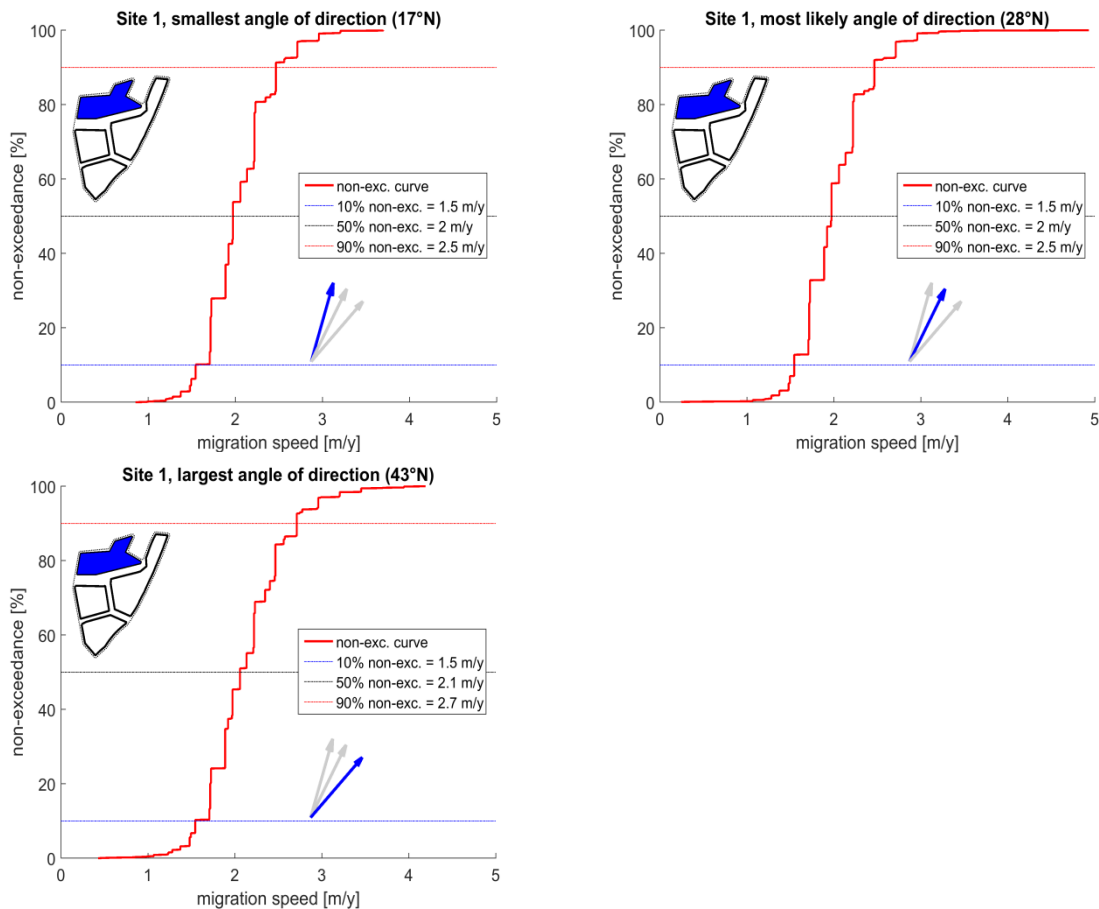


Figure 4.7 Non-exceedance plots of sand wave migration speeds for WFS-I for the period 2010-2016.. The results are shown for the three directions identified in Section 4.1.1.

4.1.2.1 Migration speeds for estimating future seabed levels.

For areas such as WFS-IV, which stretches over a large spatial area, the statistical values presented in the previous section may not be locally representative. Therefore, the prediction of future seabed levels presented in Chapter 5, are based on the local values per transect point and not the global values. To ensure that all possible variations are covered in the scenarios of future bed levels, the following three *local* migration speeds per transect are applied:

- The lowest migration speed observed in all combinations of surveys (2000 – 2010; 2000 – 2016; 2010 – 2016)
- The mean migration speed observed in all combinations of surveys
- The highest migration speed observed in all combinations of surveys

These three migration speeds are then combined with the three migration directions identified in Section 4.1.1, which, however, are assumed global values. For a further discussion of the prediction of future bed levels please see Section 5.2.

4.1.3 Sand wave characterization

For the analysis of the sand wave characterization in terms of wavelength and wave height, a Fourier analysis is used. For the analysis the same transects as used in Section 4.1.2 are

applied. For each transect the crest and trough points are automatically identified as illustrated in Figure 4.8. A Fourier series of 68 components was fitted to the identified extremes by solving an overdetermined system of equations. The sand wave heights and lengths are hence easily deduced from the corresponding Fourier series.

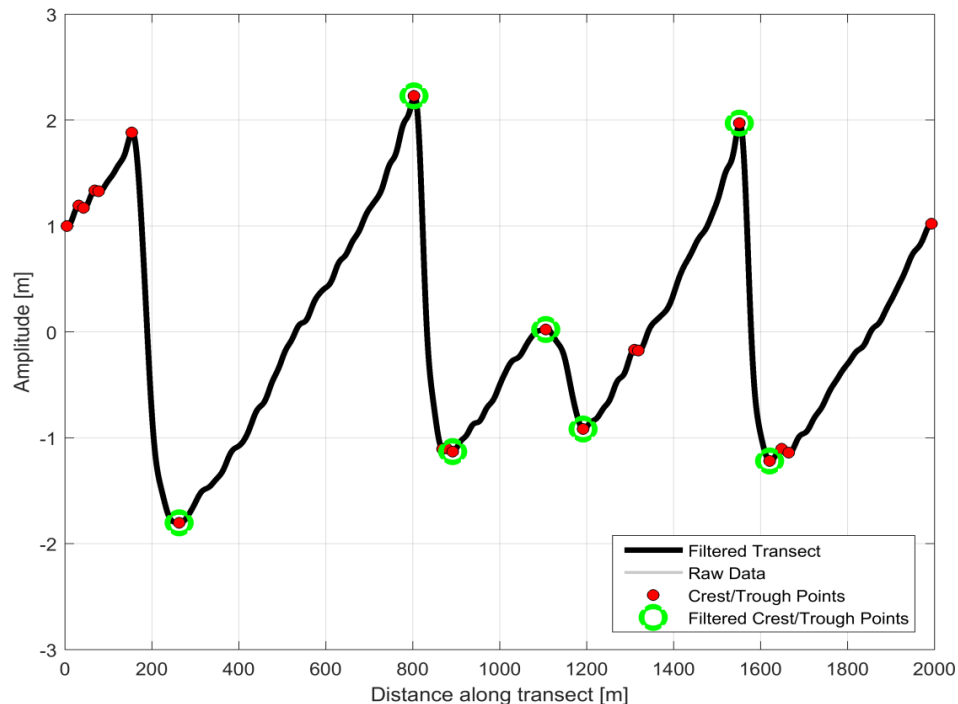


Figure 4.8 Example of Fourier analysis on one of the 2000 m long transects from SSW (left) to NNE. The plot shows the Fourier approximations of the 2016 sand wave signal (black line). Red dots indicate crest and trough point and the green circles indicate which points have been selected for analysis.

It may be noted that unlike previous studies, such as Deltares (2015b, 2016b), the Fourier method is only used for estimating the sand wave characteristics and not the migration speed as this analysis is replaced by the cross-correlation technique presented in Section 4.1.2. In Figure 4.9 and Figure 4.10 map views of the sand wave heights and sand wave lengths are shown. As seen from the figures the sand waves in the western part of the wind farm zone are in general higher and shorter, whereas the sand waves closer to shore in the eastern part, are longer and lower. It is well established that the sand wave height is correlated to the water depth where higher sand waves in general are observed at deeper water.

In order to investigate to what extent the sand waves in HKZWFZ will retain their shape over periods of several years, sand wave heights and lengths were compared between the 2010 and 2016 multibeam surveys. In this analysis only the multibeam surveys were used, because these have both similarly high resolutions and accuracies, which allows for good estimations of sand wave dimensions and minimises the differences in shape due to data artefacts. In the considered transects, 6000 sand waves were identified to correspond between both datasets. The cross-correlations of the sand wave heights and sand wave lengths are plotted in Figure 4.11 and Figure 4.12 respectively. Both plots reveal a very good correlation with values for the Pearson product-moment correlation coefficient (PMCC) of 0.996, which is very close to 1 (a value of 1 (red line in the plots) would mean that the heights and lengths in both datasets are exactly the same).

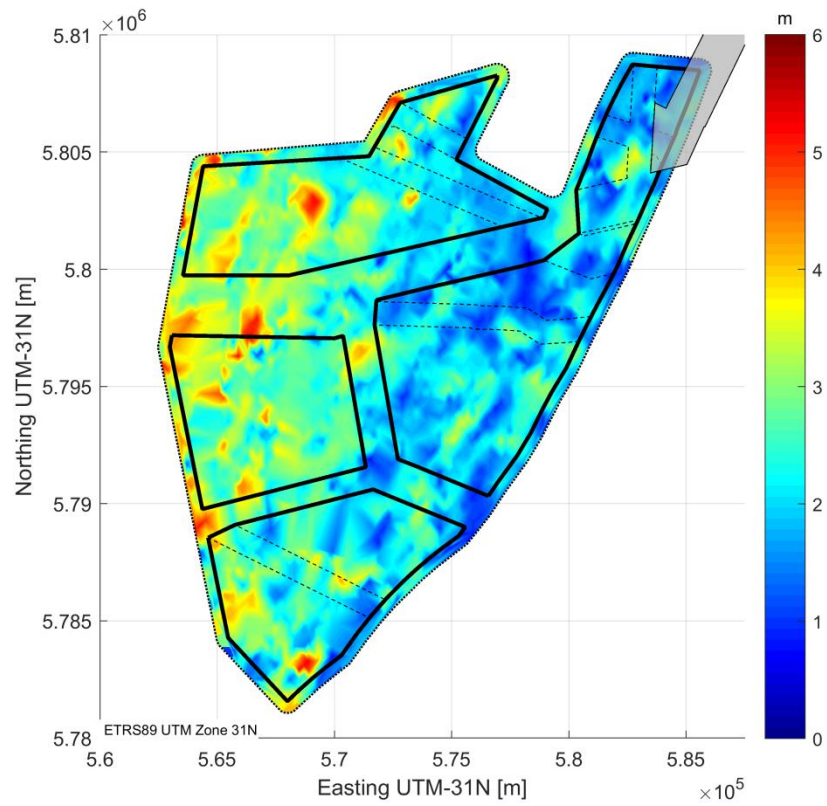


Figure 4.9 Spatial distribution of the mean sand wave height for the HKZWFZ, based on the 2016-Bathymetry.

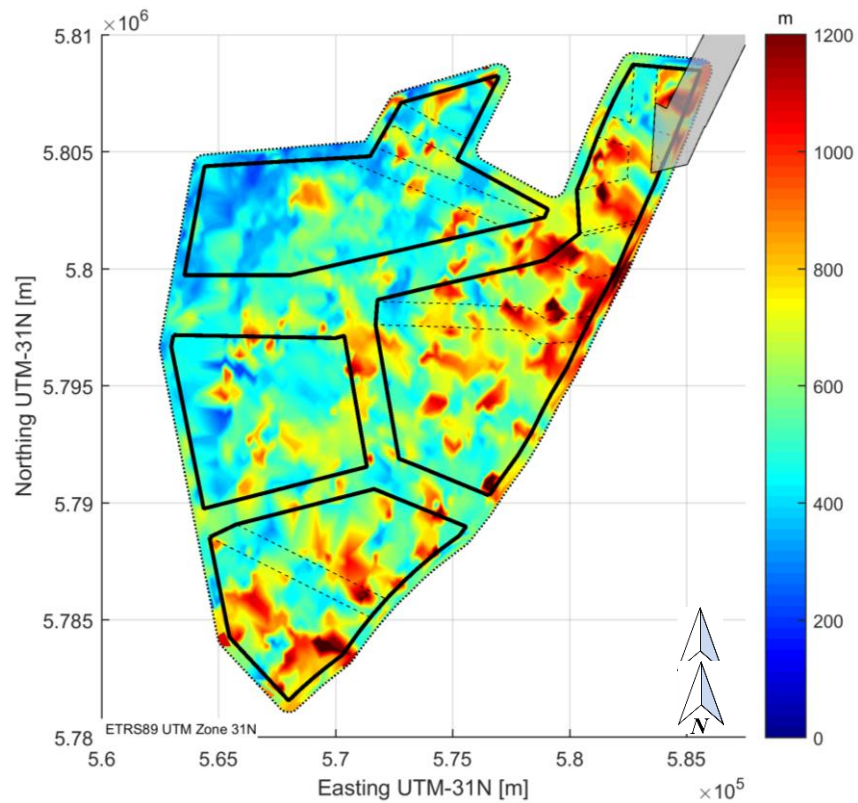


Figure 4.10 Spatial distribution of the mean sand wave length for the HKZWFZ, based on the 2016-Bathymetry.

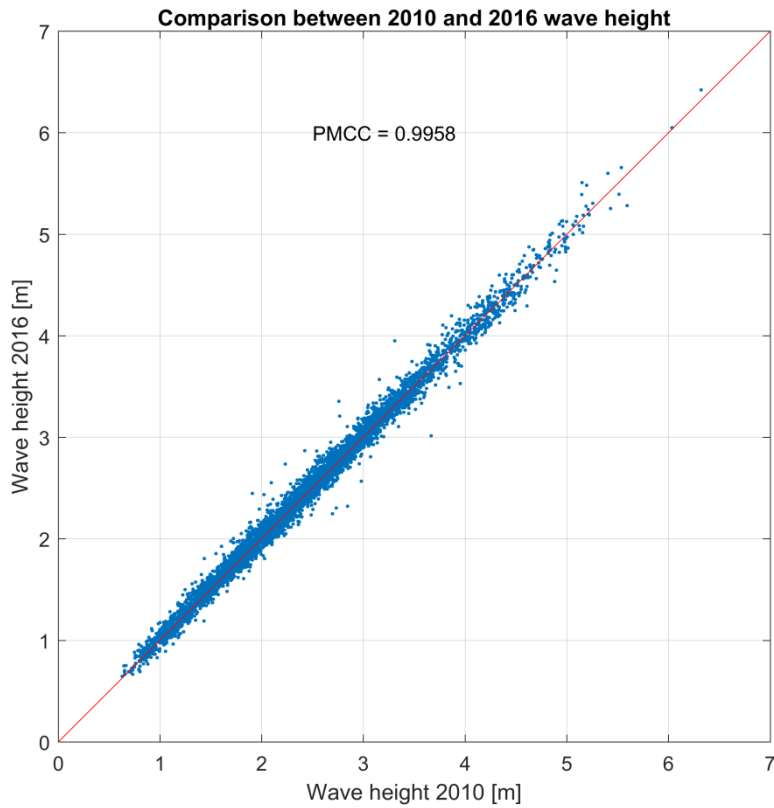


Figure 4.11 Cross-correlation scatter plot for sand wave heights in 2016 and 2010 for ~6000 identified sand waves.

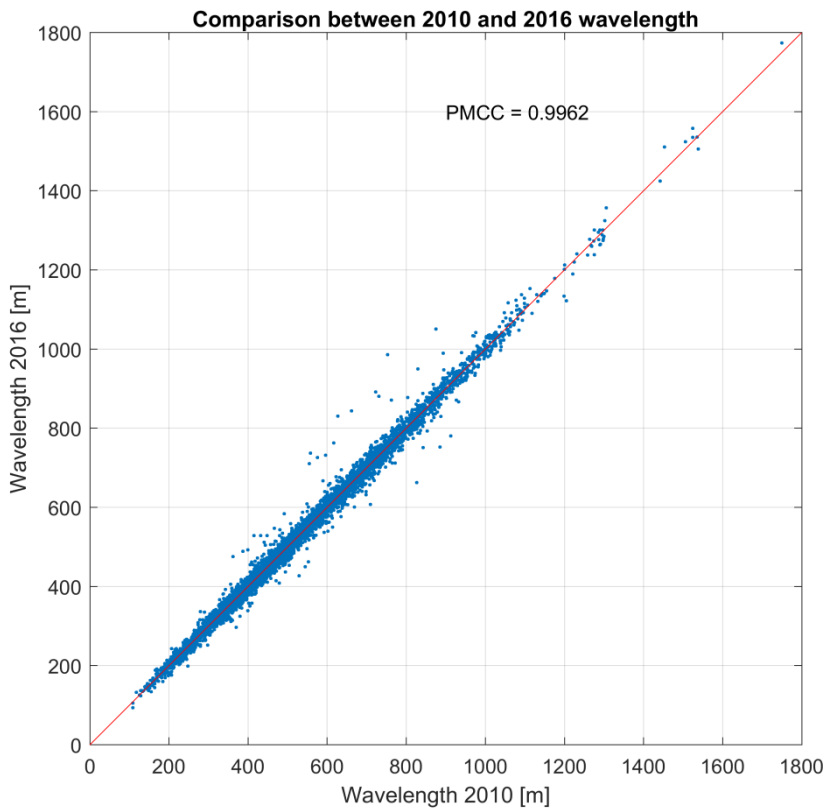


Figure 4.12 Cross-correlation scatter plot for sand wave length in 2016 and 2010 for ~6000 identified sand waves.

If the sand wave characteristics would have changed significantly in the period between 2010 and 2016, it is unlikely that the individual sand waves would have restored to such similar dimensions. Note that the potential effect of storms on sand waves is further investigated in Section 4.3.

To quantify the general sand wave characteristics per wind farm site, non-exceedance curves were created and the 10%, 50% and 90% non-exceedance values were identified (this is the same type of analysis as presented for the migration speed in Figure 4.7). From that analysis the characteristic values presented in Table 4.3 are obtained. The analysis was carried out for all dataset and the presented values represent the envelope of the results. In general the variation between the individual surveys is in the order of $O(0.1 \text{ m})$. In addition, the 10%, 50% and 90% sand wave length over sand wave height ratios (L/H ratio) are presented in Table 4.3. Note that these values are not obtained by dividing the sand wave length non-exceedance values by the sand wave height non-exceedance values, but are the non-exceedance values of all L/H ratios.

Sand wave property	Wind Farm Site				All sites
	I	II	III	IV	
Sand wave height 10% / 50% / 90% [m]	1.5 / 2.5 / 4.0	1.9 / 2.7 / 3.9	1.4 / 2.3 / 3.3	1.1 / 1.9 / 2.7	1.3 / 2.3 / 3.6
Sand wave length 10% / 50% / 90% [m]	238 / 427 / 708	265 / 503 / 757	388 / 578 / 918	391 / 631 / 950	287 / 511 / 832
Sand wave L/H ratio 10% / 50% / 90%	96 / 176 / 289	103 / 193 / 285	167 / 257 / 442	212 / 324 / 607	113 / 222 / 431

Table 4.3 Sand wave characteristics per wind farm site and for the entire area for the 2016 Bathymetry. The analysis was carried out for all bathymetries and the presented data represents the envelope of the results. Sand wave lengths are rounded off to nearest 100 m.

4.1.4 Summary of sand wave analysis

The morphodynamic characterization in the HKZWFZ is described by means of migration directions and speeds together with the sand wave heights and lengths for 3904 transects distributed over the HKZWFZ area.

With aid of the gradient method, three main migration directions were estimated, resulting in a lower bound of 17°N , a most likely direction of 28°N and an upper bound of 43°N . For each of those three directions, migration speeds were determined via a 1D cross correlation technique. In the HKZWFZ, typical migration speeds range between 0.7 m/year (WFS-III) and 3.0 m/year (WFS-IV). The observed south to north increase in migration speed is consistent with the south to north pattern observed within the hydrodynamic computations.

Furthermore, sand wave heights and wavelengths are estimated using a Fourier analysis, ranging between 1.1 and 4.0 m and 200 and 1000 m respectively. Spatially, the sand waves in the western part of the wind farm zone are in general higher and shorter, whereas the sand waves closer to shore in the eastern part are longer and lower.

4.2 Megaripple analysis

As explained in Section 2.3, megaripples have migration speeds that are so large that many megaripples will pass at each foundation throughout the lifetime of wind farms. Therefore, it was decided not to predict megaripple migration, but to analyse their dimensions and to include some representative statistical values in the uncertainty band for predicted bed levels (see also Section 5.1). This is further stimulated by the fact that megaripple occurrence and dimensions are highly variable in time.

For the analysis of the megaripples all wind farm sites were analysed using a 1x1 m grid in order to better capture the megaripple shapes. On this grid an additional filtering was carried out to separate the Sand Wave Field and the Megaripple Field. The filtering is based on the same principals and described in Section 3.2, but a smaller filter base of 15x15 m was used. This is large enough to cover the megaripples which typical have wavelengths in the order of 8 to 20 m. Note that this fine grid resolution of 1x1 m is only available for the 2016-data and hence the analysis is limited to this dataset.

In Figure 4.13, an example of this filtering method is presented for WFS-I. The left images (a) in the figure show the mobile part of the bathymetry as identified in Section 3.2. The right image (b) shows the filtered bathymetry and if this is subtracted from the Mobile Bathymetry, the Megaripple Field is obtained (c). Note that these figures are greatly zoomed in to show the megaripples with their relatively short wavelengths and small wave heights compared to the sand waves. It can be observed that the megaripple pattern is quite regular and oriented in the same direction as the sand wave crests.

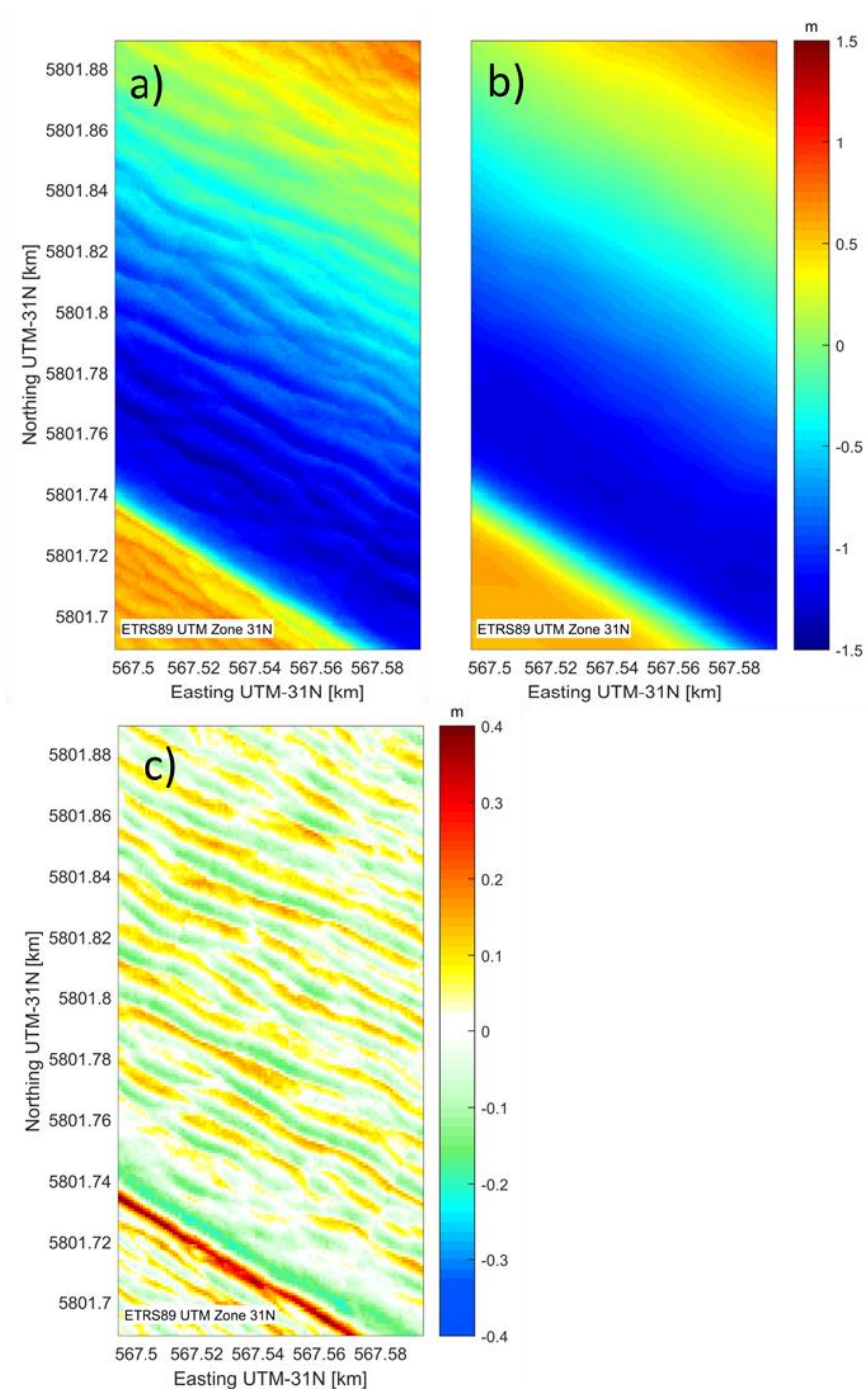


Figure 4.13 (Left) Part of the bathymetry of WFS-I, zoomed to an area of 100 x 200 m; (middle) bathymetry of same area with megaripples filtered out; (right) Megaripple Field extracted from bathymetry with in orange-red showing the megaripple crests and in green-blue the megaripple troughs.

Nearshore to offshore variation in megaripple amplitudes (crest heights and trough depths) over the HKZWFZ can be observed in Figure 4.15. Over the entire HKZWFZ, crest heights of the megaripples vary between 0 (near-shore) and 0.30 m (offshore), whereas the trough depths vary between 0 and 0.20 m. Figure 4.14 shows the megaripple amplitudes along a 1200-m long transect in WFS-I (location is depicted by the arrow in Figure 4.15).

Note that as an artefact of the filtering around the sand wave crest, the crest will be visible in the Megaripple Field as shown in Figure 4.14 and Figure 4.15. Part of the sand wave crest filtering artefacts are megaripples located at the top of the sand wave, therefore it is deemed not possible to distinguish between a sand wave crest and megaripples. I.e. filtering the megaripples out gives an underestimation of sand wave heights while disregarding the sand wave crests during filtering gives an overestimation of the sand wave height in the Sand Wave field.

Finally it should be noted that the vertical stripes visible in Figure 4.15 are artefacts related to the shipping lines sailed during the survey campaign.

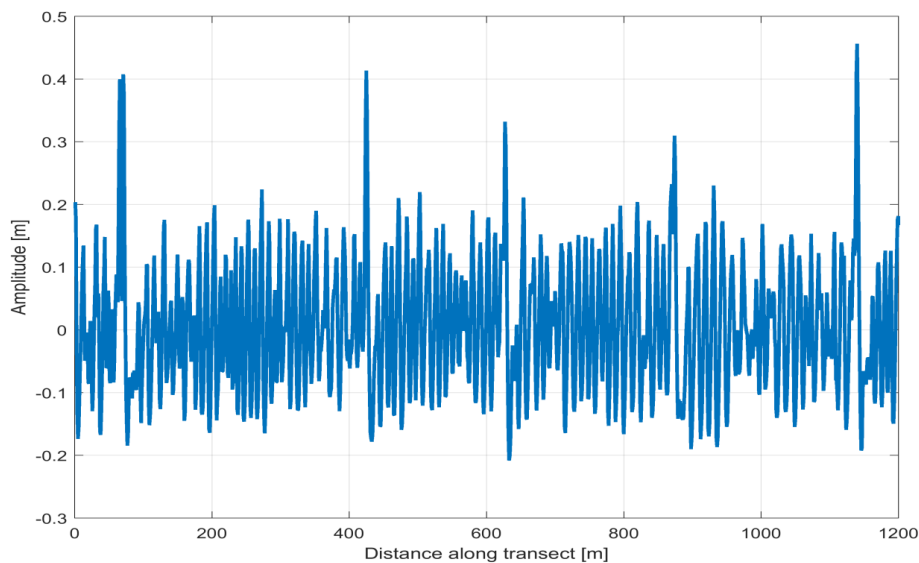


Figure 4.14 Megaripple amplitudes along a transect in WFS-I. Note that the larger upward and downward amplitudes are artefacts caused by the filtering method at the sand wave crest (here the megaripple amplitude contains part of the sand wave amplitude), which should be disregarded.

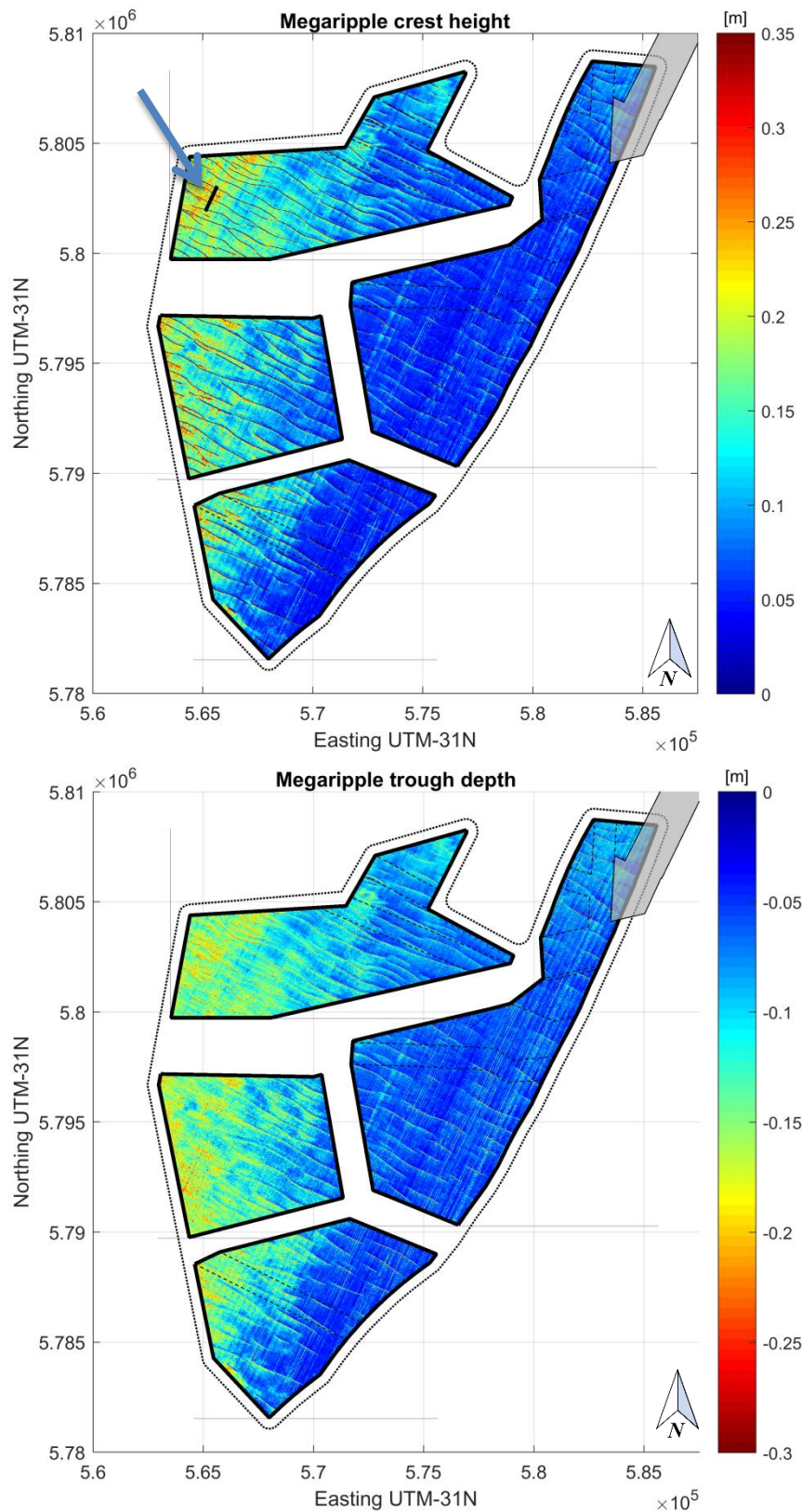


Figure 4.15 Megaripple crest heights (top plot) and trough depths (bottom plot) in the HKZWFZ. The arrow in the top plot depicts the location of the transect (black line) displayed in Figure 4.14.

4.3 Analysis of storm effects on morphodynamics

In this section the recent pre- and post-storm bathymetrical measurements carried out by Fugro as part of the measuring campaign for the HKZWFZ are analysed. The objective of the analysis is to get further insight into the effect of significant wave action associated with storm waves on the sand wave field.

The analysis was carried out on the bathymetric data from 18 March 2016 and 1 April 2016, respectively before and after the “Easter Storm” that occurred on 28 March 2016. The additional measurements were carried out for the highlighted transect shown in Figure 4.16.

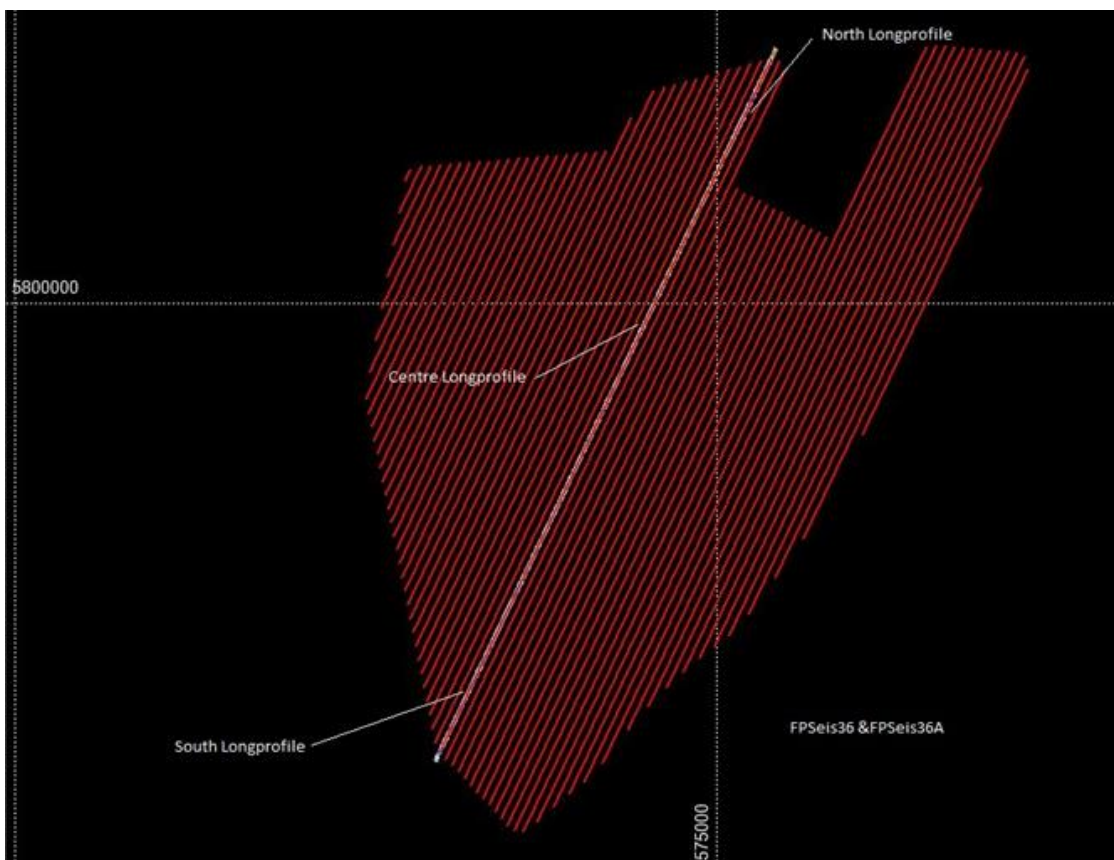


Figure 4.16 Survey lines for HKZWFZ, with the survey line that was repeated after a storm event highlighted. Figure from email communication with Fugro on 4 April 2016.

In Figure 4.17 the measured spectral significant wave heights (H_{m0}) and peak wave periods (T_p) are presented for three surrounding measurement stations Munitiestortplaats IJmuiden, Europeul-EWD and K13a-platform. The thick blue line represents the closest measurement at Munitiestortplaats IJmuiden and shows a maximum significant wave height of approximately $H_{m0} \approx 5.5$ m and a peak wave period of $T_p \approx 11$ s.

During the “Easter Storm” waves were coming from the west-southwest as shown in Figure 4.18. The waves were hence propagating with only a small angle relative to the direction of main sand wave migration. In Figure 4.19 and Figure 4.20 the current direction and the current speed are shown respectively for the same time interval. It is stressed that the standard convention for indicating directions is that waves are “coming from” whereas currents are “going to” which implies a 180 degrees shift. Furthermore it may be noted that

the current speeds and directions are originating from model computations (zuno-model) and not from measurements. In Figure 4.19, it is clearly seen that the current direction is significantly influenced by the storm, since the ebb current during the peak of the storm is almost completely suppressed. For the current speeds shown in Figure 4.20, it may be noted that the current speed during the storm is slightly increased compared to the normal tidal current.

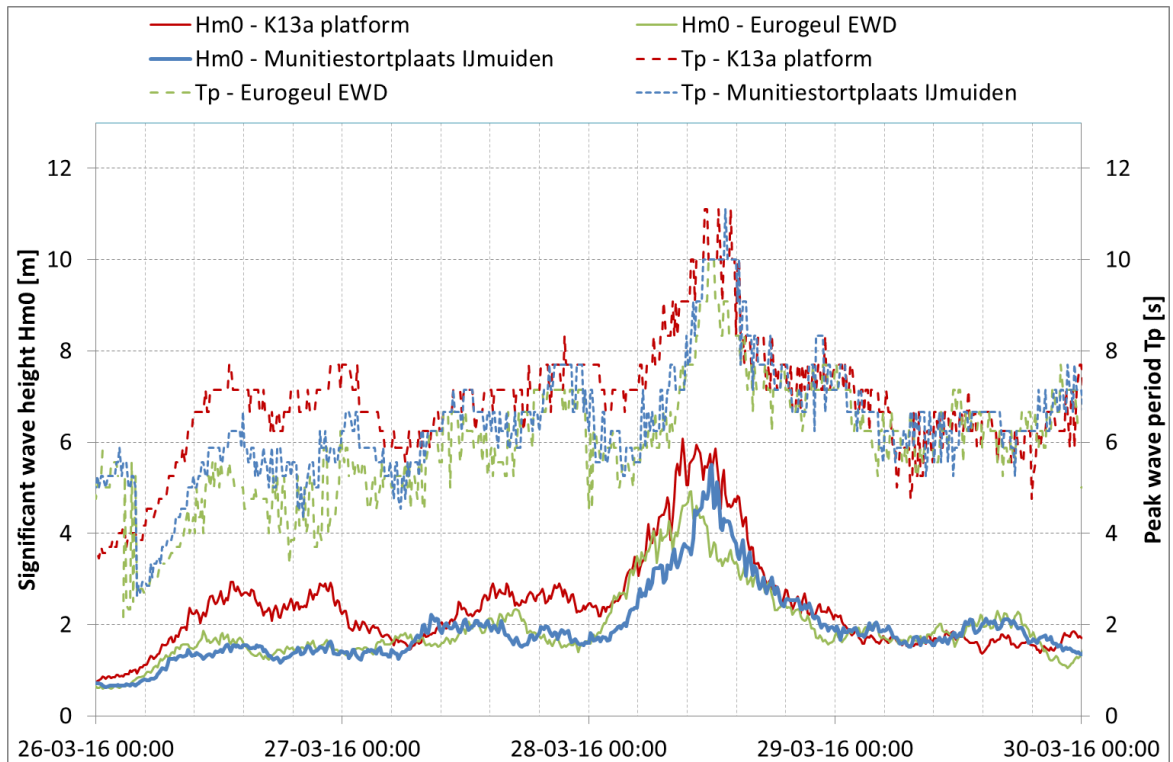


Figure 4.17 Measured spectral significant wave heights H_{m0} and peak periods T_p for the “Easter Storm” obtained at measurement stations IJmuiden Munitiestort 1 platform, K13a-platform and Eurogeul-EWD.

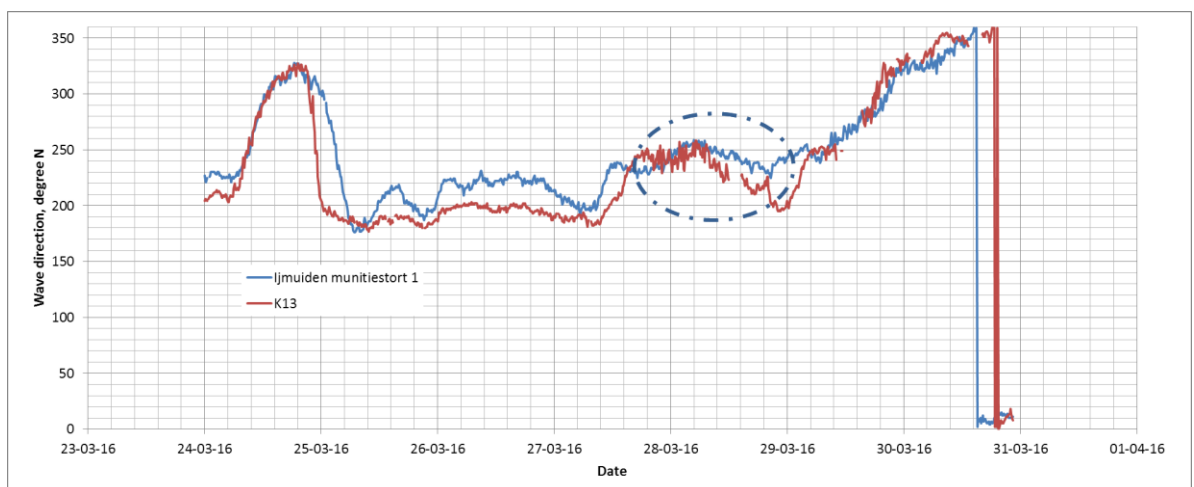


Figure 4.18 Measured wave direction for the “Easter Storm” observed at measurement stations IJmuiden Munitiestort 1 platform and the K13a-platform and Eurogeul-EWD.

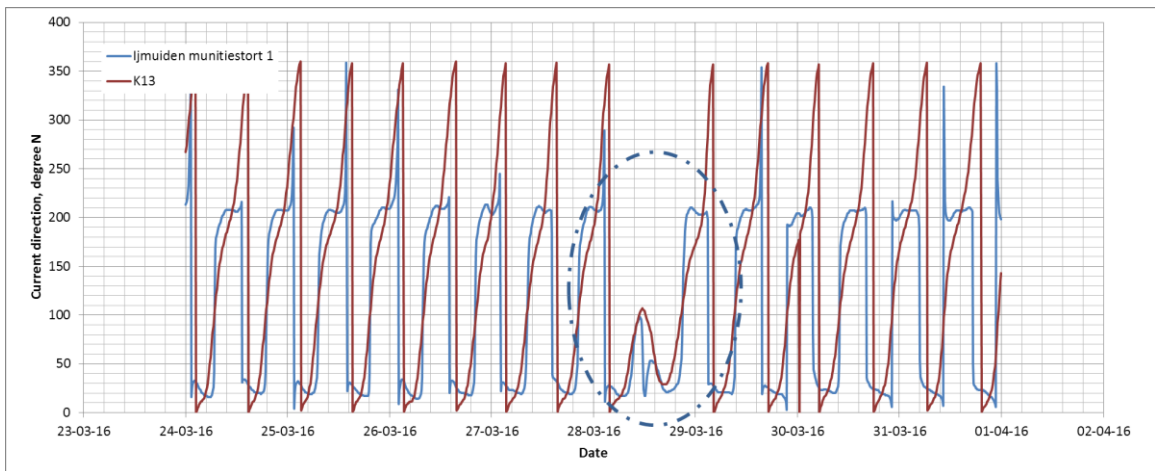


Figure 4.19 Current direction for the “Easter Storm” observed at measurement stations IJmuiden Munitiestort 1 platform and the K13a-platform. These model results are retrieved from Rijkswaterstaat (2016).

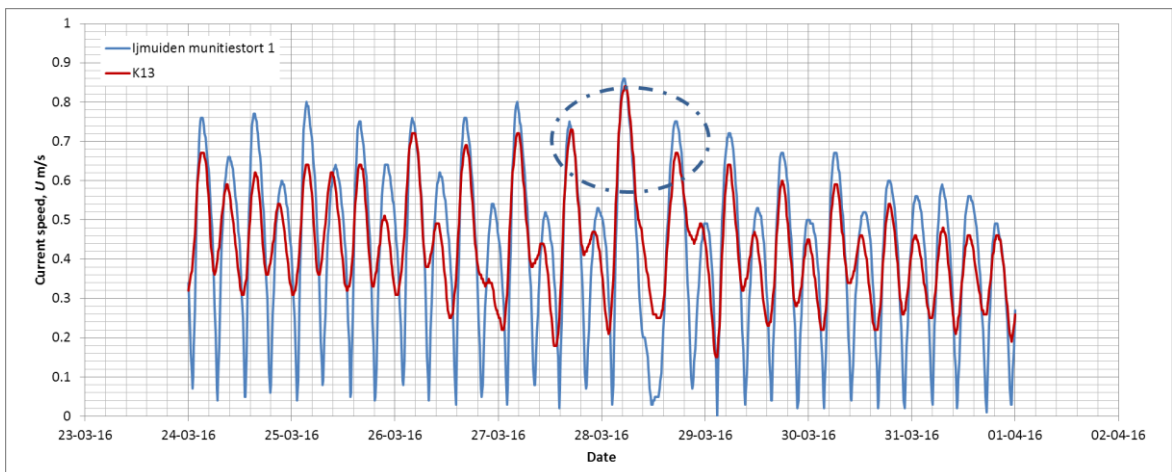


Figure 4.20 Current speed for the “Easter Storm” observed at measurement stations IJmuiden Munitiestort 1 platform and the K13a-platform. These model results are retrieved from Rijkswaterstaat (2016).

Note that both the current and the waves were quite well aligned with each other and with the main direction of sand wave migration. These conditions are considered favourable for affecting the sand waves. To determine whether the storm was actually sufficiently severe to alter the sand wave shapes, the seabed changes during the storm were analysed. In Figure 4.21 selected parts of the measured transect are shown for before and after the storm. As seen from the figure, the storm event had limited influence on the seabed and the sand wave field, where the overall sand wave shape is unaltered and changes are limited to the megaripples.

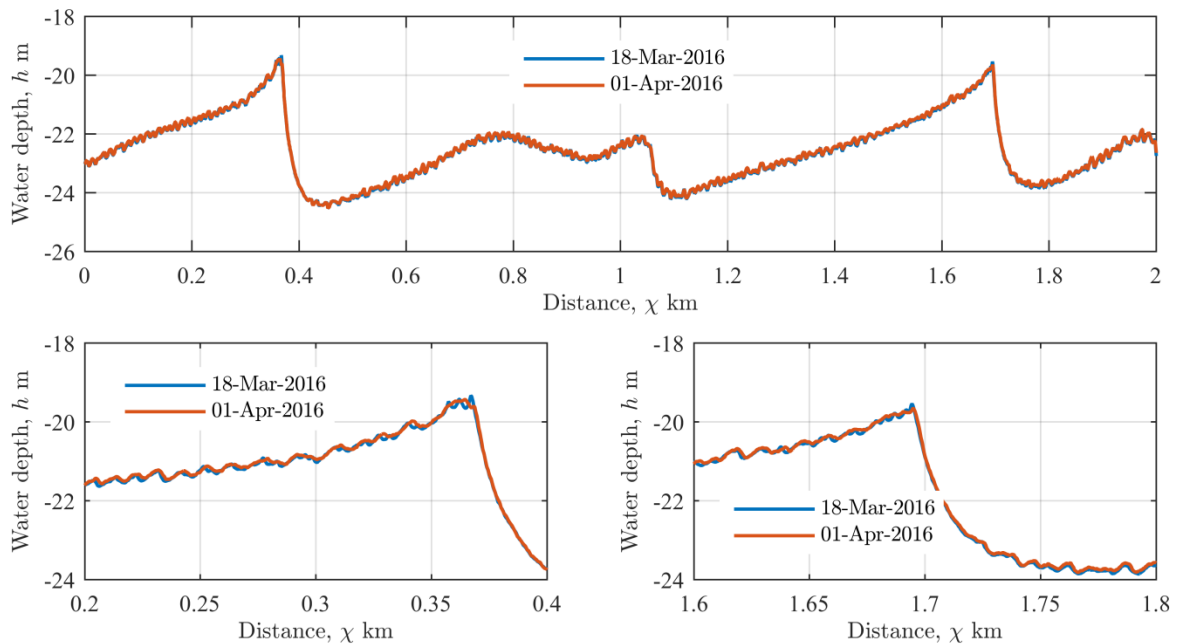


Figure 4.21 Measured seabed profiles before and after a storm event in the HKZWFZ. The bathymetry is expressed in terms of a local coordinate, χ , along the transect. Top panel: Overview of the bathymetry transects for the first 2 km of the transect. Lower panel: zoom of distinct sand wave crests.

To quantify the changes as a result of the storm, the pre and post storm profiles are analysed using the same methods as applied in Section 4.1. Figure 4.22 shows the non-exceedance curves of sand wave heights and lengths obtained from the Fourier analysis. As seen from the figure there is no significant difference between the two curves. In addition, the 1D cross correlation technique showed no displacements of individual sand waves. Hence, it can be concluded that the Easter storm did not cause measurable changes to the sand waves along the observed profile.

However, small scale features such as the megaripples experienced a reduction in the wave height in the order of 2-3 cm. This is mainly visible in the megaripple crest height which is shown in the top graph in Figure 4.23 whereas the effect for the megaripple trough depth, presented in the bottom graph in the same figure, is less pronounced. It should be stressed that the observed changes are small and without practical importance.

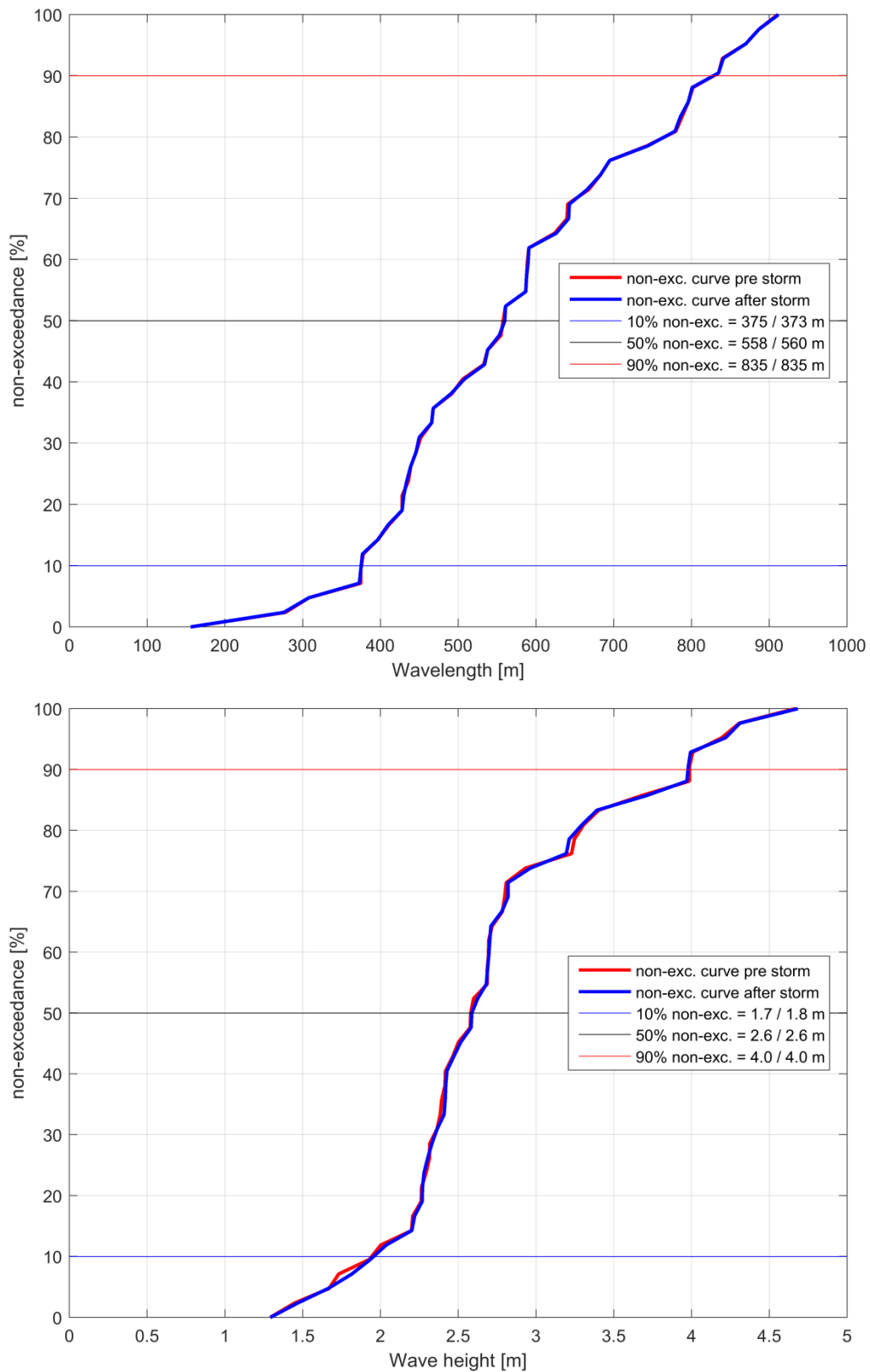


Figure 4.22 Comparison of non-exceedance curves for sand wave length (top figure) and sand wave height (bottom figure). The red lines in the figures indicate the non-exceedance curves of the pre storm survey, while the blue lines indicate the non-exceedance curves of the post storm survey.

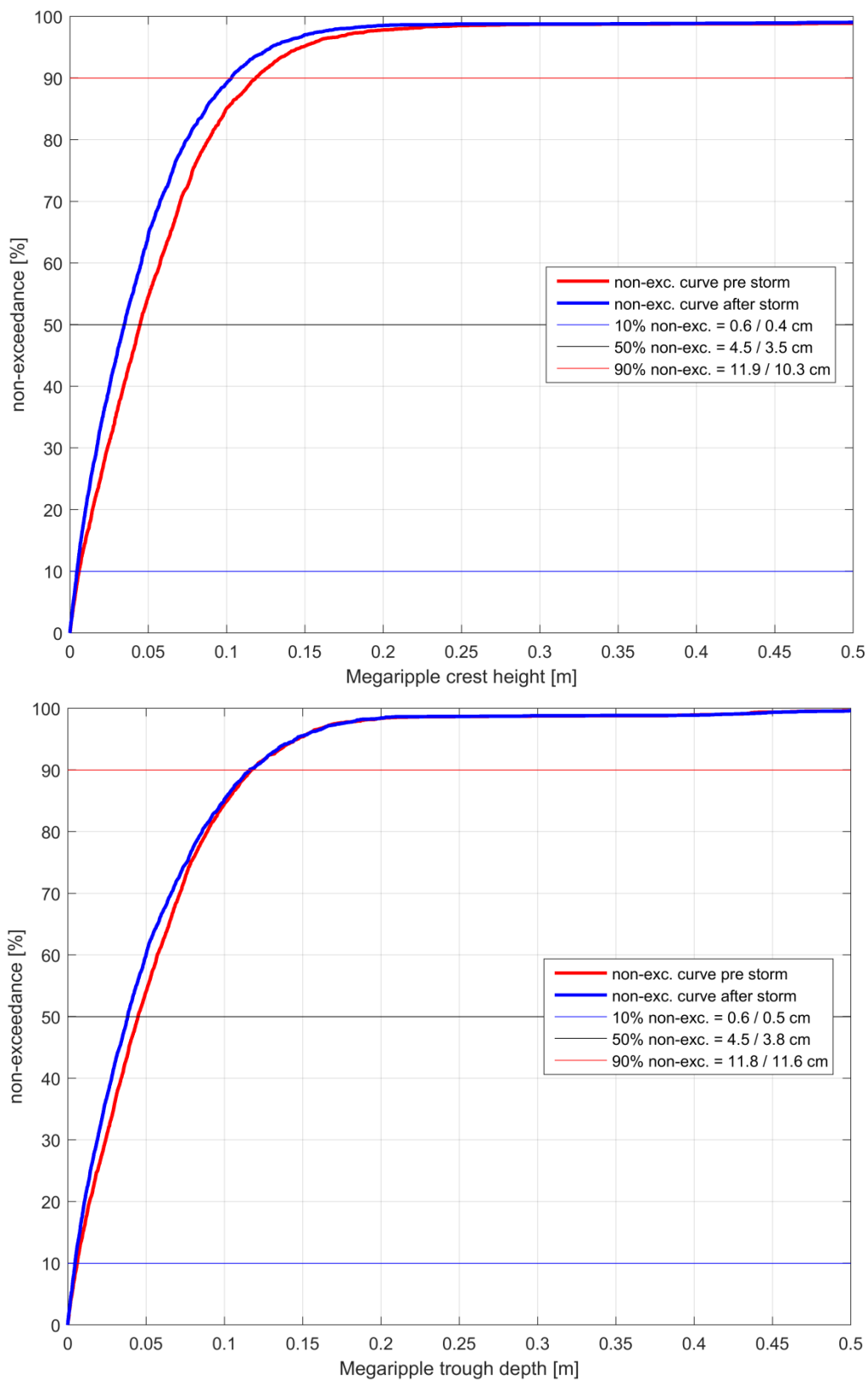


Figure 4.23 Comparison of non-exceedance curves for megaripple crest height (top graph) and megaripple trough depth (bottom graph). The red lines in the figures indicate the non-exceedance curves of the pre storm survey, while the blue lines indicate the non-exceedance curves of the post storm survey.

The limited change in the seabed is mainly related to the severity of the storm, where in particular the significant wave height and the peak period influence to what extent the seabed is affected (e.g. van Dijk et al., 2005). Using the dedicated scour and sediment mobility model OSCAR, developed by Deltares, the seabed mobility was estimated for various sea states, see Figure 4.24. The mobility is a measure of how mobile the seabed is: when the mobility (MOB) is smaller than 1 the seabed sediment is considered stable. The computed mobilities presented in Figure 4.24, should be seen as a relative indication to be able to compare storms with different wave heights. As seen from the figure, the considered storm event is relatively moderate with a corresponding return period of 1 to 5 year, which may explain why only limited change to the seabed is observed. The indicated return periods shown in the figure legend are based on preliminary results from the met-ocean study for which a final version is not yet available during this study.

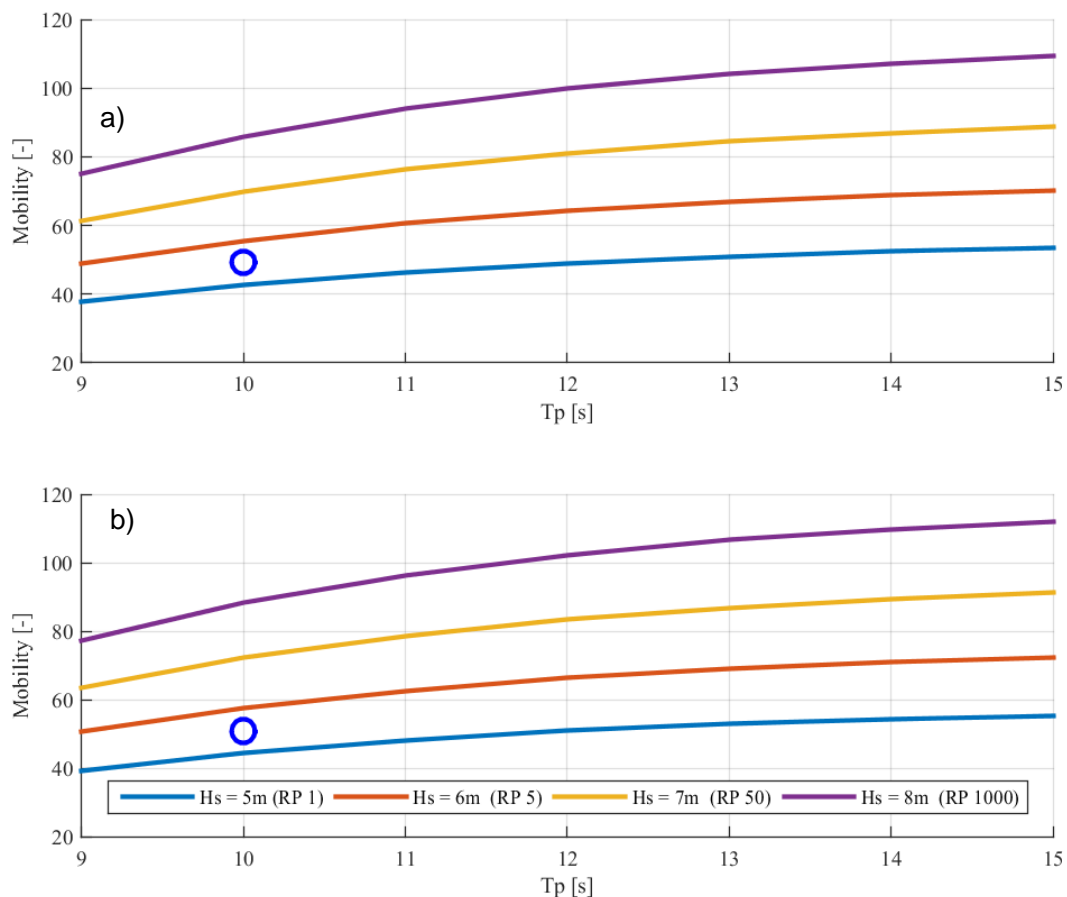


Figure 4.24 Seabed mobility for the HKZWFZ illustrated for various wave and current conditions. Blue circles indicate the considered storm event on 28 March 2016. a) Constant aligned current of 0.85 m/s. b) Constant aligned current of 0.95 m/s. RP indicates approximate return period.

4.4 Summary

A morphodynamic analysis focused on sand waves and megaripples in the HKZWFZ is presented. It is estimated that within the HKZWFZ sand waves migrate towards the north-northeast, between 17° and 43° relative to North, with typical migration speeds ranging between 0.7 m/year and 3.0 m/year. Locally, migration speeds as high as 5.2 m/year are observed. Spatially, an increasing south to north trend in migration speeds is observed.

Sand wave dimensions show a spatial trend, where sand waves in the deeper western part of the wind farm zone in general are higher and shorter, whereas the sand waves closer to shore in the eastern part are longer and lower. Within the HKZWFZ, sand wave heights and lengths range between 1.1 and 4.0 m and 200 and 1000 m, respectively.

Superimposed on the sand waves, megaripples are present. The megaripples in HKZWFZ, as measured from the 2016 survey, have wavelengths up to 20 m, crest heights up to 0.3 m and trough depths up to 0.2 m. Spatially, megaripples are almost absent in the eastern part of HKZWFZ and increase in height towards the west farther offshore. However, it may be noted that megaripple occurrence and dimensions are highly variable in time.

By analysing the recent pre- and post-storm bathymetrical measurements it is observed that the “Easter Storm” of 28 March 2016 had limited influence on the seabed and the sand wave field, where the overall sand wave shape is unaltered and changes are limited to the megaripples.

5 Prediction of future seabed levels

In this chapter the methodology for estimating future bathymetries and the corresponding seabed changes are presented. The chapter starts with a description of the various sources of uncertainty in Section 5.1. Following the description of these uncertainties, a suitable uncertainty band is determined. In Section 5.2, the methodology of predicting the future bathymetries is presented. In Sections 5.3, 5.4 and 5.5, these future bathymetries are used to determine the Best Estimate Bathymetry (BEB), Lowest SeaBed Level (LSBL) and Highest SeaBed Level (HSBL). Furthermore, the corresponding bed level changes relative to the 2016 Bathymetry are predicted. Also in Section 5.4, the LSBL is validated against the base of the Holocene formations and the non-erodible layers identified in Section 3.4.

In the final section of this chapter, Section 5.6, the LSBL and HSBL and the corresponding predicted maximum seabed level lowering and rising are translated into indicative recommendation zones for foundations and electricity cables. Note that for all figures following in this chapter, no predictions have been made within the sand mining area in the northeast of WFS-IV, denoted by a grey patch.

5.1 Sources of uncertainty

In the prediction of the future bed level changes and corresponding bathymetries, various sources of uncertainty have to be taken into account. The main sources of uncertainty in a data-driven morphological analysis based on measured bathymetrical data are:

- i) Uncertainty due to data collection and differences in the collection of data
- ii) Uncertainty in the pre-processing of data
- iii) Uncertainty in the methodology of analysis and prediction

(i): The datasets that have been used in this study are either collected by means of single beam echo sounding (SBES; 2000 combined dataset) or multi beam echo sounding (MBES; 2010 and 2016 datasets). The SBES surveys tend to have a shoal-biased nature which is caused by the fact that SBES measures the first return of the echo sounding in the wider beam. For example, when megaripples occur, the crest of the megaripple within the SBES beam width determines the measured water depth. For MBES, the separate beams also register the troughs of the megaripples. Uncertainties are however still present when using MBES data; for instance, the data becomes less accurate further away from the ship where the angle between the seabed and the echo sounding device on the ship increases.

(ii): After collection of the bathymetrical data, the raw echo sounding signals are processed before they can be applied in the further analysis. Typical examples of such pre-processing are corrections for the movement of the ship during the measurements and tidal reduction. Different methods of tidal reduction may result in relative large vertical differences between surveys in time. Furthermore, the data are typically gridded to a raster of data points with a fixed resolution in x- and y-direction. The number of data points within each grid cell is dependent on the resolution of the data and the resolution of the grid. The value of a grid cell is determined by taking the minimum, maximum, mean or another statistical value of all raw data points in the cell and also depends on the interpolation algorithm applied. In more recent MBES data, delivered on high resolution grids (2016 Fugro data on a 0.50 x 0.50 m grid), this is of less importance.

(iii): The last mentioned source for uncertainty in the data are due to the applied analysis methods. The exact timing of the measurements of individual data points in the various surveys is not known; there is a certain period in which the data are collected. This leads to an uncertainty of the estimates of the sand wave migration velocities. Furthermore, to arrive at future seabed predictions, the 2016 data is migrated using different migration directions and migration rates (see Section 5.2 for further details). This approach assumes that the seabed is in a state of dynamic equilibrium, which implies that the sand waves will retain their shape and dimensions while they are migrating. Furthermore, event-driven changes of the sand wave shape (e.g. during storms) and seasonal changes may occur (see Section 2.3 and 4.3).

The various sources of uncertainty have to be accounted for in the results by applying an uncertainty band. The uncertainty band that is applied in the analysis consists of four separate contributions:

- Survey inaccuracies;
- Existence and migration of megaripples;
- Finite and limited spatial resolution;
- The assumption of shape retaining sand waves.

Note that the uncertainty band is applied both upward and downward; the upward and downward bands do not necessarily have the same amplitude.

Finally it must be stressed that global effects such as climate change is not taken into account and it is assumed that the system will remain stable and that future seabed levels can be estimated based variations observed in the last 16 years.

5.1.1 Survey inaccuracies

The survey inaccuracies were reported by Fugro and specified as a mean vertical uncertainty of 0.182 meter, based on the characteristics of their measurement system and processing software, adapted at typical HKZWFZ-water depths. This uncertainty band captures the sources of uncertainty mentioned under points (i) and point (ii). As the 2016 MBES data was used in predictions of the future seabed levels, the additional uncertainties because of the use of the 2000 SBES do not have to be accounted for separately.

5.1.2 Megaripples

As described in Section 4.2, megaripples have migration speeds that are so large that many megaripples will pass at each foundation throughout the lifetime of wind farms. Thus, it is neither practical nor possible to make a deterministic analysis of the migration speeds. Therefore, statistical values for megaripple heights are included in the uncertainty band. Since megaripples are included in the predictions of future bathymetries, part of this uncertainty is already covered. To prevent underestimations an additional uncertainty band of 0.15 m downward and 0.20 m upward are included.

5.1.3 Finite spatial resolution

As the bathymetrical data has a finite resolution, it is unlikely that the sand wave crests and troughs are captured by the grid. To account for the loss in height a value of 0.10 m is included in the uncertainty band (upward), while for a loss in depth a value of 0.05 m is included (downward).

5.1.4 Assumption of shape retaining sand waves

The fourth contribution to the uncertainty is the assumption of shape retaining sand waves. In Section 2.3, a detailed description is presented of the physical processes behind sand waves. The conclusions of this section are that sand waves remain more or less similar over decades in HKZWFZ, but (temporary) seasonal changes may occur, mainly related to the occurrence of severe storms. In the predictions of future bed level changes, a rather wide range of migration directions (3 different directions) and migration velocities (3 different velocities) is applied, which is considered to result in a sufficiently wide range of predicted future seabed levels. It is assumed that by applying these ranges, the seasonal changes to sand wave shapes that are described in Section 2.3 and mentioned as source of uncertainty under (iii) are sufficiently accounted for. Therefore, no additional uncertainty was added to the uncertainty band.

5.1.5 Summary of the uncertainty band

The total uncertainty band that is applied on the predicted future bed level changes and corresponding bathymetry therefore becomes:

- **Uncertainty band upward:** 0.182 m (mean survey uncertainty) + 0.20 m (megaripples) + 0.10 m (spatial resolution uncertainty) = *0.482 m, taken as 0.5 m.*
- **Uncertainty band downward:** -0.182 m (mean survey uncertainty) - 0.15 m (megaripples) - 0.05 m (spatial resolution uncertainty) = *0.382 m, taken as 0.4 m*

5.2 Future bathymetries and bed level changes for the period 2016-2051

Note: In this section bed level changes are discussed and presented for the period 2016 to 2051. Additional data are available for year 2056 as part of the GIS data archive, see Appendix A.

The future bathymetries and the corresponding bed level changes are estimated by artificial shifting of the mobile seabed components of the most recent 2016 Bathymetry. Note that the megaripples are included as a mobile component since splitting the sand waves and megaripples resulted locally in a significant loss of sand wave crest height (see Section 4.2). This shifting is done with the aid of the migration directions and associated migration speeds determined in Section 4.1.1 and 4.1.2 respectively. For each transect location a shift in x- and y-direction is calculated by means of the three directions and their associated minimum, mean and maximum migration speeds found for that specific transect. Note that the maximum migration speed does not correspond to the determined 90% non-exceedance value, but is the actual maximum migration speed. In Figure 5.1, the procedure described above is illustrated showing three possible displacements for the three directions, adding up to a total of 9 predictions per transect.

The displacements for all transect locations are then combined and interpolated to a field of shifts in x- and y- directions, resulting in nine displacement fields. By shifting the Mobile Bathymetry according to these displacement fields and adding the Static Bathymetry, nine seabed predictions are constructed. This process is performed for each year in the considered period (2016-2051) by multiplying the migration speed with the number of years passed since 2016. For the total period of thirty years, this implies a total of $9 \times 30 = 270$ distinct bathymetries.

In the next step, the total envelope of all 270 predicted bathymetries plus the 2016 Bathymetry was determined. For each data point, from the stack of bathymetries, the minimum and maximum predicted seabed level changes were determined which correspond to the Lowest SeaBed Level (LSBL) and the Highest SeaBed Level (HSBL) respectively.

Uncertainties are added afterwards by applying the uncertainty band described in the previous section.

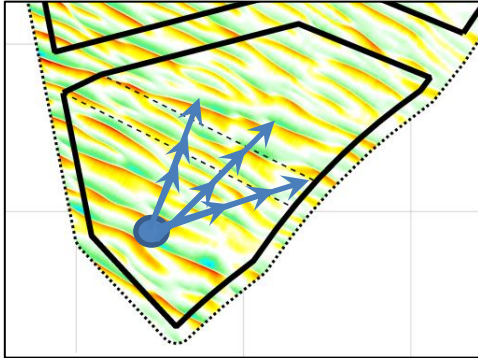


Figure 5.1 Illustration of the 9 possible displacements (blue arrows) for a transect location (blue dot), with use of the three migration directions and their associated minimum, mean and maximum migration speed. The blue arrows are extended for visualisation purposes and do not represent real distances.

An example of seabed predictions along a random transect is shown in Figure 5.2. The figure displays the seabed profile along a certain transect taken from the three available bathymetries (2000, 2010 and 2016) together with the seabed predictions for the period 2016-2051. Shown predictions are a shift of the 2016 Bathymetry towards the right with a certain migration speed. Eventually the lower and upper envelopes are determined by combining all minimum and maximum values. Note that Figure 5.2 is for illustration purpose only and represents an ideal situation where all points along the transect experience an equal shift in x- and y-direction.

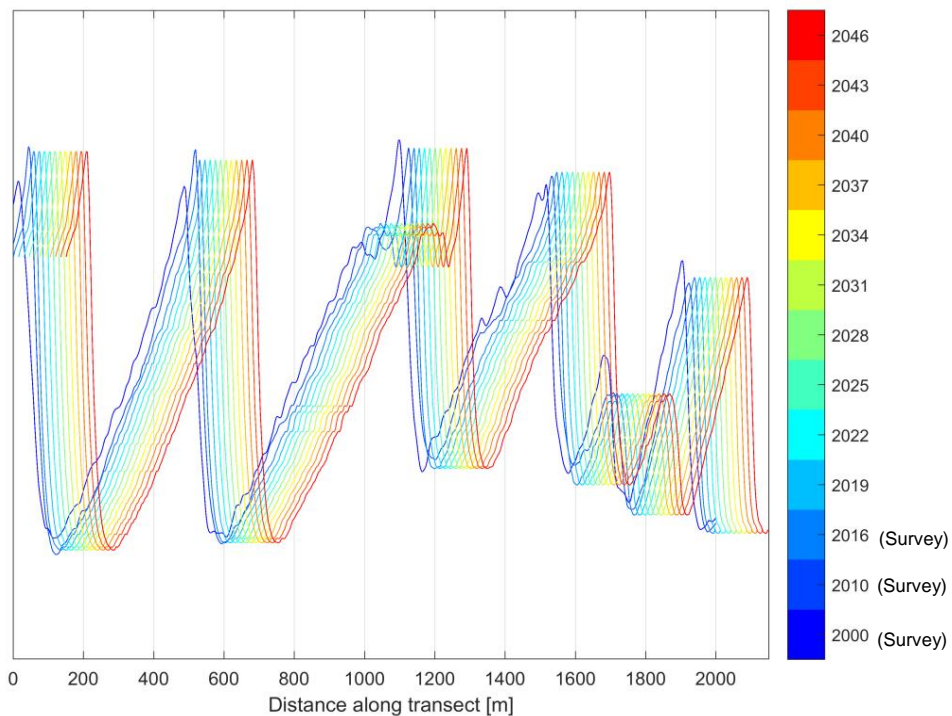


Figure 5.2 Seabed predictions along a random transect in the HKZWFZ for the period 2016-2051. Historical morphodynamic changes are denoted by transects of the 2000, 2010 and 2016 bathymetries. Note: figure for illustration purpose only.

5.3 Best Estimate Bathymetry (BEB)

The Best Estimate Bathymetry (BEB) is calculated for the best estimate migration direction of 28°N (see Section 4.1.1) and its associated mean migration speed (see Section 4.1.2). In Figure 5.3 a difference plot between the best estimate of a 2051 bathymetry and the measured 2016 Bathymetry is shown. In the difference plot the migration of the sand wave field is seen as local rising and lowering of the bathymetry.

The Best Estimate Bathymetry is expected to have the, on average, smallest overall error. In other words: when compared to the actual 2051 bathymetry the BEB₂₀₅₁ is expected to have the smallest area-averaged total difference. At specific locations it can differ significantly, but observed differences are not expected to exceed the limits provided by the LSBL and the HSBL given that the original assumptions for this analysis are satisfied.

The BEB is only provided to give a very rough indication of the possible seabed development during the lifetime of the wind farm and should not be treated as a firm design parameter. For this LSBL and HSBL provide better information (maximum predicted potential seabed level variations at each grid point). However, the BEB does provide a valuable estimate of the seabed to compute the most probable O&M costs (e.g. related to predicted cable re-burial length).

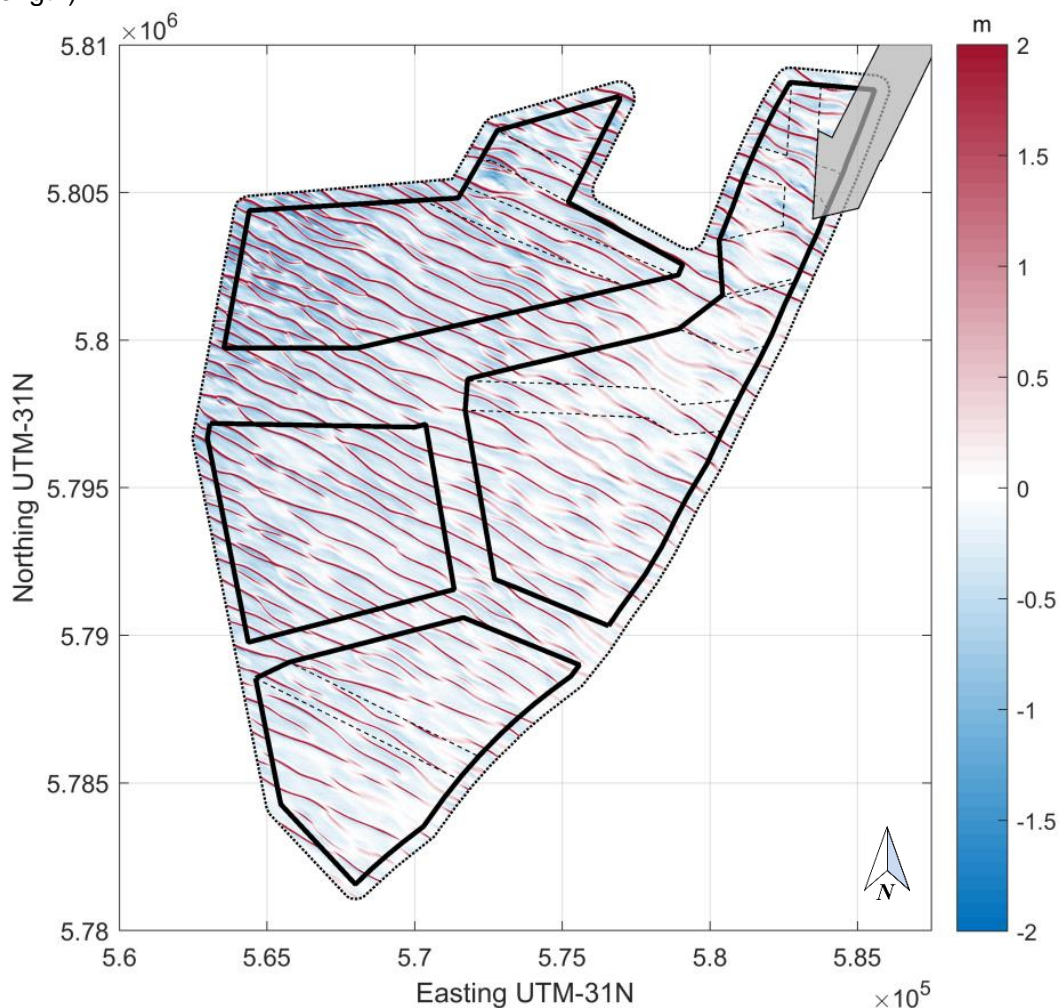


Figure 5.3 Difference between a best estimate of the 2051 bathymetry and the measured 2016 Bathymetry.

5.4 Lowest SeaBed Level (LSBL)

The LSBL is estimated by the lower envelope of all predicted bathymetries combined with the downward uncertainty band, discussed in Section 5.1. The LSBL is the expected minimum seabed level in the lifetime of the wind farm. The result is presented in Figure 5.4. The overall bathymetry of the LSBL looks very similar to the Static Bathymetry, but it is typically a few meters deeper. The LSBL varies between -17.8 m and -28.3 m LAT. The deepest parts are found in the most offshore/western parts of the HKZWFZ.

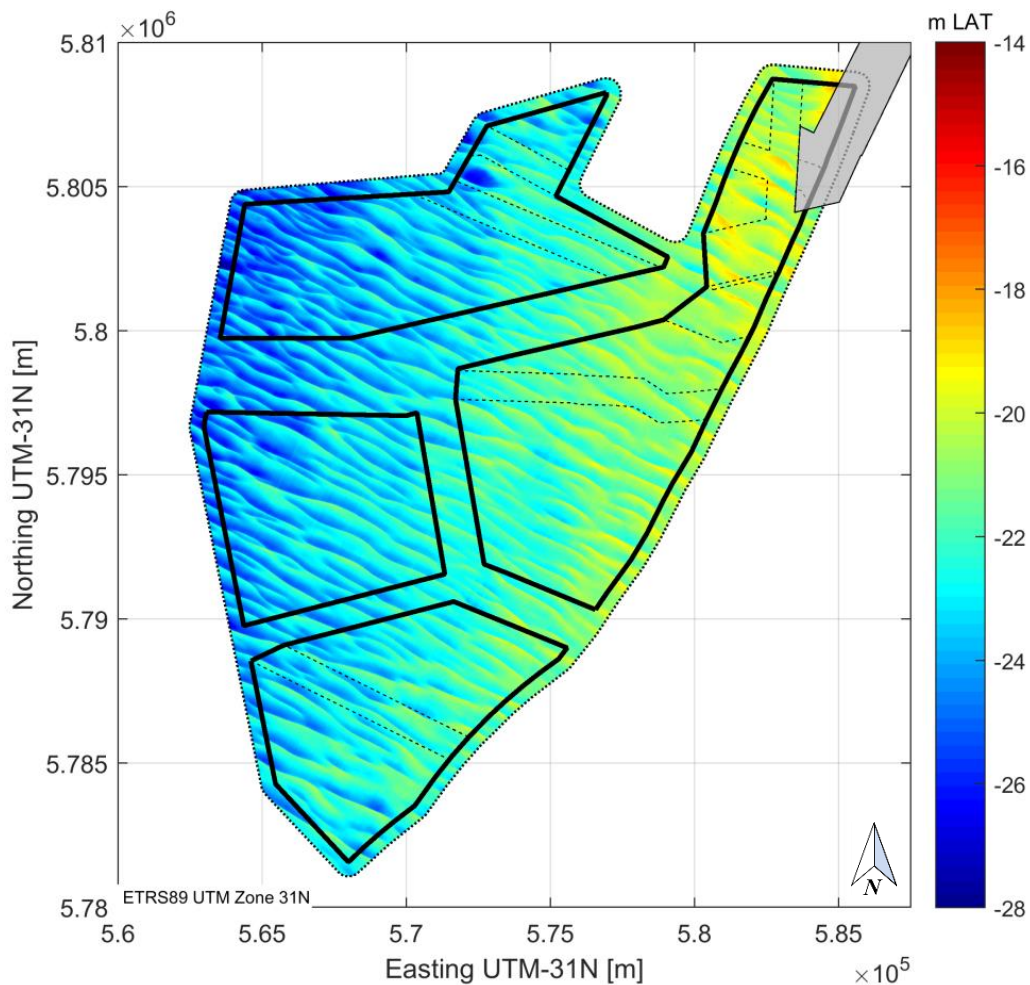


Figure 5.4 The Lowest SeaBed Level (LSBL) for the period 2016-2051. The LSBL is the summation of the lower envelope of the 270 predicted bathymetries for 2017-2051 plus the 2016 Bathymetry with addition of the upward uncertainty band.

Note that at the boundary of the surveyed area, the results are less reliable due to lack of data. It must be stressed that this is related to the survey area, which extends 1 km outside the wind farm area. However, when sand waves are migrating near the boundaries, data may not be available. The area that is potentially affected lies within 200 m from the 2016 survey boundary and the potential changes to the LSBL (and also the HSBL, see next section) will be larger when being closer to the boundary. It should be stressed that the affected area in general is outside of the HKZWFZ and results inside HKZWFZ can therefore be considered to be reliable.

By calculating the difference between the LSBL and the most recent 2016 Bathymetry, the maximum expected seabed level lowering can be predicted, as shown in Figure 5.5. It should be noted that the observed pattern follows the large-scale bedform geometry. The current sand wave crests of the 2016 Bathymetry have the largest predicted lowering in seabed level, up to -3.6 m in the west (with -1.5 m as the 99%-non exceedance value), whereas the highest troughs of the sand waves have a zero predicted lowering when excluding the uncertainty band. This pattern is observed over the entire area, but more nearshore the height variation between the crests and troughs is typically less, as the sand wave height typically decreases with decreasing water depths.

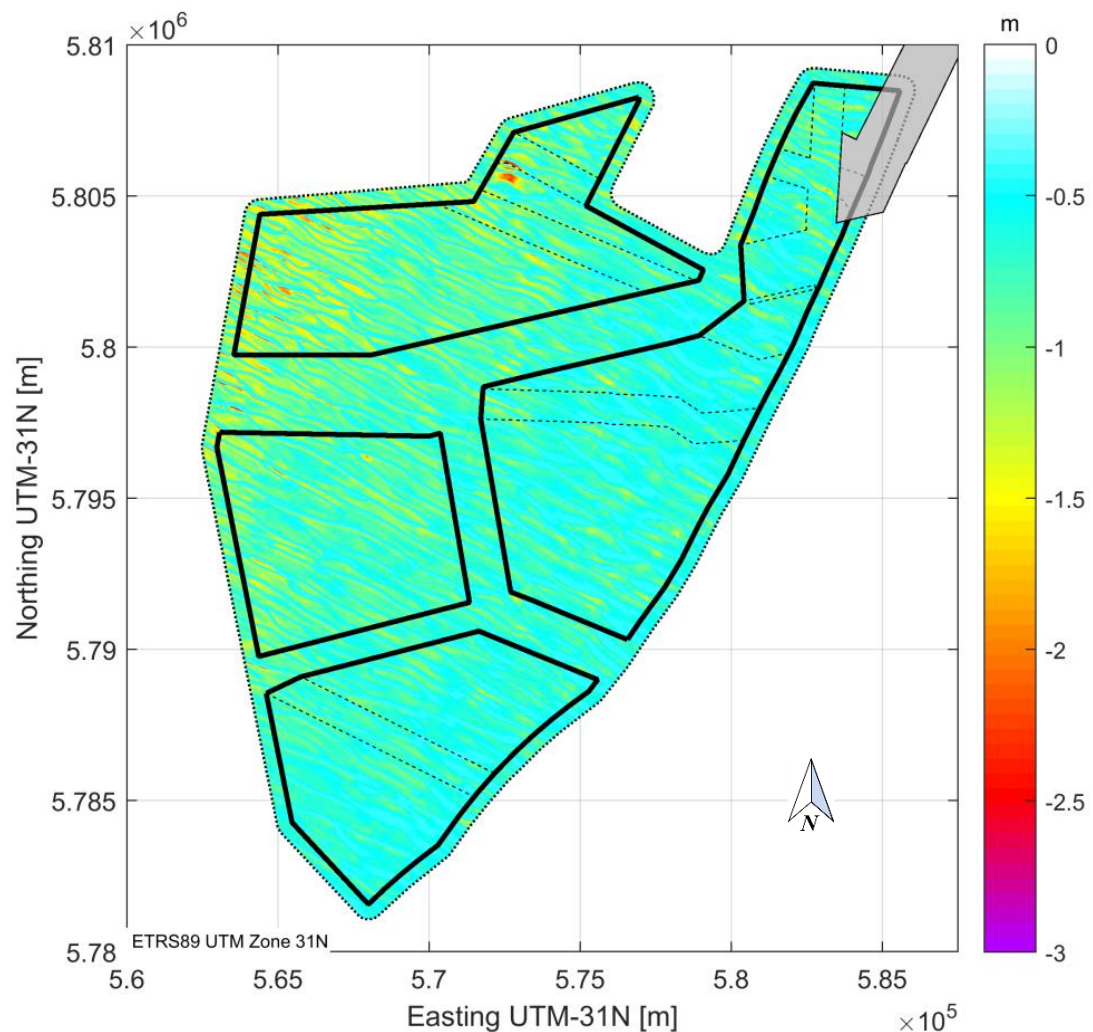


Figure 5.5 The maximum predicted seabed lowering including the downward uncertainty band based on the 2016 Bathymetry. The values indicate the difference between the 2016 Bathymetry and the LSBL (Figure 5.4).

Next, the LSBL is compared with the base of the Holocene formation and the top of the non-erodible Pleistocene layer in the HKZWFZ (see Section 3.4) to check whether the LSBL at some point penetrates one or both. By subtracting the base of the Holocene formation and the top of the non-erodible layer from the LSBL, the remaining layer thickness is calculated. Figure 5.6 indicates that the minimum remaining layer thickness between the LSBL and the base of the Holocene formation and between the LSBL and the top of the non-erodible layer is respectively 0.5 and 2.0 meter. There is hence no reason to adjust the LSBL due to the presence of non-erodible layers.

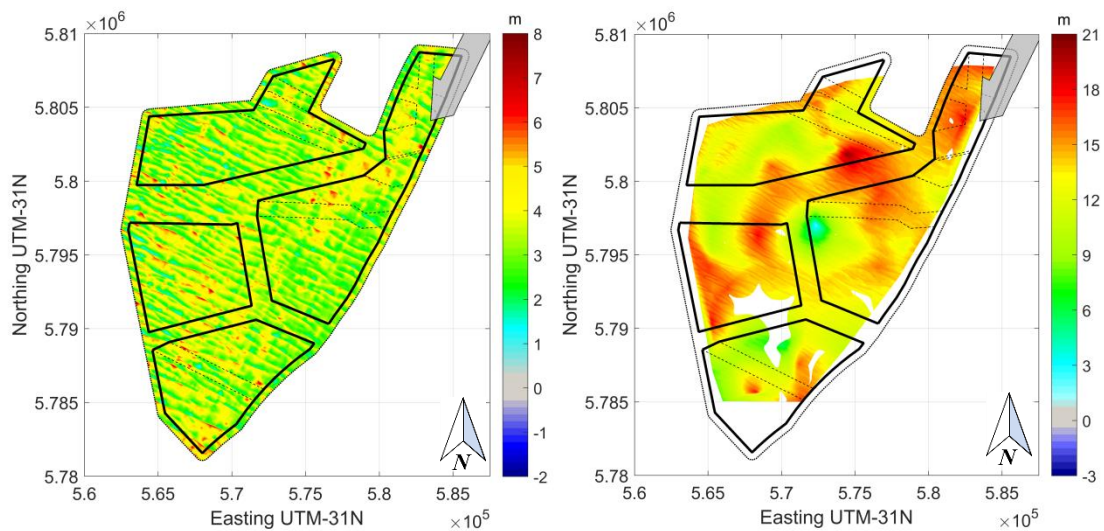


Figure 5.6 Remaining layer thickness between the LSBL and the Base of the Holocene formation (left plot) and between the LSBL and the top of the shallowest non-erodible layer (right plot). White areas indicate either missing data or complete absence of non-erodible layers.

5.5 Highest SeaBed Level (HSBL)

Similar to the procedure to determine the LSBL, the Highest SeaBed Level (HSBL) was determined. Now the upper envelope of the 270 predicted bathymetries was used and by adding the upward uncertainty band, the Highest SeaBed Level (HSBL) is obtained. The HSBL is shown in Figure 5.7. The overall bathymetry of the HSBL looks very similar to the Static Bathymetry, but it is typically a few meters shallower. The HSBL varies between -15.3 m and -27.3 m LAT.

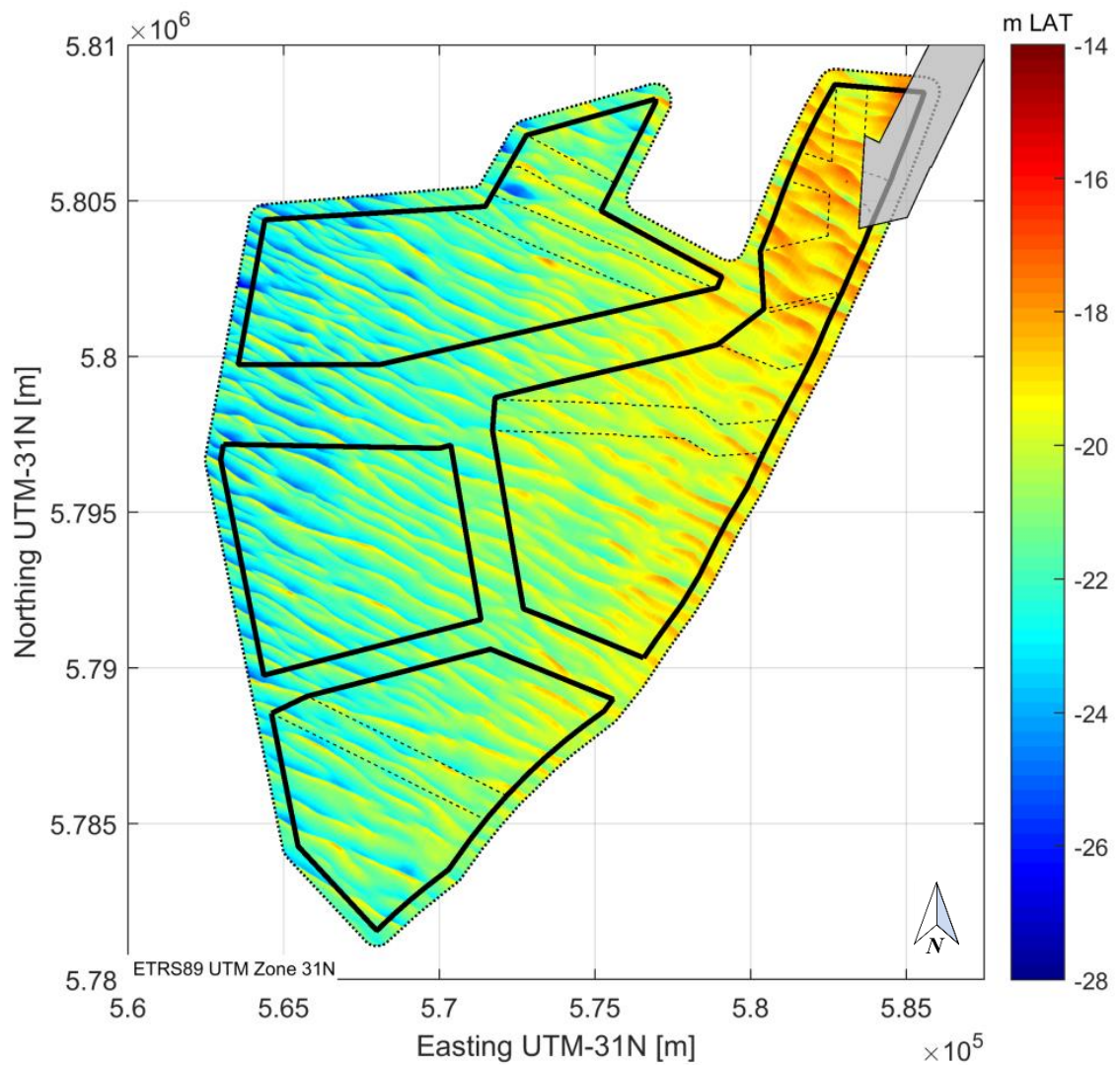


Figure 5.7 The Highest SeaBed Level (HSBL). The HSBL is the summation of the upper envelope of the 270 predicted bathymetries for 2017-2051 plus the 2016 Bathymetry with addition of the upward uncertainty band.

By calculating the difference between the HSBL and the 2016 Bathymetry, the maximum expected rise of the seabed can be predicted (Figure 5.8), which appears to be approximately 1 m in the majority of the site. The current sand wave troughs of the 2016 Bathymetry have the largest predicted rise in seabed level, up to 7.2 m in the west (with +4.1 m as the 99%-non exceedance value), whereas the highest crests of the sand waves have a zero predicted rise when excluding the uncertainty band. Note that the seabed close to the foundations will most likely not rise significantly, because local scour will counteract this. Buried electricity cables that cause no flow disturbance themselves will obviously not have this “beneficial” scour effect and therefore will experience a rising seabed if a sand wave crest passes over. This might be relevant for the maximum cable temperature (“thermal bottleneck effect”).

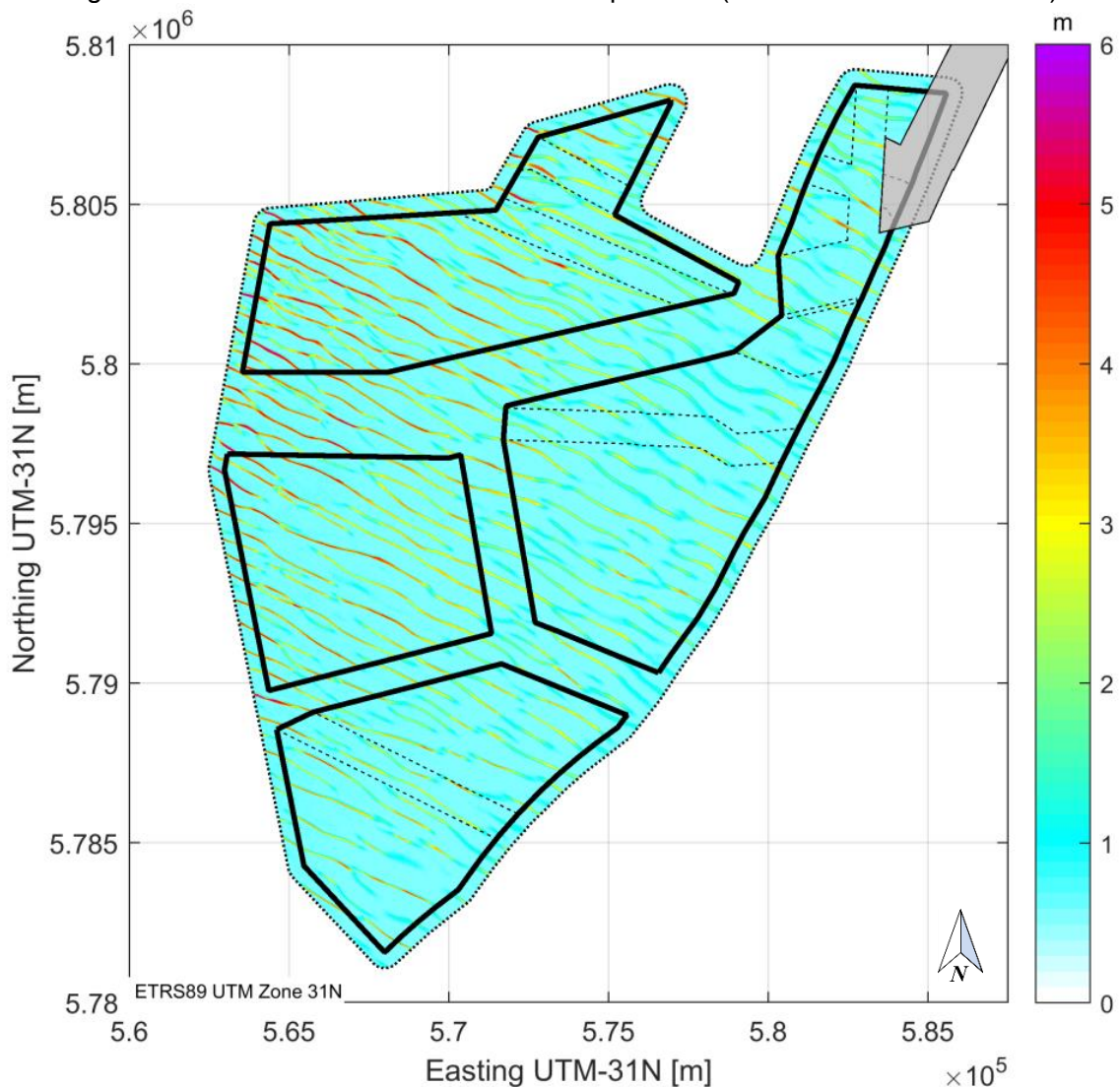


Figure 5.8 The maximum predicted seabed rising including the upward uncertainty band based on the 2016 Bathymetry. The values indicate the difference between the 2016 Bathymetry and the HSBL (Figure 5.7).

5.6 Classification zones for offshore foundations and cables

In the final step, the LSBL and HSBL and the corresponding predicted seabed level lowering and rising are translated into possible classification zones for foundations and electricity cables. The classification of these zones is based on the predicted seabed level lowering or rising (see Table 5.1). The classification was chosen less restrictively for rising seabed levels, because close to the structures, local scour will counteract rising seabed levels. This does not apply to electricity cables, which are buried in the seabed; rising seabed levels can be of influence on the maximum cable temperature.

Note that these classifications are for indicative and illustration purposes only. The actual classification is dependent on the design of the support structures and properties of electricity cables and should be adjusted accordingly once this information is available.

Classification of zones	Bed level lowering [m]	Bed level rising [m]
Preferred	$0 > dz \geq -1$	$0 < dz \leq 1$
Possible	$-1 > dz \geq -1.5$	$1 < dz \leq 2$
Better avoided	$-1.5 > dz \geq -2$	$2 < dz \leq 3$
Un-recommended	$dz < -2$	$dz > 3$

Table 5.1 Indicative classification zones for bed level lowering and rising.

Figure 5.9 shows how the classification zones are dependent on the LSBL, HSBL and the predicted seabed level changes. The top plot displays the location of transect 1001, one of the 3904 transects used in the sand wave analysis, on top of the 2016 Bathymetry. The bottom plot shows the 2016 Bathymetry together with the upper and lower envelope of the migrated Sand Wave Field and the LSBL and HSBL. The corresponding predicted bed level changes are displayed in the middle plot, together with the classification zones. The asymmetrical shape of LSBL and HSBL indicates that the sand waves will have migrated in the north-northeast direction with similar migration velocities. Furthermore, the largest seabed level changes are found respectively above and below the position of the troughs and crests in the 2016 Bathymetry. As indicated in the figure, the predicted seabed lowering is within the thickness of the Holocene formations (indicated by the dashed magenta line).

The spatial distribution of the classification zones is displayed in Figure 5.10. The classification of the zones differs for seabed lowering and rising (Table 5.1). This implies that for each data point, two classifications apply; one for the predicted seabed rising and one for the predicted seabed lowering. For each point, the more strict classification of the two is displayed in the map (with 'un-recommended' being the strictest recommendation). The full overview of classifications zones for the HKWFZ is displayed in the bottom plot of Figure 5.10. A zoom plot of the area around transect 1001 is displayed in the top plot. Spatial distributions of the classification zones for the seabed lowering and seabed rising are displayed in Figure 5.11.

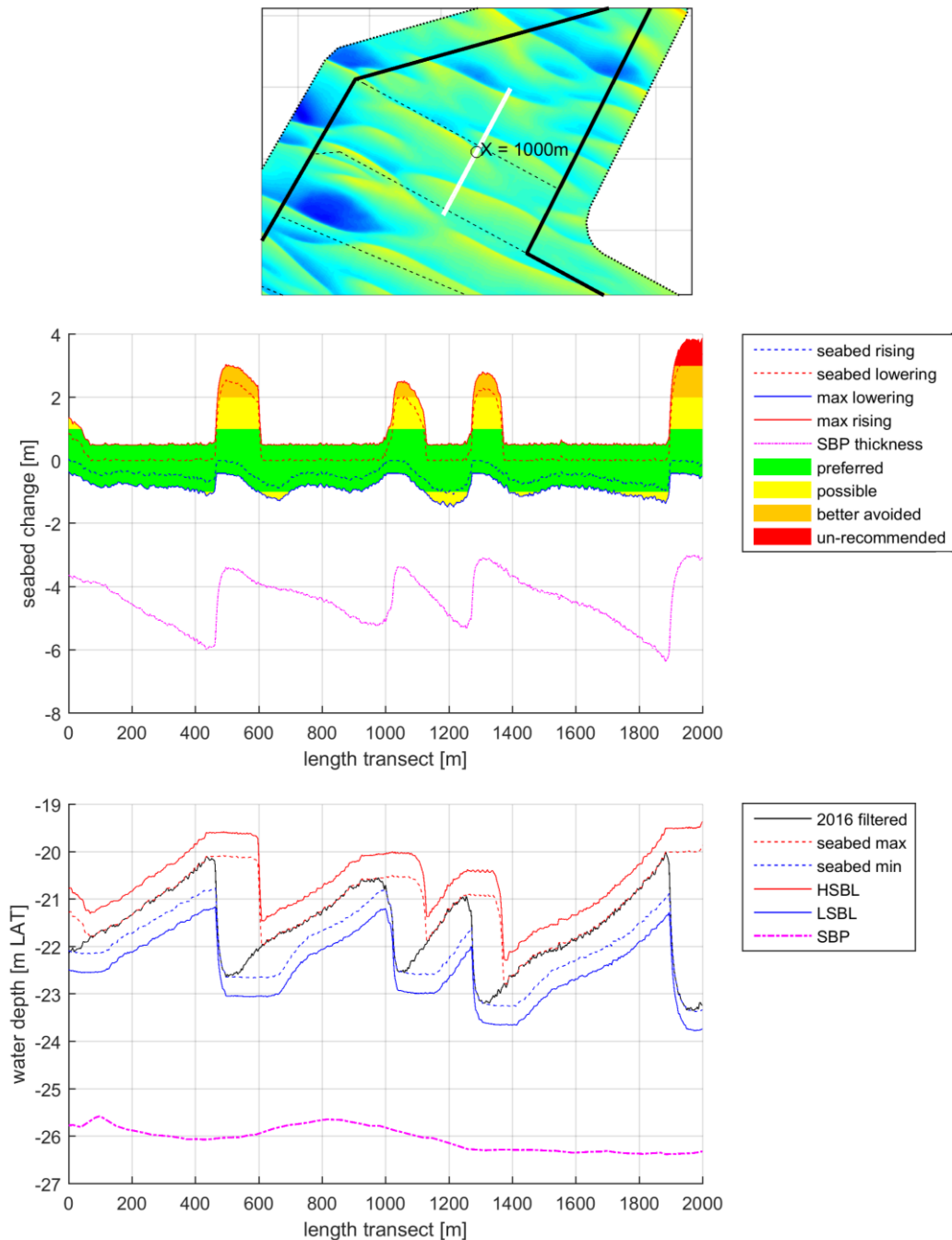


Figure 5.9 Overview of classification zones for 1 of the 3904 transects (transect 1001) used in the sand wave analysis. Top plot: Zoom plot of location of transect on top of the 2016 Bathymetry at WFS-I. Middle plot: Seabed rising and lowering relative to the 2016 Bathymetry (solid red/blue lines). The maximum rising and lowering, including the uncertainty bands, are indicated by the dashed red/blue lines. The base of the Holocene formations is indicated as thickness below the predicted bed levels by the dashed magenta line (SBP). Bottom plot: 2016 Bathymetry (solid black line), together with the upper envelope of the migrated Sand Wave Field (dashed red line), the lower envelope of the migrated Sand Wave Field (dashed blue line) and the LSBL (solid blue line) and HSBL (solid red line). The crests and troughs of sand waves are levelled, because these are already at their highest and lowest level (Sections 5.4 and 0). The base of the Holocene formations is indicated by the dashed magenta line (SBP).

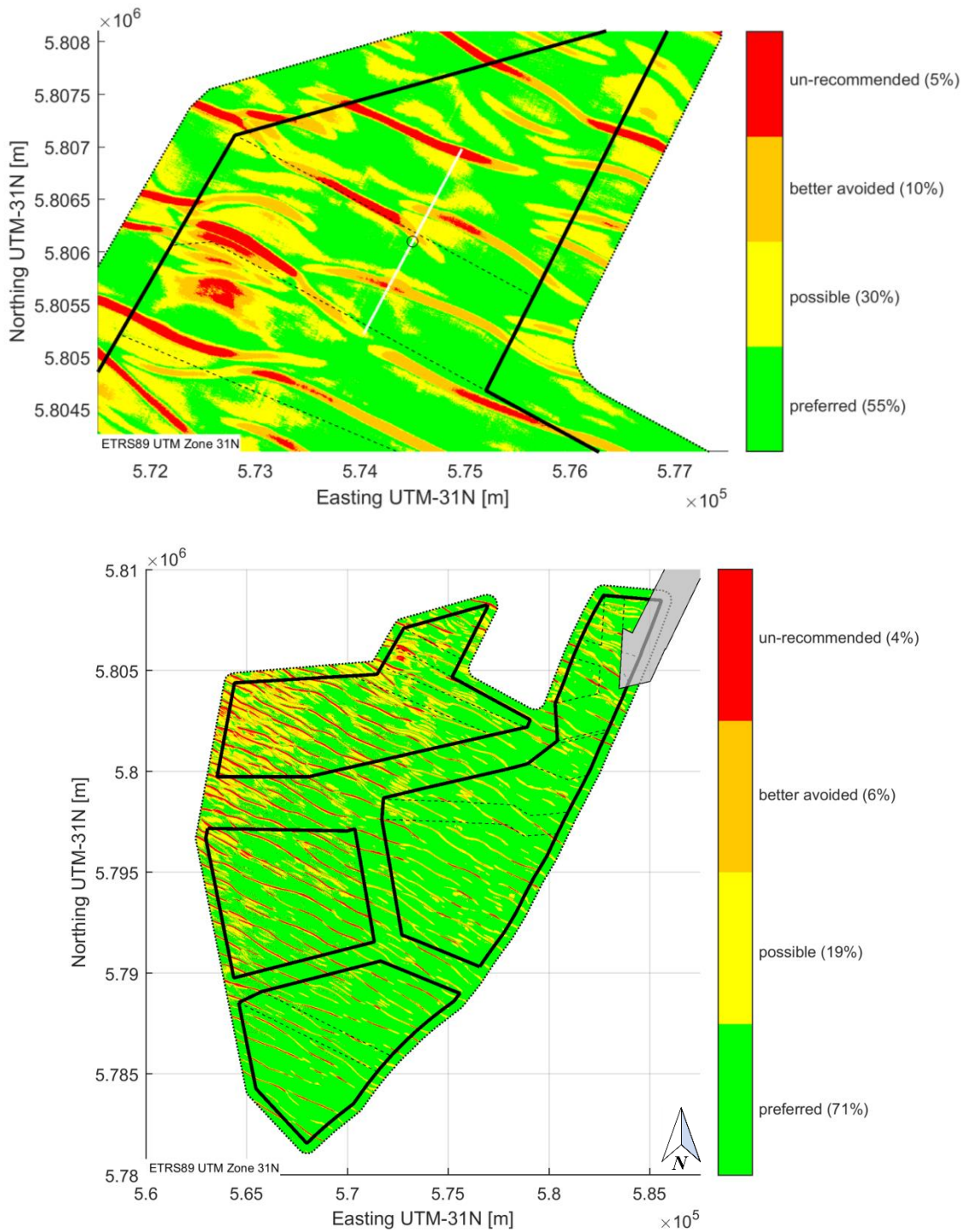


Figure 5.10 Overview map of classification zones including classification for both highest and lowest seabed levels.
 Top plot: Zoom plot of classification zones in area around transect 1001 in WFS-I (see Figure 5.9).
 Bottom plot: Overview map of classification zones of Hollandse Kust (zuid) Wind Farm Zone.

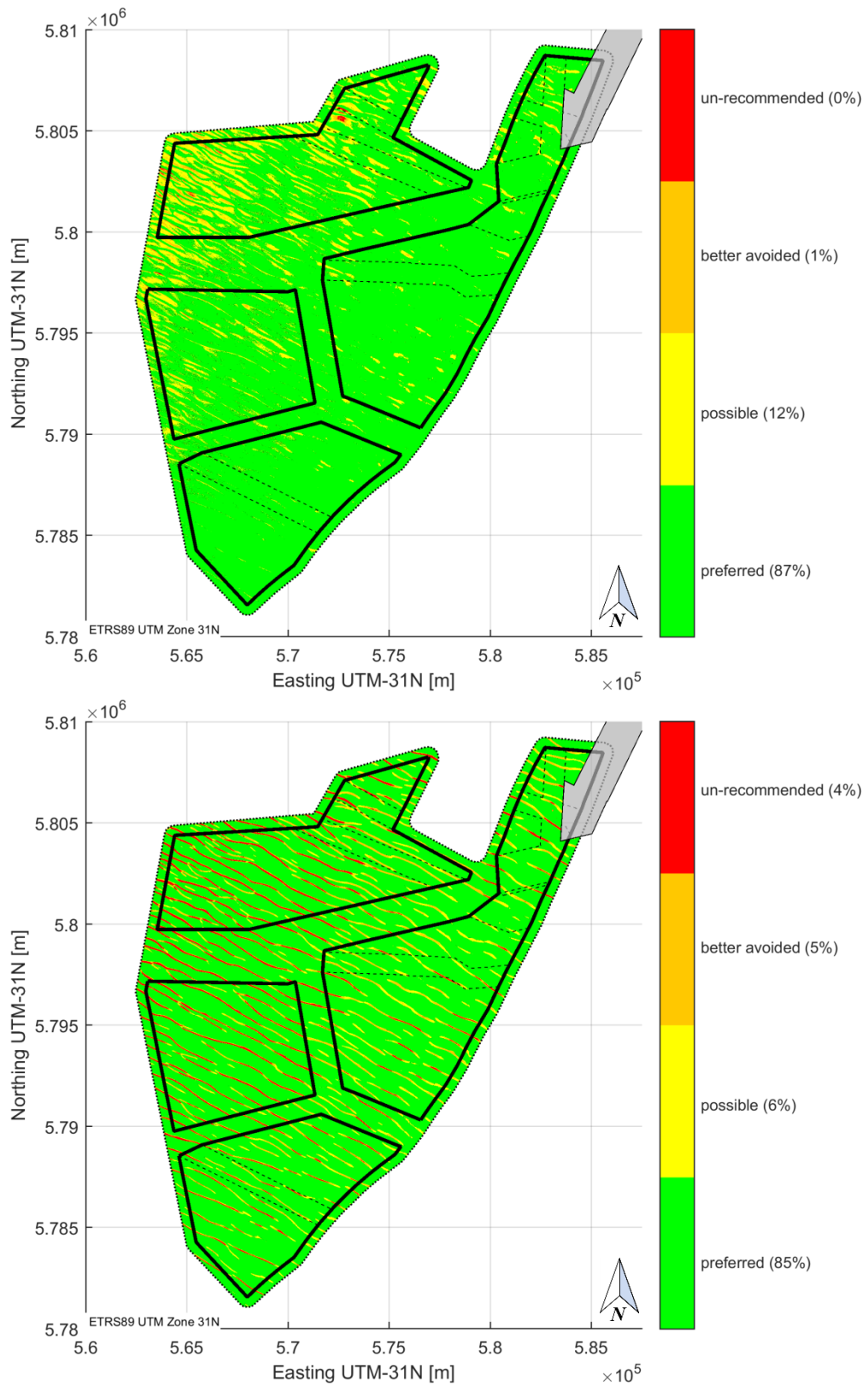


Figure 5.11 Classification zones. Top plot: Classification zones of the seabed lowering in the HKZWFZ. Bottom plot: Classification zones of the seabed rising in the HKZWFZ.

6 Conclusions and considerations

6.1 Conclusions

The bathymetry in the Hollandse Kust (zuid) Wind Farm Zone (HKZWFZ) has a relatively uniform morphology without prominent sand banks or other large-scale features. An analysis of the large-scale seabed variations shows that the underlying seabed may be considered static over the lifetime of the wind farm. The top sediment layer is mobile and covered with sand waves migrating towards the north-northeast with megaripples on top. Considering the entire HKZWFZ, the sand waves have wavelengths in the range of 200 to 1000 m, heights of 1.1 to 4 m and local migration speeds may be as high as 5.2 m/year (in north-northeast direction).

The HKZWFZ is subdivided into four wind farm sites (WFS) for offshore wind farm development. Table 6.1 summarizes the sand wave characteristics for the entire HKZWFZ and per WFS. Although some variations in sand wave dimensions and migration speeds are observed, it is clear that morphodynamic seabeds are present in the entire HKZWFZ.

Wind Farm Sites (WFS)	Sand wave height non-exceedance (2016) [m]		Sand wave length non-exceedance (2016) [m]		Migration speed [m/yr] in most frequently observed direction 28° N	
	50%	90%	50%	90%	50%	90%
WFS-I	2.5	4.0	427	708	2.0	2.5
WFS-II	2.7	3.9	503	757	1.5	2.0
WFS-III	2.3	3.3	578	918	1.2	1.6
WFS-IV	1.9	2.7	631	950	1.5	2.6
Combined HKZWFZ	2.3	3.7	511	832	1.7	2.3

Table 6.1 Selected non-exceedance values for the sand wave dimensions and migration rates for the combined HKZWFZ and per individual wind farm site (WFS); values are based on the 2016 survey for the height and length and on the 2010 and 2016 surveys for the migration rates.

A review of available geological and geophysical data indicated that non-erodible layers exist, but that they are located too deep to influence the sand wave migration. Numerical analyses of the hydrodynamics and sediment transport in the area indicate that net sediment transport is aligned with the residual tidal flow towards the north-northeast and that the net sediment transport increases from south to north. Numerical flow modelling hence confirmed the findings of the data-driven methods.

For the development of wind turbine support structures, electricity cables and high voltage stations, a Best Estimate Bathymetry (BEB), a Lowest SeaBed Level (LSBL) and a Highest SeaBed Level (HSBL) are estimated. The BEB represents the predicted bathymetry for a certain year with the smallest expected average error. The LSBL and HSBL indicate the lowest and highest seabed levels, respectively, for the period 2016-2051, including uncertainty bands.

The resulting LSBL shows a bathymetric shape similar to the existing static part of the bathymetry, but typically a few meters lower. Comparison of the LSBL with the most recent bathymetry from 2016 shows a predicted maximum local seabed level lowering of

approximately 3.5 m. As expected, the largest lowering is found at the location of the existing sand wave crests, while minimal lowering is found at the location of the sand wave troughs.

The HSBL shows a bathymetric shape similar to the existing static part of the bathymetry, but typically several meters higher and locally as much as 6.9 m. Opposite to the seabed lowering, the largest potential rise of the seabed level is found at the current locations of the troughs just in front of the steep sand wave lee sides, with minimal rising at locations of the present sand wave crests.

The predicted seabed level changes presented in this study follow from the applied morphological analysis techniques, describing the (uncertainty of the) physics and the natural variability of the analysed morphological system. Apart from the safety bands following from survey and method uncertainties, no additional safety margins for design purposes have been applied.

6.2 Considerations for cables and foundations in HKZWFZ

Morphodynamic activity such as sand wave migration may pose a threat to foundations and cables if not considered in the design and general wind farm planning. It is beyond the scope of this report to give specific design recommendations, but in the following a few general points of attention are highlighted.

When defining the initial conditions for the design basis the Best Estimate Bathymetry (BEB) at the time of foundation installation should be taken into consideration since the seabed in some areas may have changed relative to the 2016 Bathymetry. Furthermore, future morphodynamic variations should be considered when estimating the variations which may be observed during the life time of the wind farm.

6.2.1 Cables

Within the offshore wind industry currently 70-80% of insurance claims are related to failures of cables. On average in Europe one export cable and about 10 inter-array cables fail every year. Cable failures pose one of the highest risks as it can blackout an entire wind farm. In addition, cable monitoring and repair require expensive marine operations. One of the causes of cable failures is morphodynamic activity such as sand wave migration. Typical failure mechanisms are:

- Insufficient cable burial depth
- Overheating
- Internal stresses
- Free spanning
- Dragging anchors or fishnets, dropped objects

As the sand waves migrate, a cable located near the sand wave crest may experience significant seabed lowering, which may make the cable vulnerable to anchors or other threats. On the other hand, if a sand wave crest passes the cable that was formerly in a sand wave trough it may experience a significant increase in the burial depth, which locally may cause temperature increases around the cable. Depending of the specifications of the cable and environmental requirements, this may be a problem.

Cables crossing a sand wave field, which spatially migrate with different speeds, may experience a local stress build-up due to an uneven strain. When combined with e.g. thermal

stresses this may become critical. It is well known that cables exposed on the seafloor may experience local scour, which in some cases may be sufficient to undermine the cable, causing a free span. When combined with sand wave migration the risk of free spanning increases. A free span of a cable may, besides a local stress build up, also experience vortex induced vibrations.

6.2.2 Foundations

Seabed level changes may also pose a problem to the foundations of the wind turbines or sub-stations. Large seabed changes may cause problems with respect to:

- Geotechnical stability due to reduced support
- Stability of scour protection
- Change in eigen-frequencies

If a foundation is installed on a sand wave crest it may experience a significant lowering, which combined with e.g. scour may cause insufficient geotechnical bearing capacity due to reduced support from the surrounding soil. One way to prevent this is installation of scour protection systems, however, if the scour protection is not sufficiently flexible and able to adjust to the seabed variations it may become unstable and in worst case fail to protect the foundation. Therefore locations with large predicted seabed lowering are best avoided.

As the fixation level of the pile changes due to morphodynamic activity, the dynamics of the combined system including foundation and tower may change. In the worst case the natural frequencies of the system changes which may lead to an undesired amplification of harmonic loading.

6.2.3 Identification of potential risks related to morphodynamic and mobile seabeds

Similar to Table 5.1 in the report “Geological Ground Model” by Fugro (2016) potential risks are addressed for several structure types. The same classification of structure types is used as in Fugro (2016). Here, only risks related to morphodynamic and mobile seabeds are summarized in Table 6.2 3; other potential risks are not addressed. This section is indicative only and not intended to be complete or comprehensive.

Morphodynamic risks are related to large-scale seabed variations (due to natural processes, unrelated to the presence of man-made structures); risks related to a mobile seabed here refer to local interaction between the hydrodynamics, the structure and the mobile seabed.

As can be seen from this table, potential risks for all structure types can be mitigated by either a careful selection of the location with respect to expected seabed lowering or by taking appropriate mitigation measures or by a combination of both.

Structure type	Potential risks related to morphodynamics of the seabed	Potential risks related to mobile seabed (sediments)
Pile Foundation (PL)	Significant risk for change in eigen-frequency if piles are installed at unfavourable locations and morphodynamics are not taken into account in the structure and/or scour protection design. When installed at carefully selected locations the risks can be low to negligible.	Scour around the foundation might change the eigen-frequency of the pile. Pile foundations can potentially be designed for the expected scour depth in HKZWFZ, but a scour protection might be more cost-efficient, especially for larger turbines and larger pile diameters.
Jackup Platform (JU)	Negligible risk due to limited duration of jack-up operations (relative to the timescale of morphodynamic processes)	Low risk for short-term operations (of a few days), significant risk for longer operations (weeks to months) depending on the leg and spud can type and penetration depth. Scour protection might be required also for temporary operations.
Gravity Base Foundation (GB)	Low risk if installed in sand wave troughs; for other locations seabed preparation (e.g. dredging until LSBL) is recommended.	Significant risk if the GB is not protected against scour. This risk can be managed by installing a scour protection, possibly in combination with seabed preparation.
Suction Caisson Foundation (SC)	Low risk if installed in sand wave troughs; for other locations extension of the suction cans or seabed preparation (e.g. dredging) is recommended.	Scour can pose a significant risk to SC, but they can be designed with more streamlined shapes to reduce scour. Also the length of the suction cans can be increased. Otherwise a scour protection is recommended that does not interfere with the suction process during installation of the suction cans.
Cable (CB)	Negligible risk in areas with a stable seabed; low risk in areas with a (slightly) rising seabed if thermal characteristics of the cable are taken into account in cable design; significant risk on cable exposure in areas with a lowering seabed and a small initial cable burial depth.	As long as the cable is buried sufficiently deep (for other potential threats such as anchor dragging, dropped objects etc.) the risks are low to negligible. Special attention should be given to the areas just around the scour protections of the wind turbine foundations, where due to edge scour (mainly NE of the scour protection) the cables may become exposed after some years. Also cable crossings require special attention.

Table 6.2 3 Overview of potential risks related to morphodynamic and mobile seabeds for similar structure types as described in Fugro (2016); this table is indicative only and not intended to be complete or comprehensive.

References

- Ashley, G.M. (1990). Classification of large-scale subaqueous bedforms: a new look at an old problem-SEPM bedforms and bedding structures. *Journal of Sedimentary Research*, 60(1).
- Besio, G., Blondeaux, P., Brocchini, M., & Vittori, G. (2004). On the modeling of sand wave migration. *Journal of Geophysical Research: Oceans*, 109(C4).
- Besio, G., & Rodriguez, M.A.L. (2006). Sediment transport patterns in the neighbourhood of cylindrical porous structures: The "Mar de Trafalgar" offshore wind farm. *Coastal Engineering*, 2318-2329.
- Borsje, B.W., de Vries, M.B., Bouma, T.J., Besio, G., Hulscher, S.J.M.H., & Herman, P.M.J. (2009). Modeling bio-geomorphological influences for offshore sandwaves. *Continental shelf research*, 29(9), 1289-1301.
- Borsje, B.W., Kranenburg, W.M., Roos, P.C., Matthieu, J., & Hulscher, S.J.M.H. (2014). The role of suspended load transport in the occurrence of tidal sand waves. *Journal of Geophysical Research: Earth Surface*, 119(4), 701-716.
- Borsje, B.W., Roos, P.C., Kranenburg, W.M., & Hulscher, S.J.M.H. (2013). Modeling tidal sand wave formation in a numerical shallow water model: The role of turbulence formulation. *Continental Shelf Research*, 60, 17-27.
- Buijsman, M.C., & Ridderinkhof, H. (2008a). Long-term evolution of sand waves in the Marsdiep inlet. I: High-resolution observations. *Continental shelf research*, 28(9), 1190-1201.
- Buijsman, M.C., & Ridderinkhof, H. (2008b). Long-term evolution of sand waves in the Marsdiep inlet. II: Relation to hydrodynamics. *Continental shelf research*, 28(9), 1202-1215.
- Busschers, F.S., Kasse, C., Van Balen, R.T., Vandenberghe, J., Cohen, K.M., Weerts, H.J.T., . . . Bunnik, F.P.M. (2007). Late Pleistocene evolution of the Rhine-Meuse system in the southern North Sea basin: imprints of climate change, sea-level oscillation and glacio-isostasy. *Quaternary Science Reviews*, 26(25), 3216-3248.
- Cherlet, J., Besio, G., Blondeaux, P., Van Lancker, V., Verfaillie, E., & Vittori, G. (2007). Modeling sand wave characteristics on the Belgian Continental Shelf and in the Calais-Dover Strait. *Journal of Geophysical Research: Oceans*, 112(C6).
- Deigaard, R., & Fredsø, J. (1986). Offshore sand waves. *Coastal Engineering Proceedings*, 1(20).
- Deltares. (2011). The scientific validation of the hydrographic survey policy of the Netherlands Hydrographic Office, Royal Netherlands Navy. Ref: 1201907-000-BGS-0008; final report data October 2011.
- Deltares. (2014a). 3D/2D modelling suite for integral water solutions.
- Deltares. (2014b). Quick scan windfarm area Zuid-Hollandse Kust. Ref: 1210359-000-HYE-0003; final report, dated 28 November 2014.
- Deltares. (2015a). Geological study Hollandse Kust (zuid) Wind Farm Zone. Ref: 1221136-000-BGS-0006; final report, dated 22 December 2015.
- Deltares. (2015b). Morphodynamics of Borssele Wind Farm Zone WFS-I and WFS-II; Prediction of seabed level changes between 2015 and 2046. Ref: 1210520-000-HYE-0004; final report, dated 26 June 2015.
- Deltares. (2016a). Hollandse Kust (zuid) Field Measurement Campaign Validation Report. Ref: 12230377-001-HYE-0000; final report.
- Deltares. (2016b). Morphodynamics of Borssele Wind Farm Zone WFS-IV, WFS-III and WFS-V; Prediction of seabed level changes between 2015 and 2046. Ref: 1210520-000-HYE-0012; final report, dated 25 January 2016.
- Dorst, L.L., Roos, P.C., & Hulscher, S.J.M.H. (2011). Spatial differences in sand wave dynamics between the Amsterdam and the Rotterdam region in the Southern North Sea. *Continental shelf research*, 31(10), 1096-1105.

- Dorst, L.L., Roos, P.C., Hulscher, S.J.M.H., & Lindenberg, R.C. (2009). The estimation of sea floor dynamics from bathymetric surveys of a sand wave area. *Journal of applied geodesy*, 3(2), 97-120.
- Fugro. (2016). Geophysical Site Investigation Survey / Hollandse Kust (Zuid) Wind Farm Development Zone / Wind Farm Site I to IV (B ed.).
- Hijma, M.P., Cohen, K.M., Hoffmann, G., Van der Spek, A.J.F., & Stouthamer, E. (2009). From river valley to estuary: the evolution of the Rhine mouth in the early to middle Holocene (western Netherlands, Rhine-Meuse delta). *Netherlands journal of geosciences*, 88(01), 13-53.
- Hijma, M.P., Van der Spek, A.J.F., & Van Heteren, S. (2010). Development of a mid-Holocene estuarine basin, Rhine–Meuse mouth area, offshore The Netherlands. *Marine geology*, 271(3), 198-211.
- Houthuys, R., Trentesaux, A., & De Wolf, P. (1994). Storm influences on a tidal sandbank's surface (Middelkerke Bank, southern North Sea). *Marine Geology*, 121(1), 23-41.
- Hulscher, S.J.M.H. (1996). Tidal-induced large-scale regular bed form patterns in a three-dimensional shallow water model. *Journal of Geophysical Research: Oceans*, 101(C9), 20727-20744.
- Hulscher, S.J.M.H., & den Brink, G.M. (2001). Comparison between predicted and observed sand waves and sand banks in the North Sea. *Journal of Geophysical Research: Oceans*, 106(C5), 9327-9338.
- IHO. (1988). IHO Standards for Hydrographic Surveys (4th edition. ed., Vol. Special publication 44). Monaco: International Hydrographic Bureau.
- Knaapen, M.A.F., & Hulscher, S.J.M.H. (2002). Regeneration of sand waves after dredging. *Coastal Engineering*, 46(4), 277-289.
- Matthieu, J., & Raaijmakers, T. (2012). *Interaction Between Offshore Pipelines and Migrating Sand Waves*. Paper presented at the ASME 2012 31st International Conference on Ocean, Offshore and Arctic Engineering.
- McCave, I.N. (1971). Sand waves in the North Sea off the coast of Holland. *Marine geology*, 10(3), 199-225.
- Németh, A.A., Hulscher, S.J.M.H., & de Vriend, H.J. (2002). Modelling sand wave migration in shallow shelf seas. *Continental shelf research*, 22(18), 2795-2806.
- Papili, S., Wever, T., Dupont, Y., & Van Lancker, V. (2014). Storm influence on the burial of objects in a shallow sandy shelf environment. *Marine Geology*, 349, 61-72.
- Passchier, S., & Kleinhans, M.G. (2005). Observations of sand waves, megaripples, and hummocks in the Dutch coastal area and their relation to currents and combined flow conditions. *Journal of Geophysical Research: Earth Surface*, 110(F4).
- Peters, S.E., & Loss, D.P. (2012). Storm and fair-weather wave base: A relevant distinction? *Geology*, 40(6), 511-514.
- Rijkswaterstaat. (2016). MATROOS. 2016
- Rijsdijk, K.F., Passchier, S., Weerts, H.J.T., Laban, C., Van Leeuwen, R.J.W., & Ebbing, J.H.J. (2005). Revised Upper Cenozoic stratigraphy of the Dutch sector of the North Sea Basin: towards an integrated lithostratigraphic, seismostratigraphic and allostratigraphic approach. *Netherlands Journal of Geosciences/Geologie en Mijnbouw*, 84(2).
- Robertson, P.K. (2009). Interpretation of cone penetration tests—a unified approach. *Canadian Geotechnical Journal*, 46(11), 1337-1355.
- Staub, C., & Bijker, R. (1990). Dynamic numerical models for sand waves and pipeline self-burial. *Coastal Engineering Proceedings*, 1(22).
- Sterlini, F., Hulscher, S.J.M.H., & Hanes, D.M. (2009). Simulating and understanding sand wave variation: A case study of the Golden Gate sand waves. *Journal of Geophysical Research: Earth Surface*, 114(F2).
- Sterlini, F.M., van Dijk, T.A.G.P., IJzer, S., & Hulscher, S.J.M.H. (2012). *Seasonal changing sand waves and the effect of surface waves*. Paper presented at the 5th International Short Conference on Applied Coastal Research (SCACR 2011), Aachen, Germany.

- Terwindt, J.H.J. (1971). Sand waves in the Southern Bight of the North Sea. *Marine Geology*, 10(1), 51-67.
- Van Dijk, T.A.G.P., & Egberts, P.J.P. (2008). *The variability of sand wave migration in the North Sea*. Paper presented at the Proceedings of the 3rd international workshop on Marine Sand waves and River Dune Dynamics, Leeds (UK), University of Leeds.
- van Dijk, T.A.G.P., & Kleinhans, M.G. (2005). Processes controlling the dynamics of compound sand waves in the North Sea, Netherlands. *Journal of Geophysical Research: Earth Surface*, 110(F4).
- van Heteren, S., & van der Spek, A.J.F. (2008). Waar is de delta van de oude Rijn? *Grondboor & Hamer*, 62(3/4), 72-76.
- Van Santen, R.B., De Swart, H.E., & Van Dijk, T.A.G.P. (2011). Sensitivity of tidal sand wavelength to environmental parameters: A combined data analysis and modelling approach. *Continental shelf research*, 31(9), 966-978.
- Zijl, F., Verlaan, M., & Gerritsen, H. (2013). Improved water-level forecasting for the Northwest European Shelf and North Sea through direct modelling of tide, surge and non-linear interaction. *Ocean Dynamics*, 63(7), 823-847.

A Description of additional data

The following data are provided along with this report:

- Lowest SeaBed Level (LSBL) for time spans of 5 year
- Highest SeaBed Level (HSBL) for time spans of 5 year
- Best Estimate Bathymetry (BEB) for time spans of 5 year
- Classification zones for wind farm design based on seabed lowering, rising and combined lowering and rising (for the period 2016 – 2051 only)

As explained in Chapter 5, the LSBL and HSBL provide the upper and lower envelope of predicted morphological seabed level changes. But instead of a single LSBL and HSBL for the time period between 2016 and 2051, now intermediate LSBLs and HSBLs are provided. The LSBL₂₀₂₁ for example provides the lower envelope to be expected in the time period between 2016 and 2021. Each subsequent LSBL provides the envelope between 2016 and a given year (e.g. the LSBL₂₀₃₆ provides the lower envelope to be expected in the time period between 2016 and 2036). This is similar for the upper limit, which is provided by the HSBL.

The BEB is obtained by estimating the most probable migration speed and migration direction found in the various datasets. Based on these values the future bathymetry is predicted. The resulting bathymetry is expected to have on average the smallest overall error. In other words: when compared to the actual 2031 bathymetry the BEB₂₀₃₁ is expected to have the smallest area-averaged total difference. However, at specific locations it can differ significantly (but it is not expected to exceed the limits provided by the LSBL and HSBL).

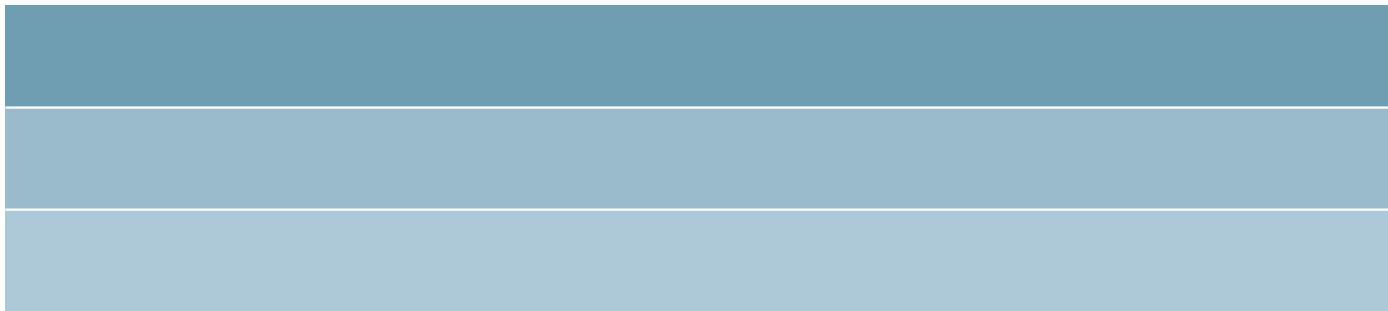
Furthermore, the classification zones as shown in Figure 5.10 and Figure 5.11 are obtained by translating the LSBL and HSBL into possible classification zones for foundations and electricity cables. The classification of these zones is based on the predicted seabed lowering and rising.

Table A1 provides an overview of the data files delivered along with this report. The data files are delivered in ASCII format and raw GIS files. The ASCII files contain three columns, respectively Easting, Northing and a z-level.

All data points are provided in the coordinate system ETRS89 / UTM Zone 31N. The z-levels for the seabed predictions are always given in metres relative to Lowest Astronomical Tide (LAT) for each of the defined z-levels (i.e. minimum expected seabed for the LSBL-files, maximum expected seabed for the HSBL-files and most probable seabed for the BEB-files). The classifications for the classification zones are addressed as 1, 2, 3 or 4 corresponding to the specific classifications (Preferred, Possible, Better avoided or Un-recommended).

Data file	Description
HKZ_20161109_Deltares_data2016_2021_D	HSBL for the period 2016 – 2021
	LSBL for the period 2016 – 2021
	BEB for the period 2016 – 2021
HKZ_20161109_Deltares_data2016_2026_D	HSBL for the period 2016 – 2026
	LSBL for the period 2016 – 2026
	BEB for the period 2016 – 2026
HKZ_20161109_Deltares_data2016_2031_D	HSBL for the period 2016 – 2031
	LSBL for the period 2016 – 2031
	BEB for the period 2016 – 2031
HKZ_20161109_Deltares_data2016_2036_D	HSBL for the period 2016 – 2036
	LSBL for the period 2016 – 2036
	BEB for the period 2016 – 2036
HKZ_20161109_Deltares_data2016_2041_D	HSBL for the period 2016 – 2041
	LSBL for the period 2016 – 2041
	BEB for the period 2016 – 2041
HKZ_20161109_Deltares_data2016_2046_D	HSBL for the period 2016 – 2046
	LSBL for the period 2016 – 2046
	BEB for the period 2016 – 2046
HKZ_20161109_Deltares_data2016_2051_D	HSBL for the period 2016 – 2051
	LSBL for the period 2016 – 2051
	BEB for the period 2016 – 2051
	Classification zones for the period 2016 - 2056
HKZ_20161109_Deltares_data2016_2056_D	HSBL for the period 2016 – 2056
	LSBL for the period 2016 – 2056
	BEB for the period 2016 – 2056

Table A1 Contents of the data files accompanying this report.



Deltares



The creative commons license 4.0 apply to this material.

This investigation was carried out by Deltares, commissioned by RVO.nl, an agency of the Ministry of Economic Affairs. Whilst a great deal of care has been taken in compiling the contents of this investigation, RVO.nl can not be held liable for any damages resulting from any inaccuracies and/or outdated information.

Contacts

Netherlands Enterprise Agency (RVO.nl)
Croeselaan 15 | 3521 BJ | Utrecht
P.O. Box 8242 | 3503 RE | Utrecht
www.rvo.nl / <http://english.rvo.nl>

Netherlands Enterprise Agency (RVO.nl) | December 2016